

Opto-Electronic Properties of Disordered Organic Semiconductors

PROEFSCHRIFT

ter verkrijging van de graad van Doctor
aan de Universiteit Leiden,
op gezag van de Rector Magnificus Dr. W. A. Wagenaar,
hoogleraar in de faculteit der Sociale Wetenschappen,
volgens besluit van het College voor Promoties
te verdedigen op donderdag 28 januari 1999
te klokke 16.15 uur

door

Michel Cornelis Josephus Marie Vissenberg

geboren te Sint Maarten in 1972

Promotiecommissie:

Promotor: Prof.dr. C. W. J. Beenakker
Co-promotor: Dr.ir. M. J. M. de Jong (Philips Research)
Referent: Dr.ir. P. W. M. Blom (Philips Research)
Overige leden: Prof.dr. H. Bässler (Philipps-Universität Marburg)
Prof.dr. G. W. 't Hooft
Prof.dr. L. J. de Jongh
Prof.dr. J. M. J. van Leeuwen
Prof.dr.ir. W. van Saarloos

Het onderzoek beschreven in dit proefschrift heeft plaatsgevonden op het Philips Natuurkundig Laboratorium te Eindhoven, als onderdeel van het Philips onderzoeksprogramma, en is tevens onderdeel van het wetenschappelijk programma van de Stichting voor Fundamenteel Onderzoek der Materie (FOM) en de Nederlandse Organisatie voor Wetenschappelijk Onderzoek (NWO).

The work described in this thesis has been carried out at the Philips Research Laboratories in Eindhoven, The Netherlands, as part of the Philips research programme, and is also part of the scientific programme of the Foundation for Fundamental Research on Matter (FOM) and the Netherlands Organization for Scientific Research (NWO).

About the cover:

A prototype of a polymer LED matrix display consisting of 87 rows and 80 columns. The polymer LED display shows a picture with 256 grey levels.

Photo: Philips Research.

Contents

1	Introduction	1
1.1	Organic semiconductors: history and applications	2
1.2	Organic semiconductors: physics	4
1.3	Polymer LEDs	9
1.4	Theoretical concepts	12
1.4.1	Resistor networks	13
1.4.2	Continuous-time random walks	16
1.4.3	Green function methods	20
1.5	This thesis	24
	References	37
2	Field-effect mobility of amorphous organic transistors	43
2.1	Introduction	43
2.2	The hopping conductivity	44
2.3	Transistor model	48
2.4	Discussion	51
2.5	Appendix	52
	References	55
3	Dispersive hole transport in poly(p-phenylene vinylene)	57
3.1	Introduction	57
3.2	Experiment	60
3.3	Results and discussion	60
3.4	Appendix	67
	References	71
4	Field-dependent mobility in disordered organic semiconductors	75
4.1	Introduction	75

4.2	Hopping conduction in one dimension	77
4.3	Model for the carrier mobility	81
	References	85
5	Exciton dynamics in disordered molecular systems	87
5.1	Introduction	87
5.2	Green function formalism	89
5.3	Photoluminescence	93
	References	99
6	Exciton migration and field-induced dissociation in conjugated polymers	101
6.1	Introduction	101
6.2	Exciton migration	102
6.3	Field-induced photoluminescence quenching	104
6.4	Conclusion	109
6.5	Appendix	109
	References	113
7	Electric field-induced photoluminescence quenching in disordered molecular solids	117
7.1	Introduction	117
7.2	Exciton migration	119
7.3	Exciton dissociation	120
7.4	Conclusion	125
	References	127
8	Photobleaching and spectral diffusion in disordered media	129
8.1	Introduction	129
8.2	Spectral diffusion	130
8.3	Photobleaching	133
8.4	Influence of quenching sites	138
8.5	Photobleaching of PPV	144
8.6	Conclusion	146
	References	147
	Samenvatting	149
	List of Publications	153
	Curriculum Vitæ	155

Chapter 1

Introduction

This thesis deals with the electrical transport and optical response properties of organic semiconductors. Due to their extremely low intrinsic conductivity, most organic semiconductors should really be designated as insulators. The use of the name semiconductor is based on the extrinsic semiconducting properties of organic systems, i.e., the capacity to transport charge generated by light, injected by electrodes, or provided by chemical dopants. For the large part, this research has been motivated by the potential application of this class of materials in opto-electronic devices, specifically polymer light-emitting diodes. Due to the weak electronic coupling between organic molecules, disorder plays a central role in the understanding of these materials. Disorder manifests itself in variations in the energy of the electronic states of different molecules and in the variations in the structure of the solid state. In this thesis we discuss the influence of these two types of disorder on the transport of charge carriers and on the dynamics of optically excited states.

In this introductory Chapter, a brief review is given of the various applications of organic semiconductors, followed by a discussion of fundamental physical concepts regarding the nature and dynamics of excited states in these materials. Since most of the work in this thesis is related to the operation of polymer-based light-emitting diodes (LEDs), some important aspects of the device physics of polymer LEDs are reviewed. Finally, several theoretical approaches to describe transport in disordered materials are introduced and the contents of the different Chapters are put into perspective through a brief outline.

1.1 Organic semiconductors: history and applications

For the past 50 years, conventional *insulating* polymers (“plastics”) have increasingly been used as substitutes for structural materials like wood, ceramics, and metals because of their high strength, light weight, ease of chemical modification, and processability at low temperatures. Traditionally, the study of *semiconducting* organic materials focused on small organic molecules in the crystalline state. Several molecular crystals like naphthalene and anthracene were found to display the semiconducting properties known from their inorganic counterparts [1]. For example, photoconductivity in organic crystals [2, 3] and electroluminescent devices based on anthracene crystals [4] have been demonstrated in the early 1960s. However, due to their poor semiconducting characteristics, organics were mostly considered as exotic materials with little potential for applications.

In molecularly doped polymers, formed by organic pigments (or *chromophores*, from the Greek “color bringers”) dispersed in an insulating polymer matrix, the semiconducting properties of small organic molecules are combined with the advantageous mechanical properties of polymers. Semiconducting polymers have been synthesized by building the chromophores into the polymer as side groups or in the main chain of the polymer itself. Since the 1970s, multilayers of these organic photoconductors have steadily replaced the amorphous-selenium and amorphous-silicon photoreceptors in electrophotographic devices like photocopiers and printers, because of their material variety, economy, flexibility, and environmental safety [5].

The first highly conducting organic polymer, chemically doped polyacetylene, was reported in 1977 [6]. Although initially these doped conducting polymers were unstable in air, brittle, and difficult to process, new generations of these materials are stable and easily processable from a wide variety of solvents. The electrical conductivities now range from those typical for insulators ($< 10^{-10}$ S/cm), to those typical of semiconductors such as silicon ($\sim 10^{-5}$ S/cm), to those greater than 10^4 S/cm (nearly that of copper, 5×10^5 S/cm) [7]. Applications of these polymers, especially polyanilines, have begun to emerge. These include coatings and blends for electrostatic dissipation and electromagnetic-interference shielding, conductive layers for opto-electronic polymer devices, and anticorrosion coatings for iron and steel [8].

The interest in undoped organic semiconductors, both polymers and small molecules, revived at the end of the 1980s as a result of (i) the demon-



Figure 1.1: *A polymer LED display. (Source: “Philips Components to set up light-emitting polymer business”, Philips Research Press release 9802e/March 1998)*

stration of high-performance electroluminescent devices made of multilayers of vacuum-sublimed dye films at Eastman Kodak [9], (ii) the report of field-effect transistors made from polythiophene [10] and from small conjugated oligomers [11], and (iii) the discovery of electroluminescence from conjugated polymer-based diodes at Cambridge University [12].

At the moment, the most promising applications are in organic electroluminescent devices, to be used as back lights for liquid crystal displays, as simple alphanumeric displays (see Fig. 1.1), and ultimately as full-color active matrix displays. Japanese researchers, as well as the group at Kodak, have improved device efficiency and lifetime of the LEDs based on vacuum-sublimed dye films to meet commercial requirements: Monochrome matrix displays are currently being produced by Pioneer and multicolor matrix displays have been demonstrated by Pioneer, TDK, and NEC. Conjugated polymers have an intrinsic advantage over these small organic molecules due to their better mechanical properties and processability, which would allow for cheaper and flexible displays. This option is currently being investigated by companies like Philips, Uniax, Cambridge Display Technologies, and Seiko Epson.

The focus in this thesis is mainly on the undoped (or better: unintentionally doped) conjugated polymers that are used in polymer light-emitting diodes (PLEDs). Before discussing the device physics of PLEDs, let us first set out some basic physical aspects of organic semiconductors.

1.2 Organic semiconductors: physics

In inorganic semiconductor crystals like silicon or germanium, the strong coupling between the constituting atoms and the long-range order lead to the delocalization of the electronic states and the formation of allowed valence and conduction bands, separated by a forbidden energy gap. By thermal activation or photo-excitation, free electrons are generated in the conduction band, leaving behind positively charged holes in the valence band. The transport of these free charge carriers is described in the quantum-mechanical language of Bloch functions, k -space, and dispersion relations familiar to solid-state physicists [13].

Structural or chemical defects in the crystal introduce states in the forbidden energy gap, spatially localized at the defect. A mobile carrier from the transport bands may get trapped at such a defect state, and no longer contribute to the conductivity until it is released again. In addition to such delocalized band transport with multiple trapping, carriers may also tunnel directly from one localized state to another when the electronic wave functions of the defect states have sufficient overlap. The carrier may overcome the energy differences between the defect states by absorbing and emitting phonons. This mechanism of phonon-assisted tunneling, or “hopping”, was originally proposed by Conwell [14] and Mott [15, 16]. The transition rates for phonon-assisted tunneling were calculated by Miller and Abrahams [17]. Hopping from a localized state j to a state i takes place at a phonon frequency ν_0 , corrected for a tunneling probability and the probability to absorb a phonon for hops upward in energy:

$$W_{ij} = \nu_0 \exp(-2\gamma R_{ij}) \begin{cases} \exp\left(-\frac{\varepsilon_i - \varepsilon_j}{k_B T}\right) & \varepsilon_i > \varepsilon_j, \\ 1 & \varepsilon_i < \varepsilon_j. \end{cases} \quad (1.1)$$

Here, γ is the inverse localization length, R_{ij} the distance between the localized states, and ε_i the energy at the state i . Since the hopping rates are strongly dependent on both the positions and the energies of the localized states, hopping transport is extremely sensitive to structural as well as energetic disorder. Reviews on hopping transport in disordered media can be found in Refs. [18, 19].

In organic solids, intramolecular interactions are mainly covalent, but intermolecular interactions are due to much weaker van der Waals and London forces. As a result, the transport bands in organic crystals are much narrower than those of their inorganic counterparts and the band structure is easily disrupted by introducing disorder in the system. Thus, even

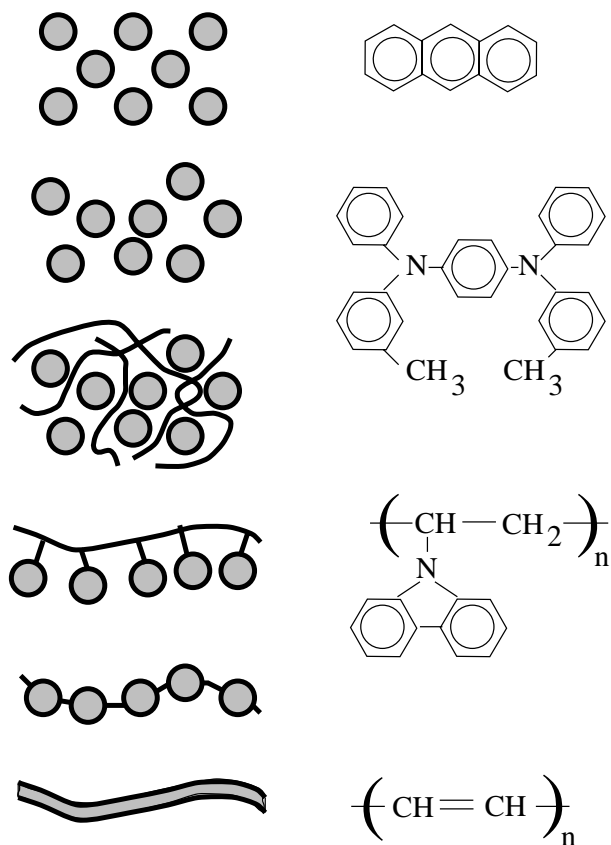


Figure 1.2: Schematic diagram depicting the classes of organic semiconducting materials (top to bottom): organic crystals, organic glasses, molecularly doped polymers, pendant-group polymers, polymers with main-chain active groups, and conjugated polymers. The shaded areas indicate the π -conjugated system. The structure formulas of some prototypical organic semiconductors are given at the right (top to bottom): an anthracene molecule, the pigment TPD [*N,N'*-diphenyl-*N,N'*-bis(3-methylphenyl)-[1,1'-biphenyl]-4,4'-diamine], the pendant-group polymer PVK [poly(vinylcarbazole)], and the conjugated polymer polyacetylene.

in molecular crystals, the concept of allowed energy bands is of limited validity and excitations and interactions localized on individual molecules play a predominant role. The common electronic feature of many organic pigments is the π -conjugated system, which is formed by the overlap of carbon p_z orbitals. Due to the orbital overlap, the π electrons are delocalized within a molecule and the energy gap between the highest occupied molecular orbital (HOMO) and the lowest unoccupied molecular orbital (LUMO) is relatively small, i.e., with transition frequencies within the visible range. Some characteristic organic semiconductors are depicted in Fig. 1.2 and the chemical structures of some π -conjugated polymers are given in Fig. 1.3. In the chemical structure formulas, the π -electrons are represented by double bonds (in phenyl groups, the double bonds are often replaced by circles, to emphasize the delocalized nature of the π -electrons). The low coupling between the molecules in the solid state ensures that the carriers in these materials are strongly localized on a molecule. Transport occurs via a sequence of charge transfer steps from one molecule to another, similar to the hopping between defect states in inorganic semiconductors.

The canonical technique for determining the charge transport properties of photoconductors is the time-of-flight technique, which originated from the use of photoconducting materials in photocopiers [5, 20]. In this technique, a flash of light generates a sheet of charge carriers close to one electrode of a parallel plate capacitor. Under an applied electric field E , the carriers move to the opposite electrode. The transit time τ_t at which the carriers reach this electrode (distance L) is then a direct measure of the carrier mobility,

$$\mu = L/\tau_t E. \quad (1.2)$$

A problem with disordered materials is that the photocurrent transients are often dispersive, i.e., the velocity of the sheet of carriers decreases as the sample is traversed. In that case the mean arrival time of the carriers, and consequently the carrier mobility, depends on the dimensions of the sample and the mobility does not reflect a genuine material parameter. The relation between disorder and dispersive transport will be discussed in more detail in Sec. 1.4.

Time-of-flight studies of disordered organic semiconductors show both dispersive and nondispersive transients, depending on, e.g., chemical purity, layer thickness or temperature. The carrier mobilities obtained from the nondispersive measurements reveal a recurrent pattern of features: (i) a field-independent activated mobility at low fields, characterized by an activation energy Δ of about 0.4 eV to 0.6 eV, independent of chemical

constitution and synthesis; (ii) a field dependent mobility of the stretched exponential form $\exp(S\sqrt{E})$ at high fields; (iii) a change of sign of the coefficient S above a certain temperature. These features may be described by the empirical law

$$\mu = \mu_0 \exp \left[-\frac{\Delta}{k_B T} + B \left(\frac{1}{k_B T} - \frac{1}{k_B T_0} \right) \sqrt{E} \right]. \quad (1.3)$$

This empirical form of the mobility was for the first time observed in poly(*N*-vinylcarbazole) (PVK) in the early 1970s [21, 22] and later in many other disordered molecular materials [23–26]. A discussion on the microscopic mechanism underlying this ubiquitous behavior can be found in Sec. 1.5 and in Chapter 4 of this thesis.

In inorganic band semiconductors, the photogeneration of charge involves the excitation of an electron from the valence band into the conduction band. Due to the delocalized nature of the electronic states and screening effects, the Coulomb interaction within the resulting electron-hole pair is weak and the carriers are either free or form very weakly bound excitons of the Mott-Wannier type [13]. In molecular systems, the primary optical excitations are localized on a single chromophore. Due to this confinement, and due to the low dielectric constant in organics, the Coulomb interaction between the electron in the LUMO and the hole in the HOMO is strong and the exciton is of the Frenkel type. Since the HOMO and LUMO vary for different chromophores in the disordered material, the excitons may relax in the course of a random walk to chromophores where the energy is low, a process known as spectral diffusion. This results in a red shift of the emission spectrum with respect to the absorption spectrum. The photogeneration of free carriers is an indirect process, requiring the dissociation of excitons into electrons and holes on different chromophores. Due to the high exciton binding energy (typically 1 eV), photoconduction in molecular systems commences about 1 eV above the absorption edge.

In conjugated polymers, the π -conjugated system extends over the whole polymer chain, thus allowing for delocalized states in one direction. Therefore conjugated polymers were initially regarded as one-dimensional semiconductors. In their pioneering work Su, Schrieffer, and Heeger [27] studied the interaction of an excitation with an ideal one-dimensional lattice, neglecting Coulomb interactions and disorder effects. They found that, in addition to direct electron and hole excitations across the semiconductor band gap, the one-dimensional system may support a host of exotic carrier types like solitons (topological defects without charge, with spin 1/2), polarons (electrons and holes, self-trapped by carrier-lattice interactions),

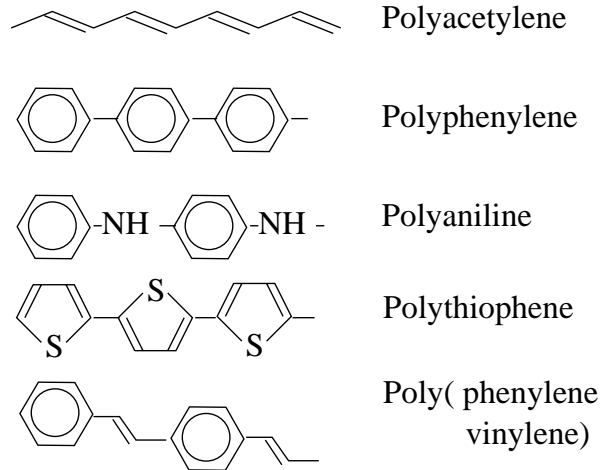


Figure 1.3: *Chemical structure of some of the most important conjugated polymers*

soliton-polarons (charged topological defects without spin, self-trapped by carrier-lattice interactions), bipolarons (two carriers with charge of the same sign, bound by lattice distortion), and polaron-excitons (two carriers with charge of the opposite sign, bound by lattice distortion) [27]. In this one-dimensional semiconductor picture, the red shift between absorption and emission is attributed to the creation of self-trapped polarons after the initial generation of free carriers. The energy shift is then a measure for the self-localization energy of the polaron. One of the major arguments in favor of the one-dimensional semiconductor picture for conjugated polymers has been the coincidence of the onset of photoconductivity with the onset of optical absorption [28], which indicates the absence of a sizeable exciton binding energy.

On the other hand, spectroscopic studies of conjugated polymers show many features that are characteristic for disordered molecular systems [29]. Among these studies are site-selective fluorescence experiments [30], where the emission spectrum is monitored as a function of excitation in a narrow spectral window, and time-resolved photoluminescence experiments [31]. Both the spectral and time dependence of the emission indicate that the primary excitation in a conjugated polymer is a neutral exciton localized on a chromophore, executing an incoherent random walk between chromophores. (We will discuss some of these experiments in Chapter 5, together with a theoretical description of exciton dynamics in disordered molecular sys-

tems.) The chromophores may be identified with segments of the polymer chain, separated by mechanical and chemical defects (twists, kinks, impurities, crosslinks, . . .). Additional experimental proof for this molecular picture is formed by the observation of luminescence quenching by high electric fields [32, 33] (attributed to the dissociation of strongly bound excitons) and the recent demonstration that the photoconduction near the absorption edge is mostly of extrinsic origin, resulting from exciton dissociation at electrodes [34]. The intrinsic photoconduction commences at much higher energies, in accord with the molecular exciton picture.

The discussion on the precise nature and dynamics of excited states in conjugated polymers—one dimensional semiconductors with strong electron-phonon interaction versus disordered molecular solids with strong Coulomb interaction—is still very much alive. A discussion on this topic can be found in Ref. [35]. The one-dimensional semiconductor nature of conjugated polymers might play a role in experiments on highly ordered, stretch-oriented materials or on isolated single chains. Furthermore, in *conducting* polymers, the influence of chemical dopants on the morphology of the polymer layer and on the charge-transporting states is still a matter of controversy: The (quasi) one-dimensional nature of the conducting states may explain the exceptionally high conductivities in doped conjugated-polymer systems [36]. Nevertheless, based on the sizeable body of experimental evidence, one must conclude that the physics of undoped amorphous conjugated polymer films can not be very different from that of other disordered organic systems. Some of the similarities between conjugated polymers and molecular systems (and their differences) are explored in this thesis.

1.3 Polymer LEDs

Since their discovery in 1990 polymer light-emitting diodes (PLEDs) have been considered promising candidates for large-area applications as a result of easy processing and mechanical flexibility [12, 37]. Additional attractive features of PLEDs as compared to other flat display systems are high contrast and resolution, the absence of viewing-angle dependence, low power consumption, low voltage operation, fast response times, and the wide range of available colors. Basically, a PLED consists of a thin layer of undoped conjugated polymer sandwiched between two electrodes on top of a glass substrate (see Fig. 1.4). Most attention has been focused on PLEDs that contain the conjugated polymer poly(-*p*-phenylene vinylene) (PPV) or its derivatives, because of the high external conversion efficiency

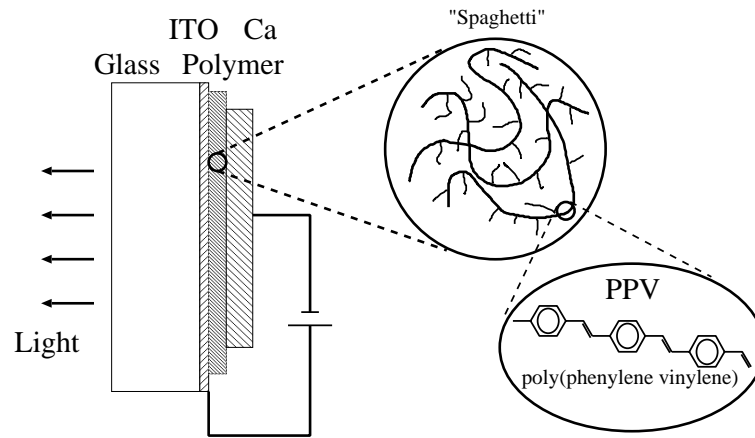


Figure 1.4: A polymer LED consists of a glass substrate with an indium-tin-oxide (ITO) coating functioning as anode, a spin-coated layer of a conjugated polymer as the active layer, and an evaporated metal cathode. The most commonly used polymers are derivatives of poly (*p*-phenylene vinylene), with different side groups to make the polymer soluble.

(> 1% photons/charge carrier). The PPV is spin-coated on top of a patterned indium-tin-oxide (ITO) bottom electrode, which forms the anode. The cathode on top of the polymer consists of an evaporated layer of a low work-function metal like calcium (Ca).

Under forward bias electrons and holes are injected into the polymer from the cathode and the anode, respectively. Driven by the applied electric field, the charge carriers move through the polymer in opposite directions until recombination takes place. The device operation of a PLED is thus determined by three processes: charge injection, charge transport, and recombination. In this Section, a short review is given of the device model for PLEDs developed at Philips Research. For more information, the reader is referred to the original papers [38–41].

The transport and injection properties of holes have been investigated by replacing the Ca cathode by a gold (Au) contact. In these hole-only devices, the work functions of both electrodes are close to the valence states (or better: HOMOs) of the PPV, preventing electron injection from the negatively biased electrode. The current density versus voltage (J - V) characteristics of such ITO/PPV/Au hole-only devices with various thicknesses

L of the PPV layer follow Child's law¹ for space-charge limited current [42],

$$J = \frac{9}{8}\epsilon_0\epsilon_r\mu_p\frac{V^2}{L^3}. \quad (1.4)$$

Here, $\epsilon_0\epsilon_r$ is the permittivity of the polymer and μ_p is the hole mobility. The observation of space-charge limited current clearly demonstrates that the hole current is determined by the transport properties of the polymer (bulk-limited) and not by the injection from the anode into the polymer (injection-limited), as proposed earlier [43, 44]. Furthermore, the hole mobility can now be obtained directly from the J - V characteristics, since it is the only unknown. Using $\epsilon_r = 3$, comparison with experiment yields a room temperature hole mobility of $\mu_p = 5 \times 10^{-11} \text{ m}^2/\text{Vs}$. A study of the J - V characteristics at high electric fields E as a function of temperature T has revealed that the hole mobility can be accurately described by the empirical law (1.3), with $\mu_0 = 3 \times 10^{-3} \text{ m}^2/\text{Vs}$, $\Delta = 0.5 \text{ eV}$, $B = 3 \times 10^{-5} \text{ eV}(\text{V/m})^{-1/2}$, and $T_0 = 600 \text{ K}$ [39]. Both the functionality and the numerical parameter values of this mobility indicate the strong similarity between the conjugated polymer PPV and the other members of the class of disordered organic semiconductors (see previous Section).

A Ca/PPV/Ca electron-only device has been used to investigate the transport properties of electrons. The work function of calcium is close to the conduction states (or LUMOs) of PPV, thus blocking the injection of holes into the polymer. The electron current appears to be orders of magnitude lower than the hole current. Furthermore, the electron current shows a much stronger field dependence, which is characteristic for an insulator with traps. Like the hole current, the electron current scales with the thickness of the PPV layer. This clearly proves that the electron current is determined by the bulk transport properties of PPV as well.

The third process underlying the operation of a PLED is the recombination of electrons and holes to produce a photon. Information about this process has been obtained by modeling the J - V characteristics of a PLED, using the information obtained from the single-carrier devices. The device model takes into account Ohmic contacts, space charge effects, the empirical form of the field and temperature dependent carrier mobility, and an exponential distribution of electron traps. In addition, the recombination of charge carriers is described by a phenomenological rate of the form Bpn ,

¹Child's law is characteristic for insulators which lack intrinsic charge. By increasing the applied voltage V the insulator is charged like a capacitor ($q \sim V$). The carrier velocity ($v = \mu V/L$) also increases with the applied voltage, which leads to the typical quadratic voltage dependence of the current density.

i.e., proportional to the electron (n) and hole (p) concentrations. Comparison of the model with experimental J - V characteristics of a ITO/PPV/Ca device reveals that the recombination constant B is thermally activated with an activation energy equal to that of the charge carrier mobility [40]. This indicates that the recombination is of the Langevin type [45], i.e., diffusion controlled. This is expected for an organic hopping system [46], since the mean free path of the carriers (the distance between two conjugated chain segments in PPV: about 10 Å) is much smaller than the capture radius $r_C = e^2/4\pi\epsilon\epsilon_r k_B T$ at which the Coulomb binding energy between an electron and a hole equals $-k_B T$ (in PPV: $r_C = 200$ Å at room temperature). As a result, the rate-limiting step in the recombination process is the diffusion of electrons and holes toward each other in their mutual Coulomb field.

The model calculations show that the recombination efficiency in the PLED is almost one: due to the high carrier densities near the Ohmic contacts and due to the scaling of the Langevin recombination strength with the carrier mobility, all carriers recombine before reaching the opposite electrode. In contrast, the conversion efficiency of a PLED is about 5% photons/carrier. This indicates that the exciton decay in the PLED is mainly nonradiative.

The important conclusions to be drawn from this device model is that in the present generation of PLEDs the injection and recombination of carriers are optimized. The limiting processes in a PLED appear to be the transport of charge and the decay of excitons. The microscopic description of these processes forms the main body of this thesis. In the next Section, we introduce the theoretical methods that form the basis of these descriptions.

1.4 Theoretical concepts

We follow the molecular approach in describing the opto-electronic properties of disordered organic semiconductors (including conjugated polymers) in terms of a series of transfer steps of an excitation between different chromophores. These chromophores may be organic dye molecules, as in organic glasses and molecularly doped polymers, active side groups or active groups on the skeletal chain of the polymer, or segments of a conjugated polymer chain that are separated by defects. In case of electrical transport, the transfer mechanism involves the thermally activated tunneling (hopping) of a positive or negative charge from a charged chromophore to a neutral chromophore. Upon optical excitation, an electrically bound electron-hole

pair (exciton) is formed, localized on the chromophore that absorbed the photon. The exciton may decay radiatively and emit a photon, decay non-radiatively and produce heat, or migrate to other chromophores and decay there.

The incoherent dynamics of charge carriers as well as excitons are described by a kinetic equation known as the master equation,

$$\frac{\partial}{\partial t} f_i(t) = - \sum_{j \neq i} W_{ji} f_i(t) [1 - f_j(t)] + \sum_{j \neq i} W_{ij} f_j(t) [1 - f_i(t)] - \lambda_i f_i(t). \quad (1.5)$$

Here, $f_i(t)$ is the occupational probability of the site i (position \mathbf{R}_i and energy ε_i) at time t . The transition from site j to site i is described by the rate W_{ij} and decay processes are taken into account through the rates λ_i ($\lambda_i = 0$ in case of charge carriers). The factors $1 - f$ are present because doubly occupied electronic states are not allowed.

In this general form, the master equation is nonlinear and very difficult to handle. Usually this equation is linearized, either by assuming small deviations from equilibrium, or by assuming uncorrelated particles, depending on the experimental situation one wants to describe. The existing approaches for solving linearized versions of the master equation may roughly be divided into three groups: (i) The resistor network method [17], combined with effective medium techniques [47], or with percolation techniques [48]. (ii) The continuous-time random walk method [49]. (iii) The Green function method [50]. In the following, these methods are discussed in relation to their application in this thesis.

1.4.1 Resistor networks

The resistor network method describes the electrical conductivity of a system with localized electronic states in the presence of a weak external electric field. The linearization of the master equation is based on the assumption that the deviation of each f_i from its equilibrium value is small. The average net flow of current between two sites can then be written in the form of a conductance times the difference in electrochemical potential. Thus the problem of hopping between localized states has been mapped on the problem of calculating the conductivity of a network of resistors. The conductivity of the whole system can then be calculated either by numerically solving Kirchhoff's equations for the whole resistor network, or by estimating the "typical" two-site conductance using effective medium techniques or percolation techniques.

In the following, we will discuss the linearization procedure to obtain a mapping of the problem of hopping between localized states onto a random resistor network. To illustrate the use of the resistor network method, the temperature dependence of the hopping conductivity is derived for a disordered system with random site positions and a constant density of states ρ near the Fermi energy. This method forms the basis of the model used in Chapter 2 to describe the carrier mobility in organic transistors.

According to the master equation (1.5) the steady-state current from site j to site i is given by

$$I_{ij} = e [W_{ij}f_j(1 - f_i) - W_{ji}f_i(1 - f_j)]. \quad (1.6)$$

The occupation f_i can be expressed in the form

$$f_i = [1 + e^{(\varepsilon_i - \mu_i)/k_B T}]^{-1}, \quad (1.7)$$

where μ_i is the quasi-electrochemical potential at site i (we say “quasi” because the system is not in equilibrium). At thermal equilibrium $\mu_i = \varepsilon_F - e\mathbf{E} \cdot \mathbf{R}_i$, where ε_F is the Fermi energy (or chemical potential). For hopping rates of the Miller-Abrahams form (1.1) the steady-state current reads

$$I_{ij} = \frac{e\nu_0 \exp(-2\gamma R_{ij} - |\varepsilon_i - \varepsilon_j|/2k_B T) \sinh[(\mu_i - \mu_j)/2k_B T]}{2 \cosh[(\varepsilon_i - \mu_i)/2k_B T] \cosh[(\varepsilon_j - \mu_j)/2k_B T]}. \quad (1.8)$$

At low bias the expression for I_{ij} may be linearized with respect to deviations in the quasi-electrochemical potential to give the Ohmic current

$$I_{ij} = G_{ij}(\mu_i - \mu_j). \quad (1.9)$$

When the energy variations are large compared to the thermal energy $k_B T$, the conductance G_{ij} can be written in the form

$$G_{ij} \approx \frac{e\nu_0}{k_B T} \exp\left(-2\gamma R_{ij} - \frac{|\varepsilon_i - \varepsilon_F| + |\varepsilon_j - \varepsilon_F| + |\varepsilon_i - \varepsilon_j|}{2k_B T}\right). \quad (1.10)$$

Thus the problem of calculating the conductivity in a disordered hopping system is reduced to calculating the conductivity in a random resistor network. To tackle this problem, several methods have been developed. Among them, the effective medium approach and the percolation approach have proven to be particularly useful.

In the effective medium approach, the disordered network is replaced by an ordered network with equal conductances G . A naive estimate for the

“characteristic” conductance G would be the average value of G_{ij} . Averaging over the initial and final site energies for a system with a constant density of localized states near the Fermi energy yields a temperature dependence $G \propto k_B T$. This averaging procedure overestimates the contribution from resistors with atypically high conductances. In the opposite approach, originally used by Miller and Abrahams [17], the random network is replaced by a set of independent conducting paths. Here the conductances are connected in series and the mean resistance calculation leads to an underestimate of the conductivity.

The following intuitive argument was used by Mott [16] to estimate the typical conductance of the disordered network. The highest conductances are those where the site energies at both ends are close to the Fermi energy. When a carrier close to the Fermi energy hops away over a distance R with an energy $\Delta\varepsilon$, it has $\frac{4}{3}\pi R^3 \rho \Delta\varepsilon$ sites to choose from. In general, the carrier will jump to a site for which $\Delta\varepsilon$ is as small as possible. The constraint to find a site within a range $(R, \Delta\varepsilon)$ is given by $\frac{4}{3}\pi R^3 \rho \Delta\varepsilon \sim 1$. Substituting this relation into Eq. (1.10) yields

$$G \propto \exp \left[-2\gamma R - \frac{1}{k_B T (4/3)\pi R^3 \rho} \right]. \quad (1.11)$$

The optimum conductance, found by maximizing G with respect to the hopping distance R , then follows the temperature dependence

$$G \propto \exp \left[- \left(\frac{T_1}{T} \right)^{1/4} \right], \quad (1.12)$$

with $k_B T_1 \sim \gamma^3 / \rho$.

A more systematic derivation of this temperature dependence, known as Mott’s law, has been given by Ambegaokar, Halperin, and Langer [48], based on percolation arguments. (Other derivations based on effective medium techniques and Green functions [50, 51] will not be discussed here.) The idea is that the electrical conductivity of the resistor network is dominated by a few easy “percolating” paths through the disordered system.² The conductivity of these percolating paths, and hence of the whole system, is dominated by the lowest conductance in the easy path. This conductance, the critical percolation conductance G_c , is calculated as follows.

²The term “percolation” was introduced by Broadbent and Hammersley [52], who described the spread of a fluid through a random medium. It is based on the resemblance to the flow of coffee in a percolator.

The percolating subnetwork consists of conductances with $G_{ij} > G_c$. Using Eq. (1.10), this can be written in the form

$$\frac{R_{ij}}{R_{max}} + \frac{|\varepsilon_i - \varepsilon_F| + |\varepsilon_j - \varepsilon_F| |\varepsilon_i - \varepsilon_j|}{2\varepsilon_{max}} < 1, \quad (1.13)$$

with

$$R_{max} = (1/2\gamma) \ln(G_c k_B T / \nu_0 e), \quad (1.14)$$

$$\varepsilon_{max} = k_B T \ln(G_c k_B T / \nu_0 e). \quad (1.15)$$

Any link with $R_{ij} > R_{max}$ or any site with $|\varepsilon_i - \varepsilon_F| > \varepsilon_{max}$ will violate the inequality (1.13) and thus cannot be part of the percolating subnetwork. Thus the density of sites that may be part of the percolating subnetwork is given by

$$N_s = 2\rho\varepsilon_{max}. \quad (1.16)$$

These sites are still randomly distributed in space. In order to form a percolating subnetwork that spans the whole system, the value of G_c must be such that each site in the subnetwork is connected to a sufficient number of other sites in the network. Since the sites in the subnetwork are linked only to sites within a range R_{max} , this criterion has the form

$$N_s R_{max}^3 = \nu_c, \quad (1.17)$$

with ν_c a dimensionless constant of order unity. A combination of Eqs. (1.14)–(1.17) yields Mott's law (1.12), with $k_B T_1 = 4\nu_c \gamma^3 / \rho$.

The power 1/4 in Mott's law (1.12) originates from the balance between tunneling in the three spatial dimensions and activation in energy. In general, this power is between 0 (activationless tunneling) and 1 (activated nearest-neighbor hopping), depending on the system dimension and on the shape of the density of localized states.

1.4.2 Continuous-time random walks

In the continuous-time random walk method the master equation is linearized by assuming uncorrelated carriers. The basis of the continuous-time random walk method lies in the observation that the variations in site positions and energies are relatively small compared to the resulting variations in the transition rates between localized states. Thus the transport of a single carrier is described as a sequence of charge-transfer events on a regular lattice, where the disorder in the system is expressed only in a

distribution $\psi(t)$ of waiting times between subsequent events. Assuming a heuristic waiting-time distribution of the algebraic form $\psi(t) \sim t^{-(1+\alpha)}$, where all the physical information about the disordered system is contained in the dispersion parameter α , continuous-time random walk theory successfully explained many anomalous features of transient charge transport in disordered materials [53].

Let us briefly describe some basic elements of continuous-time random walk theory and its application to transient transport in a time-of-flight setup. For a more elaborate description the reader is referred to the original papers [49, 53]. The amorphous system of localized sites is mapped onto a regular lattice of equivalent cells, each cell containing many randomly distributed localized states. (An alternative approach is to take a single site per cell and randomize the system after each transfer step.) For the transient transport, we are only interested in the displacement of the carrier in the direction of the electric field, thus a one-dimensional array of cells suffices. The “microscopic” probability $f_i(t)$ to find a carrier at site i is now replaced by the probability $P(l, t)$ to find the carrier in a specific cell (position l) in the time interval $(t, t + \delta t)$. Due to the disorder in the initial and final states in each cell, the time a carrier takes to move from one cell to another is a random variable. The function $\psi(l, t)$ is the probability that the transfer to a cell at a distance l occurs in the time interval $(t, t + \delta t)$. One of the central approximations in continuous-time random walk theory is the decoupling of the distance dependence and the time dependence of this function: $\psi(l, t) \approx p(l)\psi(t)$, with $p(l)$ the displacement distribution and $\psi(t)$ the waiting-time distribution. Given that all carriers start at position $l = 0$ at time $t = 0$, like in a time-of-flight experiment, the average carrier position follows from

$$\langle l \rangle = \sum_l l P(l, t). \quad (1.18)$$

This probability $P(l, t)$ can be expressed in terms of the waiting time distribution $\psi(t)$ using an auxiliary function $R_n(l, t)$, the probability to arrive at l in the time interval $(t, t + \delta t)$ in n transfer steps. The function $R_n(l, t)$ satisfies a recursion relation

$$R_{n+1}(l, t) = \sum_{l'} \int_0^t dt' p(l - l') \psi(t - t') R_n(l', t'). \quad (1.19)$$

Using the definition $R(l, t) = \sum_n R_n(l, t)$ and the initial condition $R_0(l, t) =$

$\delta_{l,0}\delta(t-0)$, we find

$$R(l, t) = \sum_{l'} \int_0^t dt' p(l-l') \psi(t-t') R(l', t') + \delta_{l,0} \delta(t-0). \quad (1.20)$$

In Fourier-Laplace space, the recursion relation is solved to give

$$\tilde{R}(k, p) = \frac{1}{1 - \tilde{p}(k) \tilde{\psi}(p)}. \quad (1.21)$$

Here $\tilde{R}(k, p)$ is the Fourier-Laplace transform of $R(l, t)$, $\tilde{p}(k)$ is the Fourier transform of $p(l)$, and $\tilde{\psi}(p)$ is the Laplace transform of $\psi(t)$. The probability $P(l, t)$ to be at position l at time t now follows from the probability to reach l in an arbitrary number of steps at a time before t , $R(l, t')$, and the probability $\phi(t) \equiv 1 - \int_0^t dt' \psi(t')$ to remain on a site:

$$P(l, t) = \int_0^t dt' R(l, t') \phi(t-t'). \quad (1.22)$$

In Fourier-Laplace space, the solution reads

$$\tilde{P}(k, p) = \frac{1 - \tilde{\psi}(p)}{p [1 - \tilde{p}(k) \tilde{\psi}(p)]}. \quad (1.23)$$

The average carrier position can now be expressed in terms of $\psi(t)$ using the definition of the Fourier transform

$$\langle l \rangle = i \left. \frac{\partial \tilde{P}(k, p)}{\partial k} \right|_{k=0} = \frac{l(E) \tilde{\psi}(p)}{p [1 - \tilde{\psi}(p)]}, \quad (1.24)$$

where we have used the definition $l(E) = \sum_l l p(l)$ and $\tilde{p}(k=0) = \sum_l p(l) = 1$. The average displacement per transfer step $l(E)$ contains the dependence on the electric field. This dependence is often approximated for low fields $l(E) \sim E$.

Let us illustrate the result (1.24) by the trivial case of the ordered system. The probability $Q(t)$ to remain on a site in a given configuration decays in time due to many parallel transfer channels, $dQ(t)/dt = -WQ(t)$, where W denotes the total sum of transition rates. Thus $Q(t)$ decreases exponentially with time, $Q(t) = e^{-Wt}$. In the ordered system, the rate W is the same for all sites. Hence the probability $Q(t)$ is equal to the average probability $\phi(t)$ to remain on a site, and

$$\psi(t) = -\frac{d\phi(t)}{dt} = W e^{-Wt}. \quad (1.25)$$

Substituting the Laplace transform $\tilde{\psi}(p) = 1/(p + W)$ into Eq. (1.24) and performing the inverse Laplace transformation, we find that the average carrier position increases with time according to

$$\langle l \rangle = l(E)Wt. \quad (1.26)$$

The carrier transit time is $\tau_t = L/l(E)W$, as follows directly from $\langle l \rangle (t = \tau_t) = L$. The carrier mobility in the ordered system is then given by $\mu = Wl(E)/E$. At low fields, $l(E) \sim E$ and the carrier mobility is a constant.

In case of a disordered system, the total transition rate W from a given site depends strongly on the configuration of the system. The probability $\phi(t)$ must then be obtained by calculating the configurational average of $Q(t)$. A typical example is the multiple trapping system with an exponential tail of localized states below the conduction band (width $k_B T_0$). At temperatures $T < T_0$ the majority of the carriers is trapped and the transport is determined by the occasional release of a carrier to the transport band. The broad density of localized states gives rise to a broad distribution in release rates $W(\varepsilon) = W_0 \exp(\varepsilon/k_B T)$, where W_0 is an attempt frequency. The average probability $\phi(t) = \int d\varepsilon \rho(\varepsilon) \exp(-W(\varepsilon)t)$ at long times ($W_0 t > 1$) then follows from

$$\begin{aligned} \phi(t) &= \frac{1}{k_B T_0} \int_{-\infty}^0 d\varepsilon e^{\varepsilon/k_B T_0} \exp(-W_0 t e^{\varepsilon/k_B T}) \\ &\approx \frac{1}{k_B T_0} \int_{-\infty}^{-k_B T \ln(W_0 t)} d\varepsilon e^{\varepsilon/k_B T_0} \\ &= (W_0 t)^{-T/T_0}, \end{aligned} \quad (1.27)$$

and the tail of the waiting-time distribution decays according to $\psi(t) = W_0(T/T_0)(W_0 t)^{-1-T/T_0}$. Accordingly, the Laplace transform $\tilde{\psi}(p)$ for small p behaves like

$$\begin{aligned} \tilde{\psi}(p) &= \int_0^\infty dt e^{-pt} \psi(t) = 1 - \int_0^\infty dt (1 - e^{-pt}) \psi(t) \\ &\approx 1 - W_0^{-T/T_0} (T/T_0) \int_0^\infty dt (1 - e^{-pt}) t^{-1-T/T_0} \\ &= 1 - cp^{T/T_0}, \end{aligned} \quad (1.28)$$

with the constant $c = W_0^{-T/T_0} (T/T_0) \int dx (1 - e^{-x}) x^{-1-T/T_0}$. Substituting this into Eq. (1.24) and performing the inverse Laplace transformation, we find that the average carrier position increases with time according to

$$\langle l \rangle \propto l(E)t^{T/T_0}. \quad (1.29)$$

Thus the speed at which the sheet of charge travels is not constant, like in the ordered system, but decreases with time. The reason for this is that initially the carriers are equally distributed over all trap depths, such that there are fast carriers and slow ones. The fast carriers give rise to the initial high velocity, but with increasing time these carriers eventually fall into a deep trap. The average transit time as obtained in a time-of-flight experiment now scales superlinearly with the sample length L according to

$$\tau_t \propto [L/l(E)]^{T_0/T}. \quad (1.30)$$

As a result, the “mobility” as determined from such a transit time scales with the sample dimensions and is no longer a genuine material parameter.

This result may be generalized to any system with an algebraic waiting-time distribution $\psi(t) \propto t^{-1-\alpha}$, with $0 < \alpha < 1$ the dispersion parameter. In case of hopping, both the variations in the hopping distance and in the hopping energies contribute to the dispersion. In general, dispersion due to structural disorder gives rise to a temperature independent α , whereas energetic disorder results in a strongly temperature dependent dispersion.

In most disordered systems, the long-time decay of the waiting-time distribution will be in between the fast exponential decay of the ordered system and the extremely slow algebraic decay resulting in anomalous transport. Furthermore, in practice there will always be an upper limit to the waiting time, determined by, e.g., the trap with the lowest energy or the spatially most isolated hopping site. Thus the algebraic waiting-time distribution is usually valid only on a limited time range (or, equivalently, a limited range of sample thicknesses). When the average carrier transit time is much larger than the maximum waiting time, the carriers have visited a representative portion of the sites in the sample and have attained dynamic equilibrium before reaching the opposite contact. The experimental sign of such behavior is a transient current that initially decreases with time and then reaches a plateau. This transition from dispersive transport to nondispersive transport is commonly observed in disordered conductors [53].

1.4.3 Green function methods

The Green function is a special solution of the linearized master equation, from which the general solution may be constructed. The linearization of the master equation may be based on small deviations from equilibrium (like in the resistor network approach) or on a single-particle approximation (like in continuous-time random walk theory). The two major difficulties one then encounters are (i) to find reasonable approximations to the path

summation problem, and (ii) to carry out the configurational averages for the quantities of interest. Several approximation schemes have been used to describe the hopping conductivity in various limits, like equilibrium or nonequilibrium, high or low site density, temperature and frequency (see, e.g., Refs. [50, 51, 54–57]). The various effective-medium and percolation methods as well as the continuous-time random walk theory may be considered as special cases of the general Green function formalism.

In this thesis, Green functions are used to describe the dynamics of excitons in disordered molecular materials. Based on spectroscopic evidence, this description is expected to hold for conjugated polymer systems as well [29–31]. In such spectroscopic studies, the system is excited by light, after which the emitted light is monitored as a function of, e.g., emission energy, time, or various system parameters. In the following, it is shown how the luminescence intensity, i.e. the number of emitted photons per unit time, may be expressed in terms of configurationally averaged Green functions. The actual path summation and configurational averaging will be discussed in detail in Chapter 5, together with some spectroscopic experiments on conjugated polymer systems.

At low illumination intensities, the occupation probabilities f_i are low and Eq. (1.5) may be linearized

$$\frac{\partial}{\partial t} f_i(t) = - \sum_{j \neq i} W_{ji} f_i(t) + \sum_{j \neq i} W_{ij} f_j(t) - \lambda_i f_i(t). \quad (1.31)$$

The Laplace transform of the master equation can be rewritten in the form of a matrix equation

$$\mathbf{R}\mathbf{f} = \mathbf{0}, \quad (1.32)$$

where \mathbf{f} is a vector with elements f_i . The relaxation matrix \mathbf{R} is an $N \times N$ matrix with diagonal elements

$$R_{ii} = p + \lambda_i + \sum_{j \neq i} W_{ji}, \quad (1.33)$$

and off-diagonal elements

$$R_{ij} = -W_{ij}. \quad (1.34)$$

The Green function $G_{ij}(p)$ is defined by

$$\mathbf{G}(p)\mathbf{R}(p) = \mathbf{1}, \quad (1.35)$$

which can be written in the form

$$G_{ij}(p) = \left(\delta_{ij} + \sum_{l \neq j} G_{il}(p) W_{lj} \right) G_{jj}^0(p), \quad (1.36)$$

with

$$G_{jj}^0(p) = \frac{1}{p + \lambda_j + \sum_{\mu \neq j} W_{\mu j}}. \quad (1.37)$$

In the time domain, $G_{ij}(t)$ is the probability to find a particle at site i at a time t , given that it was at site j at $t = 0$.

The average luminescence intensity at a time t is given by

$$L(t) = \left\langle \sum_i \lambda_i f_i(t) \right\rangle = \left\langle \sum_{i,j} \lambda_i G_{ij}(t) f_j(0) \right\rangle, \quad (1.38)$$

where the angular brackets denote a configurational average. The configurational average of a quantity A is defined as

$$\langle A(\{\mathbf{R}_\nu, \varepsilon_\nu\}) \rangle \equiv \int \left[\prod_{\mu=1}^N d\mathbf{R}_\mu d\varepsilon_\mu \right] P(\{\mathbf{R}_\nu, \varepsilon_\nu\}) A(\{\mathbf{R}_\nu, \varepsilon_\nu\}), \quad (1.39)$$

where $\{\mathbf{R}_\nu, \varepsilon_\nu\}$ denotes the configuration of sites and $P(\{\mathbf{R}_\nu, \varepsilon_\nu\})$ is a normalized distribution function. Neglecting correlations of site positions or site energies, the distribution function can be written as the product of N independent density of states functions $\rho(\varepsilon_i, \mathbf{R}_i)$

$$P(\{\mathbf{R}_\nu, \varepsilon_\nu\}) = \prod_{\mu=1}^N \frac{\rho(\varepsilon_\mu, \mathbf{R}_\mu)}{N}. \quad (1.40)$$

As the positions are taken to be randomly distributed, the medium is homogeneous: $\rho(\varepsilon_i, \mathbf{R}_i) = \rho(\varepsilon_i)$. Taking the initial occupational probability to be a function of site energy only and the recombination rate to be site-independent, i.e. $f_i(0) = f^0(\varepsilon_i)$ and $\lambda_j = \lambda$, we can now write

$$L(t) = \lambda \int \left[\prod_{\mu=1}^N d\mathbf{R}_\mu d\varepsilon_\mu \frac{\rho(\varepsilon_\mu)}{N} \right] \left\{ \sum_{i,j} G_{ij}(t) f^0(\varepsilon_j) \right\}. \quad (1.41)$$

The Green function $G_{ij}(t)$ is a function of all N positions and N energies of a given configuration $\{\mathbf{R}_\nu, \varepsilon_\nu\}$. However, we are not interested in this function itself, but in its configurational average. The configurational averages of the local Green function $G_{jj}(t)$ and the non-local Green function $G_{ij}(t)$ (with $i \neq j$) are denoted as

$$G_1(\varepsilon_j, t) \equiv \langle G_{jj}(t) \rangle_j = \int \left[\prod_{\mu \neq j} d\mathbf{R}_\mu d\varepsilon_\mu \frac{\rho(\varepsilon_\mu)}{N} \right] G_{jj}(t), \quad (1.42)$$

$$G_2(\varepsilon_i, \varepsilon_j, \mathbf{R}_{ij}, t) \equiv \langle G_{ij}(t) \rangle_{ij} = \int \left[\prod_{\mu \neq i,j} d\mathbf{R}_\mu d\varepsilon_\mu \frac{\rho(\varepsilon_\mu)}{N} \right] G_{ij}(t), \quad (1.43)$$

where $\langle \dots \rangle_j$ denotes the configurational average with the site j fixed and $\mathbf{R}_{ij} = \mathbf{R}_i - \mathbf{R}_j$.

In terms of these configurationally averaged Green functions, the luminescence intensity reads

$$\begin{aligned}
L(t) &= \lambda \int \left[\prod_{\mu=1}^N d\mathbf{R}_\mu d\varepsilon_\mu \frac{\rho(\varepsilon_\mu)}{N} \right] \left\{ \sum_j G_{jj}(t) f^0(\varepsilon_j) + \sum_{j,i \neq j} G_{ij}(t) f^0(\varepsilon_j) \right\} \\
&= \lambda \sum_j \int d\mathbf{R}_j d\varepsilon_j \frac{\rho(\varepsilon_j)}{N} f^0(\varepsilon_j) \int \left[\prod_{\mu \neq j} d\mathbf{R}_\mu d\varepsilon_\mu \frac{\rho(\varepsilon_\mu)}{N} \right] G_{jj}(t) + \\
&\quad \lambda \sum_{j,i \neq j} \int d\mathbf{R}_i d\mathbf{R}_j d\varepsilon_i d\varepsilon_j \frac{\rho(\varepsilon_i)}{N} \frac{\rho(\varepsilon_j)}{N} f^0(\varepsilon_j) \\
&\quad \times \int \left[\prod_{\mu \neq i,j} d\mathbf{R}_\mu d\varepsilon_\mu \frac{\rho(\varepsilon_\mu)}{N} \right] G_{ij}(t) \\
&= \lambda \int d\mathbf{R}_j d\varepsilon_j \rho(\varepsilon_j) f^0(\varepsilon_j) G_1(\varepsilon_j, t) + \\
&\quad \frac{N-1}{N} \lambda \int d\mathbf{R}_i d\mathbf{R}_j d\varepsilon_i d\varepsilon_j \rho(\varepsilon_i) \rho(\varepsilon_j) f^0(\varepsilon_j) G_2(\varepsilon_i, \varepsilon_j, \mathbf{R}_{ij}, t) \\
&\approx \lambda \Omega \int d\varepsilon_j \rho(\varepsilon_j) f^0(\varepsilon_j) G_1(\varepsilon_j, t) + \\
&\quad \lambda \Omega \int d\mathbf{R}_{ij} d\varepsilon_i d\varepsilon_j \rho(\varepsilon_i) \rho(\varepsilon_j) f^0(\varepsilon_j) G_2(\varepsilon_i, \varepsilon_j, \mathbf{R}_{ij}, t), \tag{1.44}
\end{aligned}$$

where we have approximated $(N-1)/N \approx 1$. The volume of the system is Ω .

The expression for the luminescence intensity $L(t)$ can be written in the form

$$L(t) = \int d\varepsilon_j L_1(\varepsilon_j, t) + \int d\varepsilon_i d\varepsilon_j L_2(\varepsilon_i, \varepsilon_j, t), \tag{1.45}$$

where $L_1(\varepsilon_j, t)$ denotes the luminescence intensity caused by excitons that recombine on a site with energy ε_j at a time t , given that they were on the same site at $t = 0$. Similarly, $L_2(\varepsilon_i, \varepsilon_j, t)$ denotes the luminescence intensity caused by excitons that have migrated from a site with energy ε_j at $t = 0$ to a site with energy ε_i in a time t . These intensities are defined as

$$L_1(\varepsilon_j, t) \equiv \lambda \Omega \rho(\varepsilon_j) f^0(\varepsilon_j) G_1(\varepsilon_j, t), \tag{1.46}$$

$$L_2(\varepsilon_i, \varepsilon_j, t) \equiv \lambda \Omega \rho(\varepsilon_i) \rho(\varepsilon_j) f^0(\varepsilon_j) \int d\mathbf{R}_{ij} G_2(\varepsilon_i, \varepsilon_j, \mathbf{R}_{ij}, t). \tag{1.47}$$

The time-dependent luminescence spectrum is defined as:

$$L(\varepsilon_i, t) \equiv L_1(\varepsilon_i, t) + \int d\varepsilon_j L_2(\varepsilon_i, \varepsilon_j, t). \quad (1.48)$$

We have now formally solved the problem of calculating the luminescence spectrum by expressing it in terms of the configurationally averaged Green functions. In Chapter 5, these Green functions are calculated explicitly. The resulting formalism is used in Chapters 5, 6, 7, and 8 to interpret a variety of spectroscopic experiments on conjugated polymers and other disordered organic semiconductors.

1.5 This thesis

Although the Chapters of this thesis are self-contained, they are related in the following manner. In the Chapters 2, 3, and 4 we study the influence of energetic and structural disorder on the transport properties of holes in organic semiconductors. To this end, the resistor network method, continuous-time random walk theory, and an analytical model system are used to interpret hole mobility data obtained from organic field-effect transistors, polymer light-emitting diodes, and from time-of-flight experiments. In Chapter 5 a Green function formalism is derived to describe the interplay of exciton migration and decay in disordered molecular materials. In the subsequent Chapters 6, 7, and 8, this formalism is extended to describe the dissociation of excitons by high electric fields, the degradation of polymers under illumination, and the quenching of excitons at defects.

Organic field-effect transistors

The principle of the field-effect transistor (FET) was first proposed by Lilienfeld in 1930 [58]. Basically, a FET operates as a capacitor where one plate is a conducting channel between two ohmic contacts, the source and the drain electrodes [59]. The density of charge carriers is modulated by the voltage applied to the second plate of the capacitor, the gate electrode. At low source-drain bias, the carrier density in the conducting channel may be varied independently using the gate voltage. Then the field-effect mobility follows directly from the slope of the drain current as a function of the gate voltage. In an ideal band semiconductor, this field-effect mobility is equal to the mobility that may be obtained from drift experiments.

The architecture of organic FETs is usually that of the thin-film transistor (TFT) (see Fig. 1.5), first introduced by Weimer in 1962 [60] and

currently used in most amorphous silicon transistors [61]. In the off-state, the current is determined by the intrinsic conductivity of the semiconductor. As a result, low off currents require a low-conductivity material. For this reason, undoped organic semiconductors must be used [62]. When all the elements of the organic FET are made out of conducting, insulating, and semiconducting polymers, the device is flexible [63], which opens up interesting perspectives for applications (see Fig. 1.6).

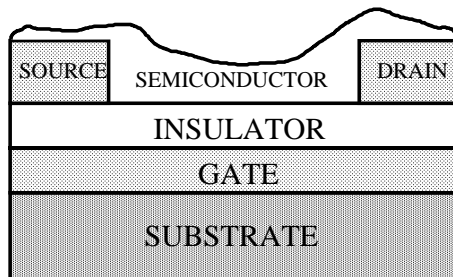


Figure 1.5: *Architecture of an organic TFT. The organic semiconductor is deposited on a patterned substrate by spin-coating or by vacuum deposition. Under an applied gate bias, charge is accumulated in the semiconductor and a current may flow from the source to the drain.*

A prominent feature shared by amorphous silicon TFTs and organic FETs is that the field-effect mobility is gate bias dependent. In amorphous silicon, this can be understood in terms of the density of localized levels that act as traps for charge carriers in the delocalized bands. At low gate bias, nearly all induced charges go to the localized levels, where their mobility is very low. With an increase of the gate voltage, the Fermi level approaches the delocalized band since more traps are filled, which leads to an increase of the concentration of mobile carriers in the delocalized levels. As a result, the effective mobility increases. Such a multiple trapping and release transport model has been applied by Horowitz *et al.* [64, 65] to rationalize the characteristics of organic FETs based on thiophene oligomers. The differences in the characteristics of FETs with different organic semiconducting layers were attributed to differences in the trap distribution.

In organic semiconductors the transport bands are very narrow and easily disrupted by disorder. Therefore, especially in amorphous organic transistors, band transport is not expected to play an important role. In Chapter 2, the characteristics of amorphous organic transistors are described



Figure 1.6: *Integrated circuits built out of all-polymer transistors still operate when the foils are sharply bent, making them ideally suited for integration as electronic identification tag or antitheft sticker into product wrappings for soft packages. (Source: “New plastic circuits are flexible enough to be folded in half”, Philips Research Press release 97005e/ 8 December 1997)*

using a transport model of hopping between localized states, rather than trapping and release to delocalized bands. In this model, the energetic disorder of the system is described by a density of localized states. We assume that the tail of this DOS is well described by an exponential distribution (the conventional choice for amorphous silicon; a crude approximation to the Gaussian DOS often used to characterize organic systems). The information about the structure of the semiconducting layer is contained in the effective overlap of the electronic wave functions of neighboring molecules. This overlap depends strongly on the relative positions and orientations of the molecules and is thus a measure of the structural packing of the molecules.

Using the resistor network method and percolation theory, we obtain an analytic expression for the field-effect mobility. This model is applied to describe the experimental data by Brown *et al.* [66] on FETs based on amorphous semiconducting films of small organic molecules (pentacene) and of the conjugated polymer polythiethylene vinylene. The field-effect mobility in the conjugated polymer-based transistor is orders of magnitude lower and

much more strongly temperature dependent than in the pentacene-based transistor. From comparison with our model, we find that these differences can not be attributed to differences in the density of localized states, like in the multiple-trapping model. The main difference lies in the effective overlap, which is larger in the pentacene semiconductor. Apparently, the stacking of the small pentacene molecules is better than that of the conjugated polymer chains. This seems plausible in view of the lower amount of steric hindrance in a system with small molecules. The effect of structure is not taken into account in the multiple trapping models, where transport is due to direct activation to a delocalized level, without involving a tunneling step. From our model, we conclude that structural order is the key parameter for improving the transport characteristics of organic FETs.

Dispersive hole transport in polymer LEDs

Chapter 3 reports on measurements of the switching characteristics of PPV-based LEDs, performed by P.W.M. Blom at Philips Research. Due to the unbalanced transport of electrons and holes through the polymer layer, the response time of a polymer LED is determined by the time the holes take to reach the opposite electrode. An analysis of these response times reveals that they do not correspond with the times expected on the basis of the hole mobility, as measured from the stationary J - V characteristics. Furthermore, the transit times are found to scale superlinearly with the PPV layer thickness. This indicates dispersive transport, i.e., that the spread in the distribution of transit times dominates over the average value. The occurrence of dispersive transport is a commonly observed feature of disordered semiconductors and it provides information about the nature of the disorder encountered by the carriers.

Applying the continuous-time random walk formalism we found that the observed transit times follow the universal Scher-Montroll scaling law as a function of electric field strength and layer thickness. An interesting result is that the dispersion parameter is independent of the temperature. When the distribution in transit times originates from a distribution in trap depths, like in the case of multiple trapping transport, the dispersion parameter is strongly temperature dependent. In a hopping system, the variation in tunneling probabilities, due to structural disorder, gives rise to a temperature independent contribution to the dispersion. Apparently, this contribution is the dominant one in our PPV. This leads to the following microscopic picture for hole transport through PPV: While traversing the material, holes get trapped in clusters of sites with relatively good electronic

overlap. The holes bounce forward and backward in this isolated cluster for a period of time, until they escape.

Field-dependent hole mobility in disordered organic semiconductors

The observation of a field and temperature dependent hole mobility in PPV-based LEDs of the empirical form (1.3) establishes the relation of the conjugated polymer PPV with the other members of the class of disordered organic semiconductors, like molecularly doped polymers and low molecular weight organic glasses. The field dependence of this mobility resembles that of the Poole-Frenkel law, which describes the escape of a charge carrier from a charged trap into a delocalized transport band. However, the magnitude of the factor B and the temperature dependence deviate from the prediction of Poole-Frenkel theory. Furthermore, the ubiquitous occurrence of this mobility with about the same parameter values, independent of chemical composition, excludes the dominance of impurity effects: It is highly unlikely that chemically different systems contain the same amount of charged traps at the same depth relatively to the transport level.

Instead, this mobility must reflect an intrinsic transport property. In disordered molecular systems, the elementary transport step is the transfer of a charge carrier among adjacent sites in the material, which can either be single molecules or segments of a conjugated polymer that are separated by defects. Due to statistical variation in the environment, the distribution of the electronic states of these molecular sites is inhomogeneously broadened. To study the hopping of carriers in a system with energetic disorder, Bäessler and co-workers have performed numerous Monte Carlo simulations [26]. Based on the information obtained from optical spectra, a Gaussian form was chosen for the density of localized states, with a width of about 0.1 eV. The transition rates were assumed to be of the Miller-Abrahams type (1.1). Indeed, these Monte Carlo simulations reproduced the ubiquitous field dependence of the carrier mobility at high electric fields (see Fig. 1.7).

The introduction of structural disorder to the system (via a distribution of overlap parameters γ) has been found to increase the prefactor μ_0 , but lower the value of T_0 [26]. The increase in μ_0 is related to the creation of easy “percolating” paths through the system, with relatively high electronic overlap between the molecular sites. These easy paths are not straight, but contain detours with hops that are against the field direction. Hence the increase of the mobility with field is weakened, as is expressed in the lower

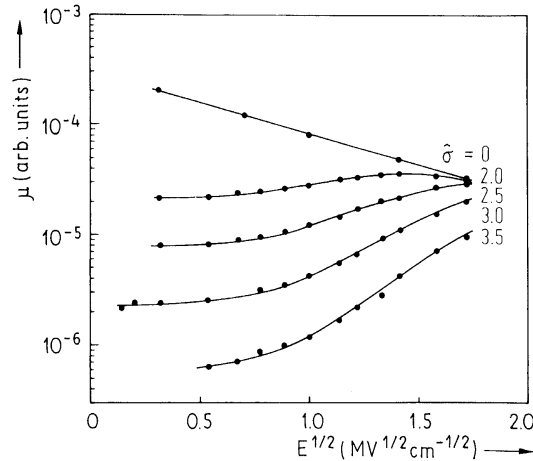


Figure 1.7: *Simulated dependence of the carrier mobility μ on the square root of the electric field E in a regular array of hopping sites with a Gaussian distribution of site energies. The parameter $\hat{\sigma}$ denotes the width of the Gaussian distribution divided by $k_B T$. Figure is taken from Ref. [26].*

value of T_0 . The simulation results further indicate that the functional form of the mobility (1.3), as well as the parameter values of Δ and B , are hardly influenced by structural disorder.

While providing a universal explanation for the observed carrier mobility in terms of energetic and structural disorder, the $\ln \mu \propto \sqrt{E}$ law is reproduced only in a narrow range of extremely high fields, $> 10^8$ V/m for typical values of the disorder parameters (see Fig. 1.7). In contrast, the experimental data exhibit this behavior starting at fields of the order of 10^6 V/m. Numerical simulations of systems with spatially correlated site energies exhibit a stretched exponential field dependence down to these low fields [67]. Analytical studies of hopping in a system with correlated energy disorder show that the empirical form (1.3) of the mobility may be attributed to correlations that arise from charge-dipole interactions, whereas other sources of energetic disorder, like van der Waals interactions or variations in conjugation length, give rise to a different form [68]. The experimental observation of the mobility (1.3) in materials without strong permanent dipoles, like for example in our PPV [39], indicates that either (i) the ubiquitously observed mobility is due to another microscopic mechanism that is not material specific, or (ii) there are other mechanisms

besides dipolar correlations that fortuitously give rise to a similar carrier mobility. In either case, an alternative mechanism must be operative in PPV and in other weakly dipolar systems.

In Chapter 4 we examine such an alternative mechanism, based on the microscopic picture of carriers getting trapped in the inhomogeneous structure (see Chapter 3). We construct an analytical model of a system that consists of relatively ordered high-mobility regions, that are connected by one-dimensional conduction paths through a low-mobility region. Calculating the ensemble average of the mobility in this system (assuming uncorrelated Gaussian energy disorder), the empirical law (1.3) is reproduced for the experimentally observed field range.

Exciton migration in disordered organic semiconductors

As discussed in previous Sections, the static and dynamic optical properties of disordered organic semiconductors, including conjugated polymers, can be explained by the spectral relaxation associated with the incoherent hopping motion of excitons. Information about the dynamics of excitons can be obtained from photoluminescence experiments, where, following excitation by light, the emitted photons may be monitored as a function of excitation energy, emission energy, or time.

In Chapter 5, we derive a Green function solution for neutral particles hopping in a disordered system at zero temperature. The following processes are taken into account (see Fig. 1.8). Photo-absorption leads to the creation of an exciton on a site (chromophore). Due to the disorder the exciton energy differs from site to site. This enables the exciton to relax in energy in the course of a random walk between sites. Finally, the exciton decays by emitting a photon or by a nonradiative process. The migration of the excitons leads to a red-shift between the absorption and emission spectrum. The dependence of this so-called Stokes shift on time and on excitation energy is discussed in Chapter 5 and illustrated by experimental results on conjugated polymers.

Exciton dissociation in disordered organic semiconductors

The concept of an exciton implies that optical generation of charge carriers is a secondary process resulting from the breaking of excitons into electrons and holes, instead of a direct transition between valence and conduction bands. In molecular systems, the dissociation of excitons requires a charge transfer step between neighboring molecules, which may be assisted by an

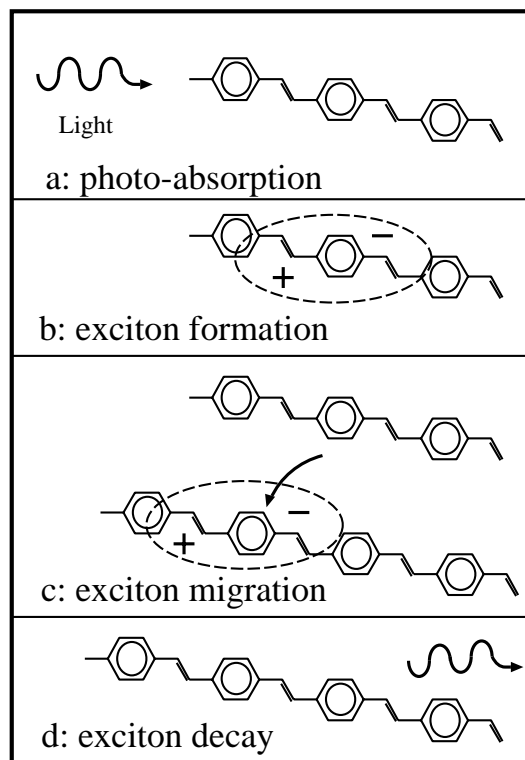


Figure 1.8: *Schematic representation of the exciton dynamics in a disordered molecular solid. The picture shows a segment of the conjugated polymer poly(-p-phenylene vinylene). a) A photon is absorbed by the molecule. b) An exciton, i.e. a bound electron-hole pair, is created on the molecule. c) The exciton migrates towards molecules with a lower exciton energy. d) The exciton recombines and a photon is emitted.*

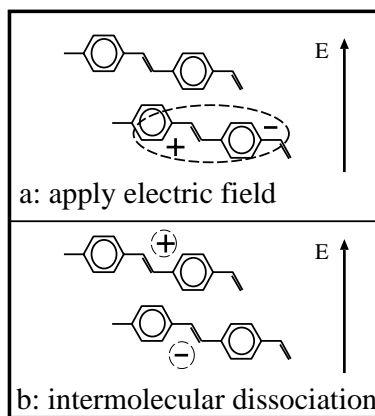


Figure 1.9: Under influence of an applied electric field, it may be energetically favorable for an exciton (a) to transfer one of its charge carriers to a neighboring molecule (b).

applied electric field (see Fig. 1.9). While this dissociation process must be optimized in, e.g., photoreceptors and solar cells, it is detrimental to the operation of organic LEDs, where the electron-hole pairs must recombine to form an exciton, instead of the other way around.

Besides being of practical relevance, the study of carrier generation processes provides fundamental information about the nature and dynamics of excited states and charge carriers in organic semiconductors. To address the ongoing discussion about the appropriate model to describe conjugated polymers (disordered molecular material or one-dimensional band semiconductor), complementary experimental studies of electric field-induced photoluminescence quenching have been performed by Bäessler and his group [32, 33, 69]. In these studies, blends were used of either the conjugated polymer poly(*p*-phenyl phenylene vinylene) (PPPV) or the small molecule tris(stilbene)amine (TSA) in an inert polymer host. The molecule TSA may be considered as one of the smallest members of the oligomer family that is related to the backbone structure of PPV type polymers, thus allowing for a direct comparison with the PPPV results. From the overall qualitative similarities in spectral, field, concentration, and matrix dependence as well as the ultrafast transient behavior, it was concluded that the appropriate model for the conjugated polymer PPPV is indeed that of a disordered molecular system, rather than a one-dimensional semiconductor. There were also some differences, most notably in the dependence of the photoluminescence quenching on the concentration of active material in the

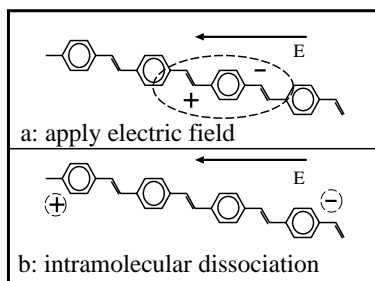


Figure 1.10: *Under influence of an applied electric field, it may be energetically favorable for an exciton (a) to dissociate along the polymer chain into a separate hole and electron (b).*

host matrix. It was speculated that these differences may be attributed to the occurrence of intrachain dissociation in the conjugated polymer, which, unlike intermolecular dissociation (Fig. 1.9), does not depend on the concentration of polymer chains. Such an intrachain dissociation mechanism is depicted in Fig. 1.10. However, the interpretation of the experimental results is not straightforward due to the interplay of several competing processes, i.e., the generation, migration, dissociation, and radiative and nonradiative decay of excitons.

In Chapters 6 and 7, we theoretically describe these complementary electric-field induced photoluminescence quenching experiments. To this end, we combine the theory of exciton migration and decay in a disordered molecular system [Chapter 5] with an exciton dissociation mechanism. In Chapter 6, we describe the experiments on the conjugated polymer PPPV. We find that good agreement can only be obtained with a completely concentration-independent dissociation mechanism. This strongly indicates that the intrachain dissociation mechanism (Fig. 1.10) is the dominant one in the conjugated polymer system. To obtain a complete picture, we model the experiments on the small molecule TSA in Chapter 7. Since intramolecular dissociation in these small molecules can be excluded *a priori*, a microscopic model of intermolecular exciton dissociation is employed here. Good agreement is obtained using the same set of migration and decay parameters as in the PPPV system. Thus we have provided a consistent picture of electric field-induced photoluminescence quenching in molecularly doped polymers as well as conjugated polymer blends.

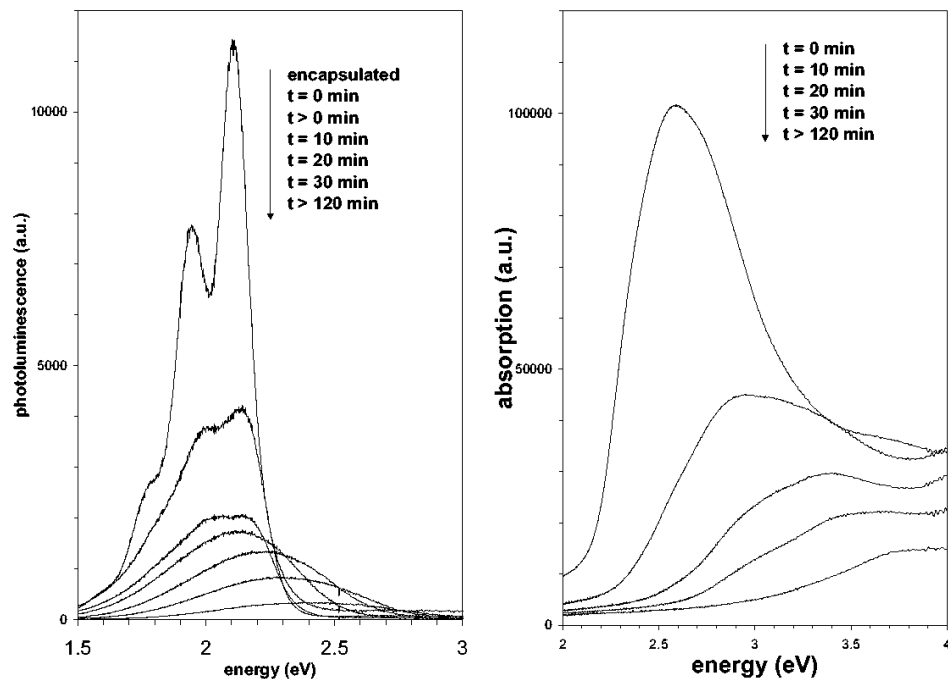


Figure 1.11: Photoluminescence spectra (left) and absorption spectra (right) of PPV during bleaching with a xenon lamp. Data provided by A.J.M. Berntsen, Philips Research.

Photochemical bleaching in disordered organic semiconductors

It is common experience that colors tend to fade when exposed to light. Each time an organic dye molecule absorbs a photon, there is a finite probability that this event causes the degradation of the molecule such that the optical activity is lost. This process poses a fundamental limit to the lifetime of optical devices based on organic materials, such as organic dye lasers, solar cells, and specifically light-emitting diodes. To investigate the degradation by light of the conjugated polymer PPV, bleaching experiments on films of PPV have been performed by A.J.M. Berntsen and R.H. Cuijpers at Philips Research. Under intense illumination by a xenon lamp, the optical absorption of the PPV film not only reduces in intensity with time, but also shifts to the blue with time (see Fig. 1.11). The photoluminescence spectrum of the PPV shows a decrease and a blue shift as well. In particular the initial decrease in photoluminescence intensity is much faster than

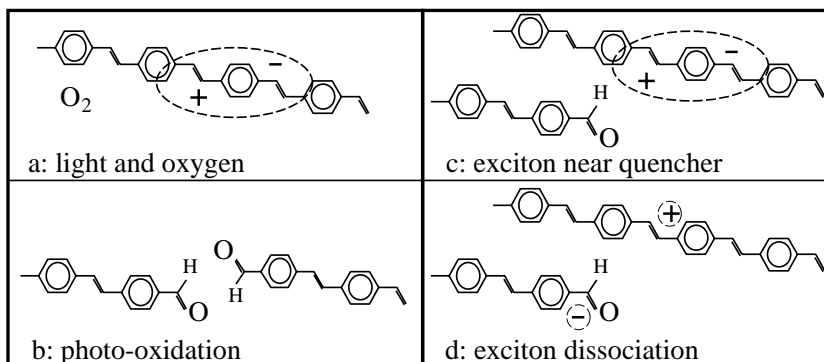


Figure 1.12: *The bleaching of the polymer PPV due to photooxidation encompasses the following processes: (a) the exciton energy can be transferred to an oxygen molecule after which (b) the excited oxygen reacts with the vinyl bond in the PPV backbone, resulting in the creation of two carbonyl groups. The presence of carbonyl groups suppresses the photoluminescence since, due to the high electron affinity of these groups, an exciton close to a carbonyl group (c) is liable to dissociate into separate charge carriers (d).*

the decrease in absorption. To illustrate this initial decrease more clearly, three different initial photoluminescence spectra are shown in Fig. 1.11, the first showing the spectrum of an encapsulated polymer layer that has not degraded at all, the second the spectrum of the unprotected polymer just before switching on the xenon lamp, the third showing the spectrum immediately after switching on the xenon lamp. This decline in the initial photoluminescence intensity implies a sharp drop in the photoluminescence efficiency upon bleaching. At longer bleaching times, a broadening of the photoluminescence spectrum is observed.

The stronger bleaching of the low-energy tail of the PPV absorption spectrum can be explained by the relaxation of excitons to polymer chain segments at a lower energy, where subsequently a degradation reaction is triggered by the presence of the exciton. The sensitivity of polymer bleaching to the presence of oxygen suggests that photo-oxidation is an important degradation mechanism. This mechanism is depicted in Fig. 1.12 a and b. In Chapter 8 we describe the bleaching of a disordered organic system by combining our theory of exciton migration and decay with such a degrada-

tion mechanism.

The strong decrease in photoluminescence efficiency upon bleaching indicates that the bleached segments of the polymer act as quenching centers for excitons. It has been suggested that the reaction products of photooxidation, i.e., carbonyl groups, induce a charge transfer reaction of excitons on neighboring chain segments, thus quenching the luminescence (see Fig. 1.12 c and d). We take this process of defect quenching into account in Chapter 8. The evolution of both the absorption and the photoluminescence spectrum as a function of the bleaching time then follows from the interplay of exciton migration, exciton decay, polymer degradation, and exciton quenching at defects.

References

- [1] K. C. Kao and W. Hwang, *Electrical Transport in Solids, with Particular Reference to Organic Semiconductors* (Pergamon, Oxford, 1981); M. Pope and C. E. Swenberg, *Electronic Processes in Organic Crystals* (Clarendon, Oxford, 1982).
- [2] O. H. Le Blanc, *J. Chem. Phys.* **33**, 626 (1960).
- [3] K. G. Kepler, *Phys. Rev.* **199**, 1226 (1960).
- [4] M. Pope, H. P. Kallmann, and P. Magnante, *J. Chem. Phys.* **38**, 2042 (1963).
- [5] For a review, see D. M. Pai and B. E. Springett, *Rev. Mod. Phys.* **65**, 163 (1993).
- [6] C. K. Chiang, C. R. Fincher, Jr., Y. W. Park, A. J. Heeger, H. Shirakawa, E. J. Louis, S. C. Gau, and A. G. MacDiarmid, *Phys. Rev. Lett.* **39**, 1098 (1977).
- [7] R. S. Kohlman, J. Joo, and A. J. Epstein, in *Physical Properties of Polymers Handbook*, edited by J. E. Mark (AIP Press, Woodbury, NY, 1996) p. 453.
- [8] For a review, see A. J. Epstein and Y. Yang (eds.), *MRS Bull.* **22**, No. 6 (1997).
- [9] C. W. Tang and S. A. VanSlyke, *Appl. Phys. Lett.* **51**, 913 (1987).
- [10] H. Koezuka, A. Tsumura, Y. Ando, *Synth. Met.* **18**, 699 (1987); A. Tsumura, H. Koezuka, and Y. Ando, *Synth. Met.* **25**, 11 (1988).
- [11] G. Horowitz, D. Fichou, X. Z. Peng, Z. Xu, and F. Garnier, *Solid State Commun.* **72**, 381 (1989); F. Garnier, G. Horowitz, X. Z. Peng, and D. Fichou, *Adv. Mater.* **2**, 592 (1990).

- [12] J. H. Burroughes, D. D. C. Bradley, A. R. Brown, R. N. Marks, K. MacKay, R. H. Friend, P. L. Burn, and A. B. Holmes, *Nature (London)* **347**, 539 (1990).
- [13] N. W. Ashcroft and N. D. Mermin, *Solid State Physics* (Saunders, Philadelphia, 1976).
- [14] E. M. Conwell, *Phys. Rev.* **103**, 51 (1956).
- [15] N. F. Mott, *Canadian J. Phys.* **34**, 1356 (1956).
- [16] N. F. Mott and E. A. Davis, *Electronic Processes in Noncrystalline Materials* (Clarendon, Oxford, 1971).
- [17] A. Miller and E. Abrahams, *Phys. Rev.* **120**, 745 (1960).
- [18] H. Böttger and V. V. Bryksin, *Hopping Conduction in Solids* (Akademie-Verlag, Berlin, 1985).
- [19] B. I. Shklovskii and A. L. Efros, *Electronic Properties of Doped Semiconductors* (Springer-Verlag, Berlin, 1984).
- [20] J. Mort and D. M. Pai (eds.), *Photoconductivity and Related Phenomena* (Elsevier, Amsterdam, 1976).
- [21] D. M. Pai, *J. Chem. Phys.* **52**, 2285 (1970).
- [22] W. D. Gill, *J. Appl. Phys.* **43**, 5033 (1972).
- [23] L. B. Schein, A. Peled, and D. Glatz, *J. Appl. Phys.* **66**, 686 (1989).
- [24] P. M. Borsenberger, *J. Appl. Phys.* **68**, 6263 (1990).
- [25] M. A. Abkowitz, *Phil. Mag. B* **65**, 817 (1992).
- [26] For a review, see H. Bässler, *Phys. Status Solidi B* **175**, 15 (1993).
- [27] For a review, see A. J. Heeger, S. Kivelson, J. R. Schrieffer, and W. P. Su, *Rev. Mod. Phys.* **60**, 781 (1988).
- [28] C. H. Lee, G. Yu, and A. J. Heeger, *Phys. Rev. B* **47**, 15543 (1993).
- [29] H. Bässler, V. Brandl, M. Deussen, E. O. Göbel, R. Kersting, H. Kurz, U. Lemmer, R. F. Mahrt, and A. Ochse, *Pure Appl. Chem.* **67**, 377 (1995).

- [30] U. Rauscher, H. Bässler, D. D. C. Bradley, and M. Hennecke, Phys. Rev. B **42**, 9830 (1990).
- [31] R. Kersting, U. Lemmer, R. F. Mahrt, K. Leo, H. Kurz, H. Bässler, and E. O. Göbel, Phys. Rev. Lett. **70**, 3820 (1993).
- [32] R. Kersting, U. Lemmer, M. Deussen, H. J. Bakker, R. F. Mahrt, H. Kurz, V. I. Arkhipov, H. Bässler, and E. O. Göbel, Phys. Rev. Lett. **73**, 1440 (1994).
- [33] M. Deussen, M. Scheidler, and H. Bässler, Synth. Met. **73**, 123 (1995).
- [34] S. Barth and H. Bässler, Phys. Rev. Lett. **79**, 4445 (1997).
- [35] N. S. Sariciftci (ed.), *Primary Photoexcitations in Conjugated Polymers: Molecular Exciton versus Semiconductor Band Model* (World Scientific, Singapore, 1997).
- [36] J. Joo, S. M. Long, J. P. Pouget, E. J. Oh, A. G. MacDiarmid, and A. J. Epstein, Phys. Rev. B **57**, 9567 (1998).
- [37] D. Braun and A. J. Heeger, Appl. Phys. Lett. **58**, 1982 (1991).
- [38] P. W. M. Blom, M. J. M. de Jong, and J. J. M. Vlegaar, Appl. Phys. Lett. **68**, 3308 (1996).
- [39] P. W. M. Blom, M. J. M. de Jong, and M. G. van Munster, Phys. Rev. B **55**, R656 (1997).
- [40] P. W. M. Blom, M. J. M. de Jong, and S. Breedijk, Appl. Phys. Lett. **71**, 930 (1997).
- [41] P. W. M. Blom and M. J. M. de Jong, IEEE J. Selected Topics Quantum Electron. **4**, 105 (1998).
- [42] M. A. Lampert and P. Mark, *Current Injection in Solids* (Academic, New York, 1970).
- [43] R. N. Marks and D. D. C. Bradley, Synth. Met. **57**, 4128 (1993).
- [44] I. D. Parker, J. Appl. Phys. **75**, 1656 (1994).
- [45] P. Langevin, Ann. Chim. Phys. **28**, 433 (1903).
- [46] U. Albrecht and H. Bässler, Phys. Status Solidi B **191**, 455 (1995).

- [47] S. Kirkpatrick, *Rev. Mod. Phys.* **45**, 574 (1973).
- [48] V. Ambegaokar, B. I. Halperin, and J. S. Langer, *Phys. Rev. B* **4**, 2612 (1971).
- [49] H. Scher and M. Lax, *Phys. Rev. B* **7**, 4491 (1973); **7** 4502 (1973); H. Scher and E. W. Montroll, *Phys. Rev. B* **12**, 2455 (1975).
- [50] B. Movaghar and W. Schirmacher, *J. Phys. C* **14**, 859 (1981); D. Bourbie, *Phil. Mag. B* **73**, 201 (1996).
- [51] O. Bleibaum, H. Böttger, and V. V. Bryksin, *Phys. Rev. B* **54**, 5444 (1996).
- [52] S. R. Broadbent and J. M. Hammersley, *Proc. Camb. Phil. Soc.* **53**, 629 (1957).
- [53] G. Pfister and H. Scher, *Adv. Phys.* **27**, 747 (1978).
- [54] M. Grünwald, B. Pohlmann, B. Movaghar, and D. Würtz, *Phil. Mag. B* **49**, 341 (1984).
- [55] P. E. Parris and B. D. Bookout, *Phys. Rev. B* **53**, 629 (1996).
- [56] B. Movaghar, B. Ries, and M. Grünwald, *Phys. Rev. B* **34**, 5574 (1986).
- [57] M. Grünwald and B. Movaghar, *J. Phys. Condens. Matter* **1**, 2521 (1989).
- [58] J. E. Lilienfeld, US Patent 1745175 (1930).
- [59] S. M. Sze, *Physics of Semiconductor Devices* (Wiley, New York, 1981).
- [60] P. K. Weimer, *Proc. IRE* **50**, 1462 (1962).
- [61] C. van Berkel, in *Amorphous & Microcrystalline Semiconductor Devices: Materials and Device Physics*, edited by J. Kanicki (Artech House, Boston, 1992).
- [62] A. R. Brown, D. M. de Leeuw, E. E. Havinga, and A. Pomp, *Synth. Met.* **68**, 65 (1994).
- [63] C. J. Drury, C. M. J. Mutsaers, C. M. Hart, M. Matters, and D. M. de Leeuw, *Appl. Phys. Lett.* **73**, 108 (1998).

-
- [64] G. Horowitz and P. Delannoy, *J. Appl. Phys.* **70**, 469 (1991).
- [65] G. Horowitz, R. Hajlaoui, and P. Delannoy, *J. Phys. III (Paris)* **5**, 355 (1995).
- [66] A. R. Brown, C. P. Jarrett, D. M. de Leeuw, and M. Matters, *Synth. Met.* **88**, 37 (1997).
- [67] Yu. N. Gartstein and E. M. Conwell, *Chem. Phys. Lett.* **245**, 351 (1995).
- [68] D. H. Dunlap, P. E. Parris, and V. M. Kenkre, *Phys. Rev. Lett.* **77**, 542 (1996).
- [69] M. Deussen, P. Haring Bolivar, G. Wegmann, H. Kurz, and H. Bässler, *Chem. Phys.* **207**, 147 (1996).

Chapter 2

Field-effect mobility of amorphous organic transistors

2.1 Introduction

Over the last decade the use of organic *p*-type semiconductors in field-effect transistors has gained considerable interest due to their potential application in low-cost integrated circuits. Most effort has been put into increasing the hole mobility of the semiconductor and increasing the on-off ratio of the field-effect transistor by optimising existing materials and by applying new materials. Mobilities as high as $0.7 \text{ cm}^2\text{V}^{-1}\text{s}^{-1}$ and on-off ratios of 10^8 have recently been reported in thin-film transistors of evaporated pentacene [1]. Furthermore, attention has been focused on the improvement of the processability of these materials by using directly soluble [2] or precursor organic semiconductors [3]. Besides the technical applicability of organic semiconductors, their electronic and structural properties have been the subject of investigation as well. Interesting questions like the connection between molecular order and hole mobility in conjugated oligomers and polymers have been addressed [1, 4–6].

Experiments have indicated that the field-effect mobility of holes in organic transistors depends on the temperature as well as on the applied gate bias [3, 7]. This has been described by Horowitz *et al.* using a multiple trapping and release model [7]. In this model the assumption is made that most of the charge carriers are trapped in localized states. Then the amount of (temporarily) released charge carriers to an extended-state trans-

port level (the valence band for classical p -type semiconductors) depends on the energy level of the localized states, the temperature, and the gate voltage. However, while extended-state transport may occur in highly ordered vacuum-evaporated molecular films [7], we do not expect it to play a role in amorphous organic films [3], where the charge carriers are strongly localized.

In this Chapter, we derive a theory for the field-effect mobility in amorphous organic transistors, where the charge transport is governed by hopping, i.e., the thermally activated tunneling of carriers between localized states, rather than by the activation of carriers to an extended state. We use the concept of variable range hopping (VRH), i.e. a carrier may either hop over a small distance with a high activation energy or hop over a long distance with a low activation energy. The temperature dependence of the carrier transport in such a system is strongly dependent on the density of localized states. In a field-effect transistor, an applied gate voltage gives rise to the accumulation of charge in the region of the semiconducting layer that is close to the insulator. As these accumulated charge carriers fill the lower-lying states of the organic semiconductor, any additional charges in the accumulation layer will occupy states at relatively high energies. Consequently, these additional charges will—on average—require less activation energy to hop away to a neighboring site. This results in a higher mobility with increasing gate voltage.

This Chapter is organized as follows. First, we study the influence of temperature and the influence of the filling of states on the conductivity of a VRH system with an exponential distribution of localized-state energies. Using percolation theory, we find an analytic expression for the conductivity. This expression is then used to derive the field-effect mobility of the carriers when the material is applied in a transistor. Finally, our result is used to interpret the experimentally observed temperature and gate-voltage dependence of the field-effect mobility in both a pentacene and a polythiethylene vinylene (PTV) organic thin-film transistor [3].

2.2 The hopping conductivity

Let us first derive an expression for the conductivity as a function of temperature T and charge carrier density. At low carrier densities and low T , the transport properties are determined by the tail of the density of (localized) states (DOS). Our model is based on the following exponential

DOS,

$$g(\epsilon) = \frac{N_t}{k_B T_0} \exp\left(\frac{\epsilon}{k_B T_0}\right), \quad (-\infty < \epsilon \leq 0) \quad (2.1)$$

where N_t is the number of states per unit volume, k_B is Boltzmann's constant, and T_0 is a parameter that indicates the width of the exponential distribution. We take $g(\epsilon) = 0$ for positive values of ϵ . We do not expect the results to be qualitatively different for a different choice of $g(\epsilon)$, as long as $g(\epsilon)$ increases strongly with ϵ .

Let the system be filled with charge carriers, such that a fraction $\delta \in [0, 1]$ of the localized states is occupied by a carrier, i.e. such that the density of charge carriers is δN_t . In equilibrium, the energy distribution of the carriers is given by the Fermi-Dirac distribution $f(\epsilon, \epsilon_F)$, where ϵ_F is the Fermi energy (or chemical potential). For a given carrier occupation δ , the position of the Fermi energy ϵ_F is fixed by the condition

$$\begin{aligned} \delta &= \frac{1}{N_t} \int d\epsilon g(\epsilon) f(\epsilon, \epsilon_F) \\ &\simeq \exp\left(\frac{\epsilon_F}{k_B T_0}\right) \Gamma(1 - T/T_0) \Gamma(1 + T/T_0), \end{aligned} \quad (2.2)$$

where $\Gamma(z) \equiv \int_0^\infty dy \exp(-y) y^{z-1}$. In Eq. (2.2), we have used the assumption that most carriers occupy the sites with energies $\epsilon \ll 0$, i.e., $-\epsilon_F \gg k_B T_0$. This condition is fulfilled when δ and T are low. Note that at $T = 0$ the gamma functions are unity and the carrier density is given by the density of states with energies lower than ϵ_F . Our approximate expression (2.2) breaks down at temperatures $T \geq T_0$, where $\Gamma(1 - T/T_0)$ diverges. At such temperatures our assumption that only the tail of the DOS is important no longer holds, as the majority of the carriers is located close to $\epsilon = 0$.

The transport of carriers is governed by the hopping of carriers between localized states, which is strongly dependent on the hopping distances as well as the energy distribution of the states. At low bias, the system can be described as a resistor network [8, 9]. In this case, one can assign a conductance $G_{ij} = G_0 e^{-s_{ij}}$ between site i and site j where

$$s_{ij} = 2\alpha R_{ij} + \frac{|\epsilon_i - \epsilon_F| + |\epsilon_j - \epsilon_F| + |\epsilon_i - \epsilon_j|}{2k_B T}. \quad (2.3)$$

Here, the first term on the right-hand-side describes the tunneling process, which depends on the overlap of electronic wave functions of the sites i and j . In a lowest-order approximation, this tunneling process may be

characterized by the distance R_{ij} between the sites and an effective overlap parameter α . The second term in Eq. (2.3) takes into account the activation energy for a hop upwards in energy and the occupational probabilities of the sites i and j .

According to percolation theory [9, 10], the conductivity of the system is given by

$$\sigma = \sigma_0 e^{-s_c}, \quad (2.4)$$

where σ_0 is an (unknown) prefactor and s_c is the exponent of the critical percolation conductance $G_c = G_0 e^{-s_c}$. This G_c is determined as follows. Take a reference conductance G and remove all conductances with $G_{ij} < G$. For high G , the remaining conductances form isolated clusters. These clusters increase in size with decreasing G . The critical percolation conductance G_c is defined as the value of G at which the first infinite cluster is formed. This G_c determines the conductivity (2.4), since it is the most difficult step required for transport through a macroscopic system. The onset of percolation, i.e., the occurrence of the first infinite cluster, is usually determined by calculating the average number of bonds (conductances with $G_{ij} > G$) per site in the largest cluster. This number of bonds B increases with decreasing G , until, at the onset of percolation, a critical number B_c is reached. For a three-dimensional amorphous system, this number is given by $B_c \simeq 2.8$ [10, 11]. The percolation criterion $B(G = G_c) = B_c$ can be written as

$$B_c = \frac{N_b}{N_s}, \quad (2.5)$$

where N_b is the density of bonds and N_s is the density of sites in the percolating system. The density of bonds is given by

$$N_b = \int d\mathbf{R}_{ij} d\epsilon_i d\epsilon_j g(\epsilon_i) g(\epsilon_j) \theta(s_c - s_{ij}), \quad (2.6)$$

where the step function $\theta(s_c - s_{ij})$ excludes all pairs of sites i, j with $s_c < s_{ij}$, or $G_{ij} < G_c$. The density of sites N_s can be estimated by excluding all sites that cannot possibly belong to an infinite cluster [12]

$$N_s = \int d\epsilon g(\epsilon) \theta(s_c k_B T - |\epsilon - \epsilon_F|). \quad (2.7)$$

Substituting Eqs. (2.1) and (2.3) into Eqs. (2.5), (2.6), and (2.7), we obtain the percolation criterion for our system,

$$B_c \approx \pi \left(\frac{T_0}{2\alpha T} \right)^3 N_t \exp \left(\frac{\epsilon_F + s_c k_B T}{k_B T_0} \right), \quad (2.8)$$

where we have assumed that the site positions are random, that most of the hopping takes place between tail states ($-\epsilon_F \gg k_B T_0$), and that the maximum energy hop is large ($s_c k_B T \gg k_B T_0$). We note that our percolation criterion (2.8) is, up to a numerical factor, in agreement with previous results [13, 14] where somewhat different approaches have been used to describe VRH in an exponential band tail.

Combining Eqs. (2.2), (2.4) and (2.8), the expression for the conductivity as a function of the occupation δ and the temperature T is obtained,

$$\sigma(\delta, T) = \sigma_0 \left(\frac{\pi N_t \delta (T_0/T)^3}{(2\alpha)^3 B_c \Gamma(1 - T/T_0) \Gamma(1 + T/T_0)} \right)^{T_0/T}. \quad (2.9)$$

Note that the conductivity has an Arrhenius-like temperature dependence $\sigma \sim \exp[-E_a/(k_B T)]$, with an activation energy E_a that is weakly (logarithmically) temperature dependent. This is in strong contrast with the well known Mott formula for VRH in a constant DOS, where the conductivity varies with temperature according to $\sigma \sim \exp[-(T_1/T)^{1/4}]$ [15]. The temperature dependence of the Mott formula is a consequence of hopping over far distances and hopping to high energies being equally important. In an exponential DOS, however, the characteristic hop is an activated jump, since there are much more available states at higher energies.¹ In fact, it has been shown that hopping in an exponential DOS can be effectively described in terms of activation from the Fermi energy to a specific transport energy [16].² This explains the Arrhenius behavior of Eq. (2.9).

In our expression (2.9), the conductivity increases superlinearly with the density of carriers ($\sigma \sim \delta^{T_0/T}$). This is due to the filling of localized states: an increase in the carrier density gives rise to an increase in the average energy, thus facilitating an activated jump to the transport energy mentioned above. When the filling of states is not taken into account, i.e., when Boltzmann statistics instead of Fermi-Dirac statistics is used in Eq. (2.2), the conductivity is simply proportional to the density of carriers [13, 14].

¹At very low temperatures ($T \ll T_0$), the jumps to higher energies are suppressed and the carriers experience a density of states that is approximately constant. In this temperature regime, the balance between hopping to higher energies and hopping over far distances is restored and Mott's law is recovered. This transition from the Arrhenius-like temperature dependence to Mott's law is demonstrated in Sec. 2.5.

²The concept of activation to a transport energy is not unique for the exponential DOS, but applies to a whole class of distributions, as has been shown by S. D. Baranovskii *et al.* [17].

2.3 Transistor model

We now apply the obtained conductivity (2.9) to describe the field-effect mobility μ_{FE} in a transistor. In bulk material, the mobility μ of the charge carriers is given by $\mu = \sigma(\delta, T)/(e\delta N_t)$. In a transistor, however, the charge density is not uniform, but it decreases with the distance x from the semiconductor-insulator interface. According to Eq. (2.2), the occupation $\delta(x)$ depends on the distance x through the gate-induced potential $V(x)$,

$$\delta(x) = \delta_0 \exp\left(\frac{eV(x)}{k_{\text{B}}T_0}\right), \quad (2.10)$$

where δ_0 is the carrier occupation far from the semiconductor-insulator interface, where $V(x) = 0$. The variations of $V(x)$ and $\delta(x)$ with the distance x are determined by the Poisson equation. For the accumulation layer, where $\delta(x) \gg \delta_0$, the following relation between the electric field $F(x) = -dV(x)/dx$ and $\delta(x)$ can be obtained [7],

$$F^2(x) = 2k_{\text{B}}T_0N_t\delta(x)/\epsilon_{\text{s}}, \quad (2.11)$$

where ϵ_{s} is the dielectric constant of the semiconductor. The field $F(0)$ at the interface can be expressed in terms of the gate voltage V_{G} and the insulator capacitance per unit area C_{i} through Gauss' law,

$$F(0) = C_{\text{i}}V_{\text{G}}/\epsilon_{\text{s}}. \quad (2.12)$$

Substituting the distance-dependent charge occupation $\delta(x)$ into Eq. (2.9) for the conductivity, the source-drain current of the transistor in the linear regime ($-V_{\text{D}} < -V_{\text{G}}$) reads

$$I = \frac{WV_{\text{D}}}{L} \int_0^t dx \sigma[\delta(x), T]. \quad (2.13)$$

Here, V_{D} is the drain voltage (the source is the ground electrode) and L , W and t are the length, width, and thickness of the channel, respectively. The field-effect mobility then follows from the transconductance (see, e.g., Ref. [3])

$$\mu_{\text{FE}} \equiv \frac{L}{C_{\text{i}}WV_{\text{D}}} \frac{\partial I}{\partial V_{\text{G}}}. \quad (2.14)$$

From Eqs. (2.9)–(2.14) we obtain the following expression for the field-effect mobility,

$$\mu_{\text{FE}} = \frac{\sigma_0}{e} \left(\frac{\pi (T_0/T)^3}{(2\alpha)^3 B_c \Gamma(1 - T/T_0) \Gamma(1 + T/T_0)} \right)^{T_0/T} \quad (2.15)$$

$$\times \left[\frac{(C_i V_G)^2}{2k_B T_0 \epsilon_s} \right]^{T_0/T-1},$$

where we have assumed that the thickness t of the semiconductor layer is sufficiently large such that $V(t) = 0$. Then the field-effect mobility is independent of the thickness t as well as the bulk carrier occupation δ_0 . We note that the N_t dependence of the charge distribution in the accumulation layer is exactly cancelled by the N_t dependence of $\sigma(\delta, T)$.

Let us now apply our result (2.16) to the experimental data of Ref. [3], where the drain current I versus gate voltage V_G characteristics have been measured of both a pentacene and a polythiénylene vinylene (PTV) organic thin-film transistor at a range of temperatures. The precursors of both organic semiconductors are spin-coated from solution on a substrate consisting of a heavily n -doped silicon (common) gate electrode, a 200 nm thick SiO₂ insulating layer ($C_i = 17$ nFcm⁻²) and a patterned gold layer as the source and drain electrodes. The precursors are converted into the organic semiconductors using a process described in Ref. [3]. Typical channel widths and lengths were $W = 10$ -20 μ m and $L = 2$ -20 μ m respectively. The film thickness t varied from 30 to 50 nm. For both semiconductors, we use a relative dielectric constant $\epsilon_r = 3$, which is appropriate for most organic solids. In Fig. 2.1 the field-effect mobility in a pentacene and in a PTV thin-film transistor is plotted against the inverse temperature for different gate voltages. Experimentally, the field-effect mobilities are determined from Eq. (2.14) at $V_D = -2$ V. The theoretical curves (solid lines) follow from Eq. (2.16), where we have used σ_0 , α , and T_0 as fitting parameters. The agreement with experiment is quite good (the parameter values are given in Table 2.1). The temperature dependence of μ_{FE} , as shown

Table 2.1: *The pre-exponential factor to the conductivity σ_0 , the overlap parameter α^{-1} , and the width of the exponential distribution of localized states T_0 for both pentacene and polythiénylene vinylene (PTV) as obtained from the fit of Eq. (2.16) to the experimental data of Ref. [3], see Fig. 2.1.*

	σ_0 (10^6 S/m)	α^{-1} (Å)	T_0 (K)
pentacene	1.6	2.2	385
PTV	0.7	0.8	380

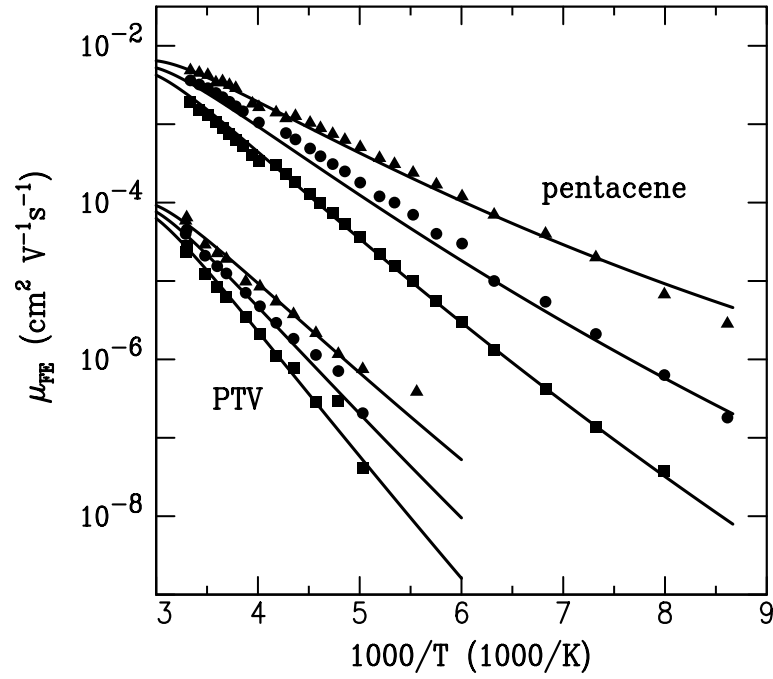


Figure 2.1: Field-effect mobility μ_{FE} in a pentacene and a polythienylene vinylene (PTV) thin-film transistor as a function of the temperature T for different gate voltages $V_G = -20 \text{ V}$ (triangles), -10 V (circles) and -5 V (squares). The experimental data (symbols) are taken from Ref. [3]. The solid lines are according to Eq. (2.16), using the parameters given in Table 2.1.

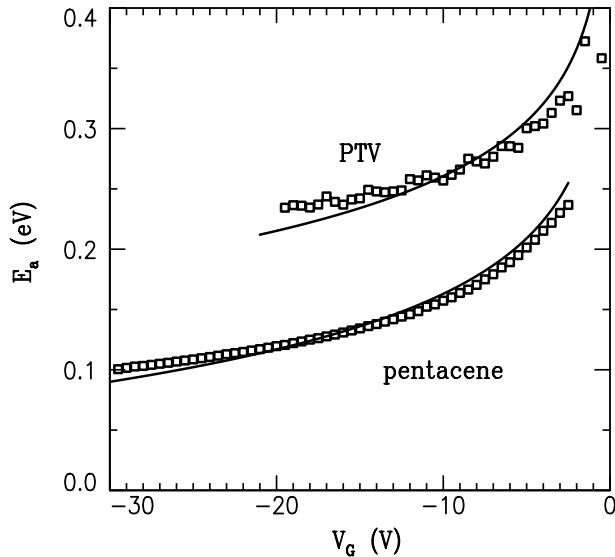


Figure 2.2: *Activation energy E_a for the field-effect mobility in a pentacene and a polythienylene vinylene (PTV) thin-film transistor as a function of the gate voltage V_G . The experimental data (squares) are taken from Ref. [3]. The solid lines are calculated from Eq. (2.16), using the parameters given in Table 2.1.*

in Fig. 2.1, follows a simple Arrhenius behavior $\mu_{\text{FE}} \sim \exp[-E_a/(k_{\text{B}}T)]$, where the activation energy E_a depends on V_G as plotted in Fig. 2.2. The decrease of E_a with increasing (negative) gate voltage is the direct result of accumulated charges filling the lower-lying states. As a result, any additional charge carriers in the system will occupy sites with—on average—a higher energy and less energy will be required for the activated jumps to neighboring sites.

2.4 Discussion

The field-effect mobility in PTV is more than two orders of magnitude lower than the field-effect mobility in pentacene. Furthermore, the activation energy for PTV is about twice the activation energy for pentacene. Surprisingly, these differences cannot be attributed to differences in the prefactor σ_0 nor to the width of the energy distribution T_0 , as these pa-

rameters have similar values for PTV as well as pentacene (see Table 2.1). The main difference between pentacene and PTV appears to be in the overlap parameter α , which determines the tunneling process between different sites. We note that this key parameter is absent in a multiple-trapping model, where the transport is governed by thermal activation from traps to a conduction band and subsequent retrapping, without involving a tunneling step. As the length scale α^{-1} is smaller than the size of a molecule, one must be cautious not to interpret α^{-1} simply as the decay length of the electronic wave function. The size and shape of the molecules and the morphology of the organic film are expected to have an important influence on the tunneling probability as well. The observed difference in α^{-1} may be due to the fact that there is more steric hindrance in the polymer PTV than in a system of small pentacene molecules. The better stacking properties of pentacene give rise to a larger area of overlap of the electronic wave functions, which results in a larger effective overlap α^{-1} in our model.

In conclusion, we have derived an analytic expression for the field-effect mobility in a thin-film transistor of an amorphous organic semiconductor, using percolation theory and the concept of hopping in an exponential density of localized states. The calculated temperature dependence and gate-voltage dependence agree well with those of the the observed field-effect mobility in both a pentacene and a PTV thin-film transistor. According to the theory, the differences in the magnitude and in the temperature dependence of the field-effect mobility of pentacene and PTV transistors are mainly due to differences in the structural order of the organic films.

2.5 Appendix

At very low temperatures, the assumption $s_c k_B T \gg k_B T_0$ [used in the derivation of the percolation criterion (2.8)] breaks down. Since the maximum energy hop $s_c k_B T$ becomes smaller than the width of the DOS ($k_B T_0$), the carriers experience a DOS that is approximately constant. In this regime, the temperature dependence of the conductivity should follow Mott's law. This can be described as follows. Without the assumption $s_c k_B T \gg k_B T_0$, the percolation criterion (2.8) may be generalized to

$$B_c \approx \pi \left(\frac{T_0}{2\alpha T} \right)^3 N_t \exp \left(\frac{\epsilon_F}{k_B T_0} \right) \left[\frac{\sinh(2s_c T/T_0) + 6s_c T/T_0}{\sinh(s_c T/T_0)} - 8 \right]. \quad (2.16)$$

For $s_c T/T_0 > 4$, the factor between square brackets reduces to $\exp(s_c T/T_0)$ and Eq. (2.8) is recovered. For $s_c T/T_0 < 4$, this factor behaves like

$(s_c T/T_0)^4/5$. Following a derivation analogous to the one for high temperatures, we then find for the conductivity in the low-temperature regime

$$\sigma(\delta, T) = \sigma_0 \exp \left(- \left[5 \frac{T_0}{T} \frac{(2\alpha)^3 B_c \Gamma(1 - T/T_0) \Gamma(1 + T/T_0)}{\pi N_t \delta} \right]^{1/4} \right). \quad (2.17)$$

Thus at very low temperatures, the conductivity indeed follows Mott's law $\sigma \sim \exp[-(T_1/T)^{1/4}]$ [15]. In agreement with Mott VRH in a constant DOS, the parameter T_1 can be written in the form $k_B T_1 = \lambda \alpha^3 / \rho(\varepsilon_F)$, with $\lambda = 40 B_c / \pi$ a dimensionless constant [9, 15]. However, unlike for VRH in a constant DOS, the value for $\rho(\varepsilon_F)$ in the exponential DOS varies with temperature and carrier concentration. For the PTV and pentacene transistors studied in this Chapter, the transition in the temperature dependence is expected to take place well below 100 K.

References

- [1] D. J. Gundlach, Y. Y. Lin, T. N. Jackson, S. F. Nelson, and D. G. Schlom, *IEEE Electron Device Lett.* **18**, 87 (1997).
- [2] Z. N. Bao, Y. Feng, A. Dodabalapur, V. R. Raju, and A. J. Lovinger, *Chem. Mater.* **9**, 1299 (1997).
- [3] A. R. Brown, C. P. Jarrett, D. M. de Leeuw, and M. Matters, *Synth. Met.* **88**, 37 (1997).
- [4] F. Garnier, G. Horowitz, D. Fichou, and A. Yassar, *Synth. Met.* **81**, 163 (1996).
- [5] J. G. Laquindanum, H. E. Katz, A. J. Lovinger, and A. Dodabalapur, *Chem. Mater.* **8**, 2542 (1996).
- [6] A. Dodabalapur, L. Torsi, and H. E. Katz, *Science* **268**, 270 (1995).
- [7] G. Horowitz, R. Hajlaoui, and P. Delannoy, *J. Phys. III (France)* **5**, 355 (1995).
- [8] S. Kirkpatrick, *Rev. Mod. Phys.* **45**, 574 (1973).
- [9] V. Ambegaokar, B. I. Halperin, and J. S. Langer, *Phys. Rev. B* **4**, 2612 (1971).
- [10] For a review, see e.g. M. Sahimi, *Applications of Percolation Theory* (Taylor & Francis, London, 1994).
- [11] G. E. Pike and C. H. Seager, *Phys. Rev. B* **10**, 1421 (1974).
- [12] P. N. Butcher, in *Linear and Nonlinear Electron Transport in Solids*, edited by J. T. Devreese and V. E. van Doren (Plenum, New York, 1976).

- [13] M. Grünewald, P. Thomas, and D. Würtz, *Phys. Status Solidi B* **94**, K1 (1979); M. Grünewald and P. Thomas, *ibid.* **94**, 125 (1979).
- [14] F. R. Shapiro and D. Adler, *J. Non-Cryst. Solids* **74**, 189 (1985).
- [15] N. F. Mott and E. A. Davis, *Electronic Processes in Non-Crystalline Materials* (Clarendon press, Oxford, 1979).
- [16] D. Monroe, *Phys. Rev. Lett.* **54**, 146 (1985).
- [17] S. D. Baranovskii, T. Faber, F. Hensel, and P. Thomas, *J. Phys.: Condens. Matter* **9**, 2699 (1997).

Chapter 3

Dispersive hole transport in poly(p-phenylene vinylene)

3.1 Introduction

The advantage of easy processing and mechanical flexibility makes polymer light-emitting diodes (PLEDs) suitable candidates for large area display technologies. Electrical characterization of poly(phenylene vinylene) (PPV) based LEDs has mainly been focused on the direct current (DC) device characteristics [1–4]. Recently, current density-voltage (J - V) measurements on PPV-based hole-only and electron-only devices have revealed that the hole current is dominated by space-charge effects, whereas the electron current is strongly reduced by traps [5]. At low electric fields a hole mobility of $5 \times 10^{-11} \text{ m}^2/\text{Vs}$ is obtained at room temperature, independent of electric field. The fact that electrons are relatively immobile has also been observed in photoconductivity experiments [6]. Investigation of the J - V characteristics as a function of temperature T and layer thickness L has shown that at high fields the DC hole mobility μ_p in PPV can be accurately described as a function of electric field E according to [7]

$$\mu_p(E) = \mu_0 \exp \left[-\frac{\Delta}{k_B T} + B \left(\frac{1}{k_B T} - \frac{1}{k_B T_0} \right) \sqrt{E} \right], \quad (3.1)$$

with typically $\Delta = 0.48 \text{ eV}$, $B = 2.9 \times 10^{-5} \text{ eV}(\text{V/m})^{-1/2}$, $T_0 = 500\text{--}600 \text{ K}$, and $\mu_0 = 2 \times 10^{-3} \text{ m}^2/\text{Vs}$. The DC mobility (3.1) appears to be generic for a large class of disordered materials [8–10] like molecularly doped polymers and amorphous glasses, with relatively small variations in the parameters Δ , B , and T_0 . At present the physical origin of this universal field and

temperature dependence of the DC hole mobility [Eq. (3.1)] is not quite clear. Monte Carlo simulations of hopping between sites that are subject to both positional and energetic disorder agree with Eq. (3.1) over a limited field range [11]. This range may be increased by taking into account spatial correlations in the energetic disorder [12].

Transient experiments provide additional information on the microscopic origin of charge transport in disordered materials. Studies of the transient hole transport in a number of disordered solids [13] have revealed dispersive current traces which were attributed to a broad distribution in transit times of the individual carriers. The dispersion of transit times has been described in a stochastic transport model by Scher and Montroll (SM) [14], in which the transport is represented as a chain of hopping events. If one describes the waiting-time between two hops by a distribution $\psi(t)$ with an algebraic time-dependence $\psi(t) \sim t^{-(1+\alpha)}$, all of the essential features of dispersive transport are reproduced. The dispersion is characterized by a parameter α ($0 < \alpha < 1$) which depends on the microscopic transport mechanism. In the case of hopping small variations of the hopping distance introduce a broad distribution in hopping times. The corresponding dispersion parameter α is then temperature independent, as has been observed in amorphous arsenic triselenide (*a*-As₂Se₃) [15] and polyvinylcarbazole [16]. Similarly, in case of multiple trapping transport, broad release time distributions can be obtained for small variations in the trap depth. This gives rise to a temperature dependent α , as found in triphenylamine doped polycarbonate [13]. Furthermore, Monte Carlo simulations have demonstrated that hopping between sites which are exponentially distributed in energy also gives rise to a similar temperature-dependent dispersion [17]. Thus the observation of dispersive transport is common to many disordered conductors and it provides information on the microscopic transport mechanisms.

In various conjugated polymers, e.g. polyacetylene [18], poly(dodecyl thiophene) [19] and poly(*p*-phenylene vinylene) [20], transient photocurrents decaying as a power-law have been observed, which suggests that the transport in this class of materials is dispersive as well. However, it should be noted that disordered conductors often exhibit some spread in the transit times leading to an approximate power-law decay, whereas the transport is not dispersive in the sense of the SM theory [11, 21]. An unambiguous sign of SM dispersive transport is a universal scaling of the transit time with sample thickness and electric field, arising from the algebraic waiting-time distribution. To our knowledge this universal scaling has not been observed in conjugated polymer systems.

Usually, transient transport is studied using the time-of-flight (TOF) technique, where charge carriers are optically created close to one of the electrodes. As a result film thicknesses of at least several μm are required in order to prevent a homogeneous illumination throughout the film. Experimentally, TOF experiments on thick films of conjugated polymers are difficult due to the extremely low mobilities of these materials. From TOF measurements Meyer *et al.* [22] have determined the hole mobility of poly(1,4-phenylene-1,2-diphenoxyphenyl vinylene) (DPOP-PPV), which is a high-mobility derivative of PPV ($\mu_p \sim 10^{-8} \text{ m}^2/\text{Vs}$ at room temperature). The mobility of this material exhibits the same temperature and field dependence as given in Eq. (3.1), which has been interpreted in terms of a multiple trapping model. However, for standard PPV with a mobility which is typically a few orders of magnitude lower [5], their photocurrent showed a featureless decay without a discernible transit time and a mobility could not be determined.

Recently, studies by Vestweber [23] and Karg [24] have revealed that there is a time lag between the application of a voltage pulse and the onset of the electroluminescence (EL) in a PLED. As a result of the unbalanced charge transport [5] in a PLED the EL is confined to a region close to the cathode [25]. After application of a voltage the injected holes will first have to flow to the cathode before light generation occurs. Thus the observed time lag is directly related to the transit time of holes towards the cathode. The equivalence of transit times obtained from delayed electroluminescence and from TOF measurements has been confirmed experimentally by Ranke *et al.* [26]. An advantage of this method compared to the TOF technique is that it can be applied to PPV-films with a thickness less than the penetration depth of light.

In the present study we investigate the response time of PPV-based PLEDs after application of a voltage pulse as a function of electric field and temperature. Our study reveals that the observed response times are faster than the hole transit times as expected from the DC hole mobility (3.1). This discrepancy originates from the fact that the hole transport is dispersive as is demonstrated from the universal scaling of the response times with sample thickness and electric field. The observed response times are dominated only by the fastest part of the injected holes, whereas the DC mobility represents the transport of holes on a time scale much longer than the observed response times.

3.2 Experiment

The devices used in this study consist of a single polymer layer sandwiched between two electrodes on top of a glass substrate. The polymer is soluble poly(dialkoxy-*p*-phenylene) [5], which is spin coated on a patterned indium-tin-oxide (ITO) bottom electrode. As a top electrode an evaporated Ca contact is used. The measurements are performed in a nitrogen atmosphere. Pulses of known voltage V and duration τ_{pulse} are applied to our devices at a repetition rate of 4kHz using a HP214B pulse generator. As a result light pulses will be generated, typically delayed with regard to the voltage pulse with a delay time τ_d , as schematically indicated in the inset of Fig. 3.1. The integrated light-output I_{int} , represented by the shaded area, is measured by a Keithley 617 electrometer in current mode. In Fig. 3.1, I_{int} vs τ_{pulse} is shown for various applied voltages for a device with thickness $L = 100$ nm. For long τ_{pulse} ($\gg \tau_d$) the integrated light-output I_{int} increases linearly with τ_{pulse} , as expected since the missing light output as a result of τ_d can be neglected. The intercept of the linear part with the τ_{pulse} axis is then a measure for τ_d . The observed delay time τ_d decreases from 38 μs at 2V to 2.8 μs at 2.8 V and is used as a measure for the responsivity of the PLED throughout this paper. An advantage of this method is that it is very sensitive: at low voltages, where the light-emission is small, delay times can still be obtained. The RC time constant of the PLED circuit, which limits the time resolution of our setup, was determined from the response of the device current using a digital oscilloscope and amounts to 0.1-0.3 μs for the various devices.

3.3 Results and discussion

As stated above the response time is expected to be dominated by the transit time of holes towards the cathode, where light generation occurs. In the case of non-dispersive transport the hole transit time then directly provides information about the DC hole mobility μ_p according to

$$\mu_p = \frac{L^2}{\tau_d (V - V_{\text{bi}})}, \quad (3.2)$$

with τ_d the observed response time and V the applied voltage. It should be noted that we have corrected the applied voltage with a built-in voltage V_{bi} of 1.5 V, which is present due to the work function difference between ITO and Ca. The electric field pulling the front of the charge carriers is

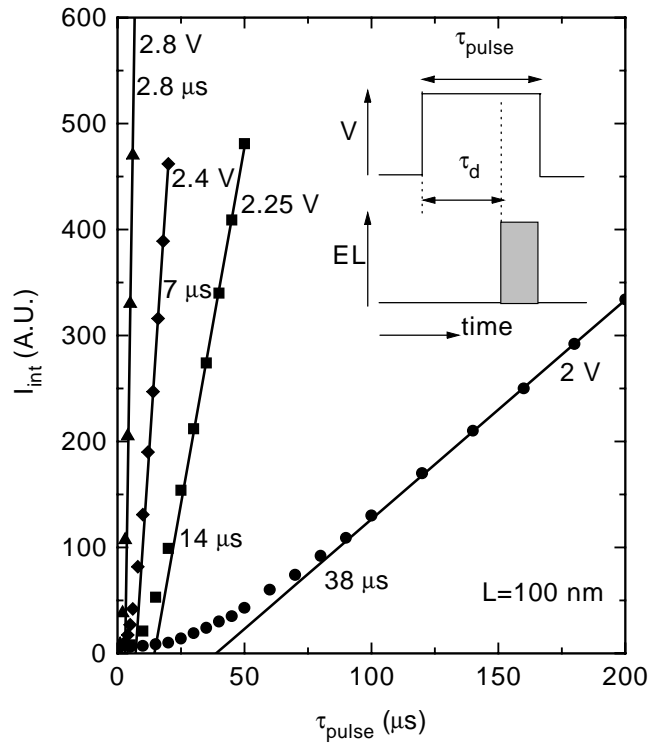


Figure 3.1: Time-integrated light output I_{int} vs pulse length τ_{pulse} for a PLED with a thickness of 100 nm at $T = 295$ K. The inset shows a schematic representation of a PLED exhibiting a delay time τ_d between the application of a voltage pulse and the first observation of EL. For voltage pulses with τ_{pulse} comparable to τ_d the integrated light-output I_{int} , represented by the shaded area, is relatively small. With increasing pulse length I_{int} will strongly increase until τ_{pulse} is much longer than τ_d . Then the missing light output during τ_d can be neglected and I_{int} vs τ_{pulse} will approach a linear behavior. By extrapolating the linear regime to $I_{\text{int}} = 0$ the delay time τ_d is obtained. The extrapolated τ_d decreases from 38 μs at $V = 2$ V, which is just above the threshold for light emission, to 2.8 μs at $V = 2.8$ V.

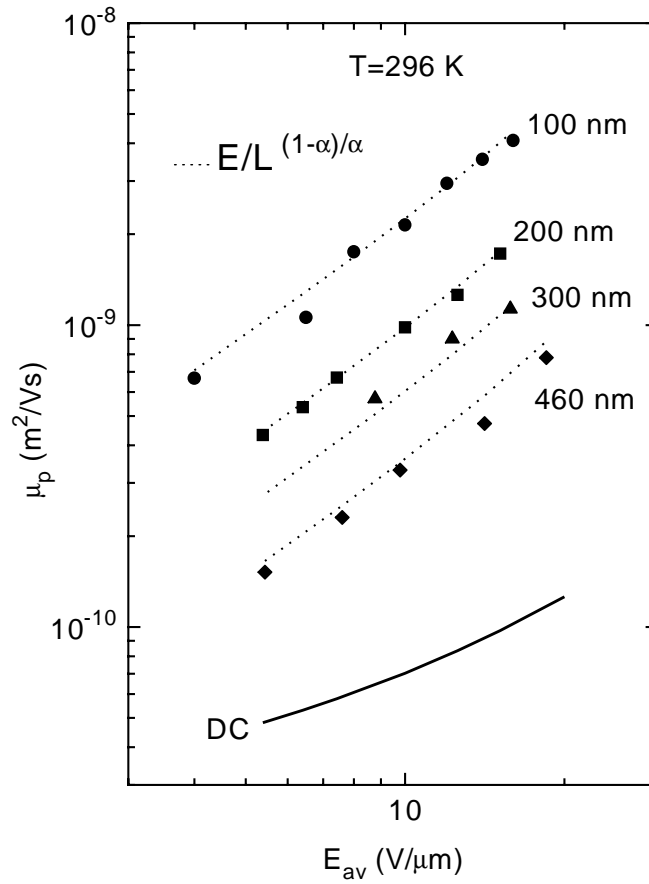


Figure 3.2: Hole mobility μ_p calculated from the observed response times using Eq. (3.2) as a function of applied electric field E_{av} (symbols) for PLEDs with $L = 100, 200, 300,$ and 460 nm together with the hole mobility of Eq. (3.1) as obtained from DC J-V measurements [7] (solid line).

unaffected by space charge, as has been shown both experimentally [27] and theoretically [28]. As a result an eventual inhomogeneous distribution of the electric field due to space charge in the device can be neglected in Eq. (3.2). From the observed response times, as shown in Fig. 3.1, μ_p can now be calculated using Eq. (3.2) as a function of $E_{av} \equiv (V - V_{bi})/L$. In Fig. 3.2, μ_p following from the response times as observed for $L = 100, 200$ and 300 nm are shown together with μ_p as obtained from the DC J - V measurements [Eq. (3.1)]. The most striking feature is that the “mobility” as obtained from the response times depends on the device thickness. Furthermore, these “mobilities” are larger than the DC mobility [Eq. (3.1)] and they exhibit a stronger field dependence.

The difference between DC and transient mobilities [29] as well as a thickness dependent transient mobility [15, 30] are strong indications of dispersive transport. According to the SM theory [14] the transit time τ_d of the fastest charge carriers is given by the universal scaling law

$$\tau_d \sim \left(\frac{L}{l(E)} \right)^{1/\alpha} \exp \left(\frac{\Delta_0}{k_B T} \right), \quad (3.3)$$

where Δ_0 is the average zero-field activation energy, $l(E)$ is the mean displacement of the carrier between two pausing events (hopping, trapping), and α is the dispersion parameter. At low fields, one may assume [14] $l(E) \sim E$, such that τ_d is given by

$$\tau_d \sim \left(\frac{L}{E} \right)^{1/\alpha} \exp \left(\frac{\Delta_0}{k_B T} \right). \quad (3.4)$$

Clearly, in a system with dispersive transport an analysis in terms of a mobility using Eq. (3.1), which leads to a thickness dependent “mobility” $\mu \sim (E/L)^{(1-\alpha)/\alpha}$, is not meaningful. According to Eq. (3.4), the observed response times at a given temperature are expected to scale as (E/L) . In Fig. 3.3, the observed response times τ_d are plotted against E_{av}/L for various temperatures. We find that for $T = 296$ K the observed τ_d for $L = 100, 200$ and 300 nm coincide on a single curve when plotted against E_{av}/L , in contrast to the “mobility” plot of Fig. 3.2. This demonstrates that at room temperature the hole transport follows the SM scaling law.

At lower temperatures, however, the response times start to deviate from the scaling law (3.4), as becomes evident in Fig. 3.3. This deviation is due to the fact that the linear approximation $l(E) \sim E$ no longer holds at low temperatures or high fields. In order to describe the high field dispersive transport in a -As₂Se₃ Pfister has introduced the phenomenological expression $l(E) \sim \sinh(eRE_{av}/2k_B T)$ [31]. This expression describes

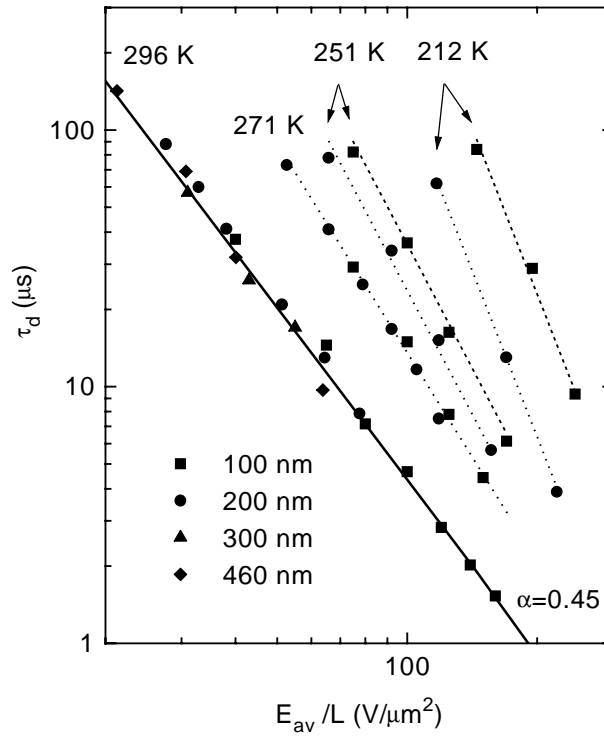


Figure 3.3: Response time τ_d of PLEDs with thicknesses $L = 100$, 200, 300 and 460 nm as a function of E_{av}/L for various temperatures. The built-in voltage V_{bi} results from the work function difference between the ITO anode and Ca cathode. At $T = 296$ K the response times follow the scaling law [Eq. (3.4), $\alpha = 0.45$] as predicted by Scher and Montroll for stochastic transport at low electric fields.

the asymmetry between hops in the direction of and against the applied field between two sites at a distance R , when the applied field lowers the activation energy for jumps in the field direction [32]. Note that, at low fields or high temperatures, $l(E)$ still approaches linear behavior. Using this expression for the field enhancement of the mean step displacement $l(E)$, we find that the response times obey the scaling law [Eq. (3.3)] for all temperatures and fields. Using an average activation energy $\Delta_0 = 0.34$ eV and an average site distance $R = 30$ Å, all data coincide on one curve characterized by a single dispersion parameter $\alpha = 0.45$ (see Fig. 3.4). From the average hopping distance $R = 30$ Å a site density $N_h = (4\pi R^3/3)^{-1}$ of 10^{25} m $^{-3}$ can be estimated. A temperature independent α , as also observed in *a*-As $_2$ Se $_3$ [15], indicates that the dispersion in the transit times in PPV is mainly due to structural disorder, i.e., disorder in the positions and local orientations of the polymer chains, rather than due to energetic disorder. This observation strongly favors hopping as the dominant transport mechanism in PPV rather than extended state transport with trapping in a distribution of trapping levels, which would give rise to a temperature dependent dispersion.

The response time τ_d of a PLED at high electric fields is relevant for its use in pixilated displays where multiplexing is required. Because of the dispersive character of the charge transport the response time of a PLED is determined only by the fastest part of the injected charge carriers. As a result the field dependence of the observed response times cannot be compared directly to the field dependence of the DC mobility [Eq. (3.1)], which reflects the time-averaged behavior of the charge transport. Extrapolating Eq. (3.4) towards high fields [without including the nonlinear field dependence of $l(E)$] we deduce as an upper limit for a 100 nm PLED operated at 10 V a response time of only 20 ns at $T = 295$ K. Thus at high fields PLEDs are extremely fast devices, in agreement with the observation of Braun *et al.* [33].

In conclusion we have demonstrated that the response of PPV-based PLEDs under pulsed operation is dominated by the dispersive transport of holes towards the cathode. The transit times of the holes follow the universal SM scaling law as a function of layer thickness, electric field and temperature. As a result an interpretation in terms of a charge carrier mobility is not meaningful. The dispersion in transit times appears to be independent of temperature, indicating that it originates from structural disorder, rather than energetic disorder.

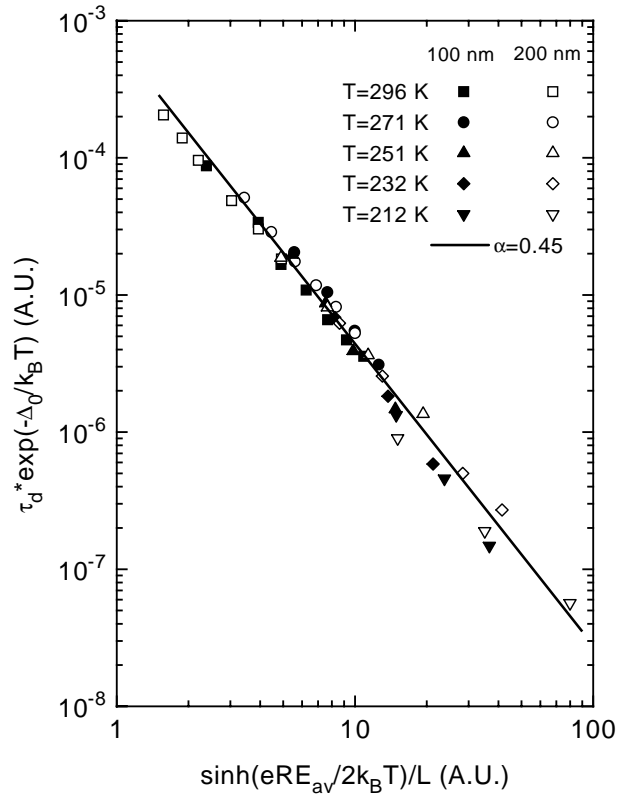


Figure 3.4: Response time τ_d of Fig. 3.3 multiplied by $\exp(-\Delta_0/k_B T)$ as a function of $\sinh(eRE_{av}/2k_B T)/L$. Using the approximation $l(E) \sim \sinh(eRE_{av}/2k_B T)$ the observed τ_d (symbols) follow Eq. (3.3) with $\Delta_0 = 0.34$ eV, $R = 30$ Å and $\alpha = 0.45$ (solid line) for various electric fields, temperatures and sample thicknesses ($L = 100$ and 200 nm).

3.4 Appendix

Recent TOF experiments on PPV by Lebedev *et al.* [34] seem to be at variance with the results described in the previous Chapter. Lebedev *et al.* interpreted the power-law decay of the transient photocurrent in terms of temperature-dependent dispersion parameters. However, as stated in the introduction, energetic disorder often gives rise to a power-law decay, even when the transport is not dispersive. The distinction between dispersive and nondispersive transport can only be made through the scaling with L . When the transient mobility scales with L , the transport is dispersive. For nondispersive transport, the mobility is a genuine material parameter, independent of L . Although the scaling with L is not discussed by Lebedev *et al.* [34], they observed a transient mobility that agrees well with the DC mobility, which indicates nondispersive transport.

In this Appendix, we demonstrate that the differences between our results, based on delayed EL, and the results in Ref. [34] based on TOF, can be attributed to the different length scales used. By increasing the thickness of the PPV layer up to 820 nm, which is in the range used for TOF [34], we observe a transition from dispersive to nondispersive transport, in agreement with theoretical predictions.

In Fig. 3.5, the transient hole mobility, as calculated from the observed delay times τ_d according to Eq. (3.2), is shown as a function of the electric field E_{av} for different layer thicknesses at room temperature. While the mobilities in the samples with thickness up to 460 nm clearly follow the scaling law (3.4) as a function of E_{av} and L , the mobility in the 820 nm sample is much lower and shows a weaker field dependence. Instead, this mobility agrees well with the DC mobility (3.1), which strongly suggests a transition towards nondispersive transport. Furthermore, as shown in Fig. 3.5, the temperature dependence of the mobility in the 820 nm sample is also in reasonable agreement with the DC mobility.

Let us now compare this result with a theoretical estimate for the dispersive-nondispersive transport transition. Monte Carlo simulations [35] as well as analytic theory [36] predict that dispersive transport in a structurally disordered material can only be observed on time scales shorter than a certain demarcation time $t_0 = \nu^{-1} \exp(1.73\gamma n^{-1/3})$. Here, ν is an attempt rate, γ is the wave-function overlap parameter, and n is the site density. After this time, the carrier has surveyed a representative fraction of the sample sites and the transport becomes nondispersive. Using a phonon frequency $\nu_0 = 10^{13}$ Hz and the average activation energy $\Delta_0 = 0.34$ eV, the attempt frequency $\nu = \nu_0 \exp(-\Delta_0/k_B T) \approx 10^7$ Hz at room temper-

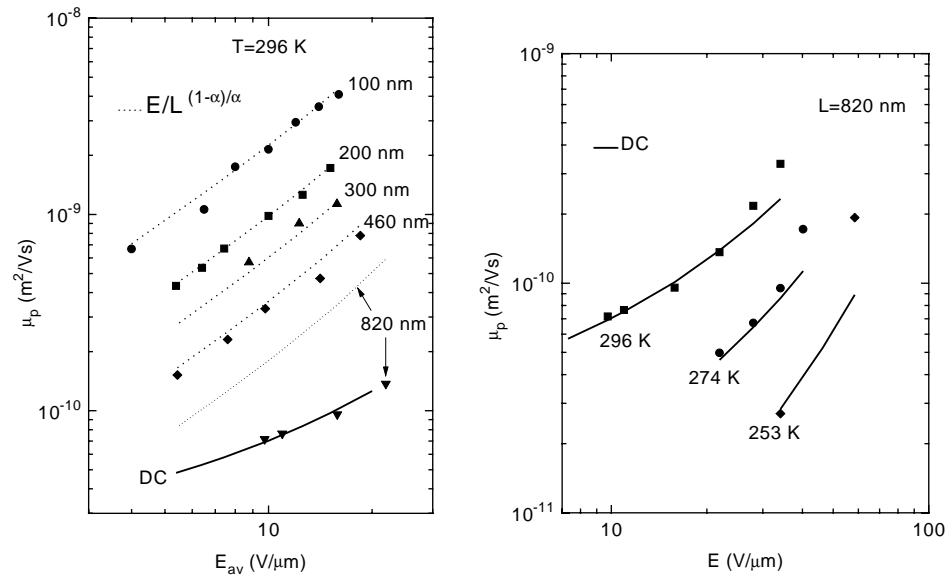


Figure 3.5: Hole mobility μ_p calculated from the observed response times using Eq. (3.2) as a function of applied electric field E_{av} (symbols). The dotted lines denote the hole mobilities as expected from SM theory; the solid lines denote the DC hole mobility [Eq. (3.1)] as obtained from DC J-V measurements [7]. The left figure shows room-temperature mobilities for PLEDs with various L ; the right figure shows the mobility for a LED with $L = 820\text{ nm}$ at different temperatures.

ature. Substituting this result, together with the relation $\alpha = 3\gamma^{-1}n^{1/3}$ (Ref. [36]) and $\alpha = 0.45$ into the expression for the demarcation time, we find that t_0 lies in the millisecond regime, which is in fair agreement with the observed transit times for $L = 820$ nm.

In conclusion, the transit time of holes in PPV based LEDs is governed by structural disorder-induced dispersive transport. Upon increasing the PPV layer thickness a transition to nondispersive transport is observed. In this regime, the hole transit time corresponds well with the DC hole mobility found in stationary experiments. Since time-of-flight experiments on PPV require layer thicknesses ≥ 700 nm [34], structural disorder-induced dispersive transport is not likely to be observed with this technique.

References

- [1] J. H. Burroughes, D. D. C. Bradley, A. R. Brown, R. N. Marks, K. MacKay, R. H. Friend, P. L. Burn, and A. B. Holmes, *Nature (london)* **347**, 539 (1990).
- [2] D. Braun and A. J. Heeger, *Appl. Phys. Lett.* **58**, 1982 (1991).
- [3] R. N. Marks, and D. D. C. Bradley, *Synth. Met.* **55–57**, 4128 (1993).
- [4] I. D. Parker, *J. Appl. Phys.* **75**, 1657 (1994).
- [5] P. W. M. Blom, M. J. M. de Jong, and J. J. M. Vlegaar, *Appl. Phys. Lett.* **68**, 3308 (1996).
- [6] M. Abkowitz, and M. Stolka, *Philos. Mag. Lett.* **58**, 239 (1988).
- [7] P. W. M. Blom, M. J. M. de Jong, and M. G. van Munster, *Phys. Rev. B.* **55**, R656 (1997).
- [8] D. M. Pai, *J. Chem. Phys.* **52**, 2285 (1970).
- [9] W. D. Gill, *J. Appl. Phys.* **43**, 5033 (1972).
- [10] P. M. Borsenberger and D. S. Weiss, *Organic Photoreceptors for Imaging Systems* (Dekker, New york, 1993), chap. 8, p. 181 , and articles referenced therein.
- [11] H. Bässler, *Phys. Status Solidi B* **175**, 15 (1993).
- [12] Yu. N. Gartstein and E. M. Conwell, *Chem. Phys. Lett.* **245**, 351 (1995); D. H. Dunlap, P. E. Parris, and V. M. Kenkre, *Phys. Rev. Lett.* **77**, 542 (1996).
- [13] G. Pfister and H. Scher, *Adv. Phys.* **27**, 747 (1978).
- [14] H. Scher and E. W. Montroll, *Phys. Rev. B* **12**, 2455 (1975).

- [15] G. Pfister and H. Scher, *Phys. Rev. B* **15**, 2062 (1977).
- [16] F. C. Bos and D. M. Burland, *Phys. Rev. Lett.* **58**, 152 (1987).
- [17] M. Silver, G. Schoenherr and H. Bässler, *Phys. Rev. Lett.* **48**, 352 (1982).
- [18] S. Etemad, T. Mitani, M. Ozaki, T. C. Chung, A. J. Heeger, and A. G. MacDiarmid, *Solid State Commun.* **40**, 75 (1981); H. Bleier, S. Roth, Y. Q. Shen, D. Schäfer-Siebert, and G. Leising, *Phys. Rev. B* **38**, 6031 (1988).
- [19] N. T. Binh, L. Q. Minh, and H. Bässler, *Synth. Met.* **58**, 39 (1993).
- [20] J. Obrzut, M. J. Obrzut, and F. E. Karasz, *Synth. Met.* **29**, E103 (1989); B. R. Hsieh, H. Antoniadis, M. A. Abkowitz, and M. Stolka, *Polym. Prepr.* **33**, 414 (1992).
- [21] J. C. Scott, B. A. Jones, and L. Th. Pautmeier, *Mol. Cryst. Liq. Cryst.* **253**, 183 (1994).
- [22] H. Meyer, D. Haarer, H. Naarmann, and H. H. Hörhold, *Phys. Rev. B* **52**, 2587 (1995).
- [23] H. Vestweber, R. Sander, A. Greiner, W. Heitz, R. F. Mahrt, and H. Bässler, *Synth. Met.* **64**, 141 (1994).
- [24] S. Karg, V. Dyakonov, M. Meier, W. Rieß, and G. Paasch, *Synth. Met.* **67**, 165 (1994).
- [25] P. W. M. Blom, M. J. M. De Jong, C. T. H. F. Liedenbaum, and J. J. M. Vlegaar, *Synth. Met.* **85**, 1287 (1997); J. Grüner, M. Remmers, and D. Neher, *Adv. Mater.* **9**, 964 (1997).
- [26] P. Ranke, I. Bleyl, J. Simmerer, D. Haarer, A. Bacher, and H. W. Schmidt, *Appl. Phys. Lett.* **71**, 1332 (1997).
- [27] M. Abkowitz and M. Morgan, *Solid State Commun.* **47**, 141 (1983).
- [28] G. F. Leal Ferreira and L. E. Carrano de Almeida, *Phys. Rev. B* **56**, 11579 (1997).
- [29] M. Abkowitz and D. M. Pai, *Philos. Mag. B* **53**, 193 (1986).
- [30] D. M. Pai, and M. E. Scharfe, *J. Non-Cryst. Solids* **8–10**, 752 (1972).

-
- [31] G. Pfister, and H. Scher, Bull. Am. Phys. Soc. **20**, 322 (1975); G. Pfister, Philos. Mag. **36**, 1147 (1977); N. Crisa, Phys. Status Solidi B **116**, 269 (1983).
- [32] N. F. Mott and E. A. Davis, *Electronic Processes in Non-Crystalline Materials* (Clarendon press, Oxford, 1979).
- [33] D. Braun, D. Moses, C. Zhang, and A. J. Heeger, Synth. Met. **55–57**, 4145 (1993).
- [34] E. Lebedev, Th. Dittrich, V. Petrova-Koch, S. Karg, W. Brütting, Appl. Phys. Lett. **71**, 2686 (1997).
- [35] B. Ries and H. Bässler, Phys. Rev. B **35**, 2295 (1987).
- [36] B. Movaghar, B. Grünewald, B. Pohlmann, D. Würtz, and W. Schirmacher, J. Stat. Phys. **30**, 315 (1983).

Chapter 4

Field-dependent mobility in disordered organic semiconductors

4.1 Introduction

Charge transport phenomena in disordered molecular solids are of practical interest because of their role in, e.g., electrophotography [1] and polymer light-emitting diodes [2, 3]. An outstanding theoretical challenge is the construction of one model that accounts for the similar features in materials with a wide variety of chemical and physical structures. Such an intriguing feature is the functional form of the field E and temperature T dependence of the carrier mobility μ ,

$$\mu = \mu_0 \exp \left[-\beta\Delta + B (\beta - \beta_0) \sqrt{E} \right], \quad (4.1)$$

with $\beta = 1/k_B T$ and $\beta_0 = 1/k_B T_0$. This stretched exponential form has first been observed for poly(N-vinyl carbazole) [4, 5]. Numerous experimental studies on molecularly doped polymers, pendant group polymers, amorphous molecular glasses, and conjugated polymers have revealed a similar behavior, with typical parameter values $\Delta \simeq 0.5$ eV, $B \simeq 3 \times 10^{-5}$ eV(m/V)^{1/2}, and $T_0 \simeq 600$ K (see, e.g., Refs. [6–9]).

To explain this ubiquitous E and T dependence, Bäessler and co-workers [9, 10] have performed numerical simulations of charge transport in a regular array of hopping sites with a Gaussian distribution of site energies. They were able to reproduce Eq. (4.1) for a temperature range around room temperature, but only for relatively high electric fields (100 MV/m $< E < 300$

MV/m). Adding structural disorder to the system yields a larger β_0 [9, 10], but the precise dependence on structural disorder is quite sensitive to the way the disorder is implemented in the simulations [11]. Experimentally, Eq. (4.1) often holds for fields down to 1 MV/m [4–8]. As already noted by Gill [5], the strong field dependence observed at low fields requires a length scale of at least several molecular spacings (note that a potential energy difference eEl over a length l must at least be of order $k_B T$ in order to be effective). Due to translational symmetry, the only length scale in models with homogeneous disorder [9–11] is the average distance between nearest neighbors. Longer length scales have been introduced by Gartstein and Conwell [12] by taking into account spatial correlations between the energies of neighboring sites. This extends the stretched exponential behavior to lower fields. Using an analytical one-dimensional model, Dunlap *et al.* [13] have attributed the specific form (4.1) to energy correlations associated with charge-dipole interactions, whereas other types of interaction gave a different form. This was recently confirmed by simulations for three dimensions [14]. Nevertheless, there are numerous experimental observations of the mobility (4.1) in systems *without* strong dipoles [7, 8].

In this Chapter we point out that an alternative cause for translational symmetry breaking is inhomogeneity in *structure*, instead of site energies. To investigate this idea an analytical model is employed, similar to the one by Dunlap *et al.* [13]: we show that Eq. (4.1) holds generically for systems consisting of a series of ordered high-mobility regions that are connected by parallel one-dimensional conduction paths of low mobility (see Fig. 4.1). The rationale for this model is that, due to the strong localization of charge carriers in disordered organic materials, relatively modest variations in structural order—e.g. in density or alignment of molecules—give rise to large variations in electronic coupling between clusters of molecules. We describe this by alternating regions of high mobility and of low mobility (a similar morphology has been suggested for doped conducting polymers [15]). Carriers get caught in the ordered regions, bouncing forward and backward with zero net velocity for a period of time before they escape [16]. When this time is sufficiently long, the ordered region contains a relatively large amount of equilibrated carriers and acts as a reservoir of charge.¹ The long length scale in our model is the distance l that a carrier has escaped from a reservoir: the potential energy difference eEl suppresses the process of returning, which leads to a strong increase in carrier mobil-

¹We note that the ordered regions need not be metallic, like in the model for doped polymers [15].

ity at relatively low fields. We stress that our model is independent of the microscopic source of the disorder, like charge-dipole interactions, van der Waals interactions, or variations in conjugation length. The characteristic field dependence of the mobility follows directly from the topology of the inhomogeneous structure.

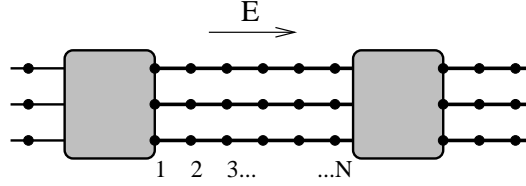


Figure 4.1: *Schematic representation of charge transport through a disordered material. The material is represented by relatively ordered clusters of sites (shaded), with negligible internal resistance, that act as reservoirs of charge carriers. These clusters are connected in series through parallel one-dimensional percolating paths that govern the conductivity of the material. A uniform electric field E drives a current from left to right.*

This Chapter is organized as follows. First, following Ref. [13], we analytically describe the hopping transport along a one-dimensional conduction path. The advantage of this approach is that the influence of high fields on the non-equilibrium charge distribution is taken into account exactly [17], instead of through a field-dependent effective temperature [18]. We demonstrate that, for uncorrelated Gaussian disorder in site energies, this model, like the simulations [9, 10], follows a stretched exponential for high fields only. The model is then extended by introducing a charge reservoir (the ordered region) at both ends of the conduction path. As a result, the mobility in our model system with inhomogeneous structural order and Gaussian energetic disorder follows a $\mu \propto \exp \sqrt{E}$ law for a broad field range.

4.2 Hopping conduction in one dimension

Starting point of our model is a one-dimensional chain of N sites (separation a) with periodic boundary conditions. Charge carriers hop from site n to one of its nearest-neighbors $n \pm 1$ at a transition rate $W_{n\pm 1,n}$. For low carrier densities, the time evolution of the system is described by a

linearized master equation, which gives the occupation probability $f_n(t)$ of site n at time t :

$$\begin{aligned} \frac{df_n}{dt} &= W_{n,n+1}f_{n+1} + W_{n,n-1}f_{n-1} \\ &\quad - (W_{n+1,n} + W_{n-1,n})f_n. \end{aligned} \quad (4.2)$$

The periodic boundary conditions are $W_{m,n} = W_{m+N,n+N}$ and $f_n = f_{n+N}$. The steady-state solution ($df_n/dt = 0$) has been given by Derrida [19]

$$f_n = Cr_n, \quad (4.3)$$

$$r_n = \frac{1}{W_{n+1,n}} \left[1 + \sum_{i=1}^{N-1} \prod_{j=1}^i \left(\frac{W_{n+j-1,n+j}}{W_{n+j+1,n+j}} \right) \right]. \quad (4.4)$$

The constant C is fixed by the average occupation

$$\bar{f} = N^{-1} \sum_{n=1}^N f_n. \quad (4.5)$$

The current I through the system reads

$$\begin{aligned} I &= e(W_{n+1,n}f_n - W_{n,n+1}f_{n+1}) \\ &= eC \left\{ 1 - \prod_{j=1}^N \frac{W_{j-1,j}}{W_{j+1,j}} \right\}, \end{aligned} \quad (4.6)$$

with e the elementary charge.

This solution is brought to a simpler form using the detailed balance relation

$$\frac{W_{n,n+1}}{W_{n+1,n}} = e^{\beta(\varepsilon_{n+1} - \varepsilon_n - eEa)}. \quad (4.7)$$

Here ε_n is the energy at site n for zero electric field and eEa is the difference in potential energy of two neighboring sites due to the electric field E . Substitution into Eq. (4.4) yields

$$r_n = \sum_{i=0}^{N-1} e^{\beta(\varepsilon_{n+i} - \varepsilon_n - ieEa)} W_{n+i+1,n+i}^{-1}. \quad (4.8)$$

Furthermore, in the limit $N \rightarrow \infty$ the term between braces in Eq. (4.6) tends to 1, so that the expression for the current simplifies to

$$I = eC = e\bar{f}/\bar{r}, \quad (4.9)$$

where we have defined $\bar{r} \equiv N^{-1} \sum_{i=1}^N r_n$.

In the simulations by Bässler and co-workers [9, 10], the transition rates $W_{m,n}$ are of the Miller-Abrahams form [20], i.e., the rate is ν for hops downwards in energy and $\nu e^{-\beta\Delta\varepsilon}$ for hops upwards in energy. The attempt frequency ν depends on the overlap of the electronic wave function of the adjacent sites, which we take identical for all hops along the conduction path. For convenience, we take rates of the slightly different Glauber form [21],

$$W_{n+1,n} = \nu \left[1 + e^{\beta(\varepsilon_{n+1} - \varepsilon_n - eEa)} \right]^{-1}, \quad (4.10)$$

which, for energy differences larger than $k_B T$, are identical to the Miller-Abrahams rates. The corresponding r_n are given by

$$r_n = \nu^{-1} \left[1 + 2 \sum_{i=1}^{N-1} e^{\beta(\varepsilon_{n+i} - \varepsilon_n - ieEa)} + e^{-\beta N eEa} \right]. \quad (4.11)$$

The charge-carrier mobility μ is defined by the drift equation

$$j = ep\mu E, \quad (4.12)$$

where j is the current density and p is the average carrier density. For our one-dimensional system, $j = I$ and $p = \bar{f}/a$. Using Eq. (4.9), the mobility reads

$$\mu = \frac{a}{\bar{r}E} = \frac{a}{\langle r \rangle E}. \quad (4.13)$$

Here the average \bar{r} over sites in one chain has been replaced by the average $\langle r \rangle$ over an ensemble of disordered chains, the two averages being the same for large N . For uncorrelated site energies ε_n the mobility then follows from Eqs. (4.11) and (4.13):

$$\mu = \frac{\nu a/E}{1 + 2 \langle e^{\beta\varepsilon} \rangle \langle e^{-\beta\varepsilon} \rangle [e^{\beta eEa} - 1]^{-1}}. \quad (4.14)$$

For a model of a Gaussian density of states (DOS) with standard deviation σ this evaluates to

$$\mu = \frac{\nu a/E}{1 + 2e^{\beta^2\sigma^2} [e^{\beta eEa} - 1]^{-1}}. \quad (4.15)$$

The mobility (4.15) is plotted in Fig. 4.2 as a function of E for various temperatures. We can distinguish three different regimes for the field dependence. At low fields, $\beta eEa \ll 1$, the mobility is independent of E . At

moderately high fields, $1 < \beta e E a < \beta^2 \sigma^2$, the mobility increases exponentially with E , since the activation energies for all hops in the field direction are lowered by $e E a$. In this regime, $\mu = \nu a e^{-\beta^2 \sigma^2} e^{\beta e E a} / 2E$. At very high fields, $e E a \gg \beta \sigma^2$, the drift velocity $v = \mu E$ saturates, since all hops are downward in energy. The mobility then *decreases* with field ($\mu = \nu a / E$). We note that, like in the simulations [9], a stretched exponential field dependence is observed only at the narrow transitional region from moderate to high fields ($e E a \simeq \beta \sigma^2$).

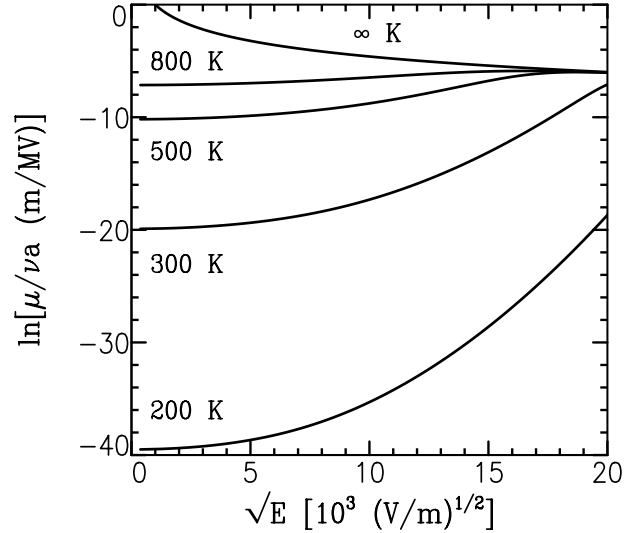


Figure 4.2: *Logarithm of the mobility μ in a one-dimensional chain of sites [Eq. (4.15)] as a function of the square root of the electric field E for different temperatures T . The site energies are distributed according to a Gaussian with standard deviation $\sigma = 0.1$ eV. The sites have a spacing $a = 1.0$ nm.*

To improve on this model, we now assume that the conduction path is connected at both ends to a reservoir of charge carriers, as indicated in Fig. 4.1. We take the first site to be in direct contact with the charge injecting reservoir. The second reservoir acts as a drain for charges located on site N . For long conduction paths, the boundary condition on the drain site $N + 1$ may be chosen arbitrarily, since it does not influence the occupation probabilities f_n in the limit $N \rightarrow \infty$ at finite n and E . It is convenient to take again periodic boundary conditions, $f_{N+1} = f_1$, so that

the solution for the f_n is still given by Eq. (4.3). The difference with the isolated conduction path is that the total charge on the chain is no longer fixed, since the path is connected to a reservoir of charge carriers. The constant C in Eq. (4.3) is determined by the occupation probability on site 1, which is in direct contact with the reservoir:

$$f_1 = Cr_1 = p_r e^{-\beta\varepsilon_1}/Z. \quad (4.16)$$

Here p_r is the density of charge carriers in the reservoir, $Z = \int d\varepsilon \rho(\varepsilon) e^{-\beta\varepsilon}$ is the partition function, and $\rho(\varepsilon)$ is the DOS in the reservoir. Note that we have used Maxwell-Boltzmann statistics, which is valid at the low carrier densities we have assumed throughout the paper.

The current through a single conduction path in the large N limit now follows from Eq. (4.9), with Eq. (4.16) fixing the constant C :

$$\begin{aligned} I &= eC = ep_r e^{-\beta\varepsilon_1}/Zr_1 \\ &= \frac{\nu ep_r Z^{-1}}{e^{\beta\varepsilon_1} + 2 \sum_{i=1}^{\infty} e^{\beta(\varepsilon_{i+1} - iEa)}}. \end{aligned} \quad (4.17)$$

We have again assumed transition rates of the Glauber form. We note that the field and temperature dependence of I is strongly dependent on the configuration of site energies near the source reservoir. The influence of the energy on site k decreases exponentially with the distance from the source, due to the factor $e^{-\beta(k-1)Ea}$. The mobility μ of the carriers in the conduction path is still given by Eq. (4.13), independent of the configuration. Thus the configuration dependence of $I = e(\bar{f}/a)\mu E$ originates from the configuration dependence of \bar{f} .

4.3 Model for the carrier mobility

So far we have considered the carrier mobility on a single conduction path. What is measured experimentally is the mobility of the entire system of charge reservoirs (high-mobility regions) in series connected by several parallel paths of low mobility (see Fig. 4.1). Since the charge in the one-dimensional paths is negligible compared to the charge in the reservoirs, the charge density p in the entire system is proportional to the charge density p_r in the reservoirs. The current density j through the entire system is proportional to the density of parallel conduction paths and to the ensemble average $\langle I \rangle$ of the current per conduction path [Eq. (4.17)]. We thus

obtain the mobility $\mu = j/epE$ of the entire system

$$\mu = \frac{\nu c}{ZE} \left\langle \frac{1}{e^{\beta\varepsilon_1} + 2 \sum_{i=1}^{\infty} e^{\beta(\varepsilon_{i+1} - ieEa)}} \right\rangle. \quad (4.18)$$

The proportionality constant c depends on the structural properties of the material, like the size and number of the high-mobility regions and the density of parallel conduction paths, and is independent of temperature and field. For the Gaussian DOS, the partition function is $Z = \rho e^{\beta^2 \sigma^2 / 2}$, with $\rho \equiv \int d\varepsilon \rho(\varepsilon)$ the density of sites.

In contrast to Eq. (4.13) for the single-path mobility, the ensemble average in Eq. (4.18) for the mobility of the entire system is over the whole fraction, not just the denominator. To compute this average, we use that the first few energy values have the strongest influence: the terms $e^{\beta(\varepsilon_{i+1} - ieEa)}$ in Eq. (4.18) may be neglected for sufficiently large i . Replacing the site energies beyond site k by their average value $\langle \varepsilon \rangle = 0$, we find the expression

$$\begin{aligned} \mu = & \frac{\nu c}{ZE} \int \left[\prod_{l=1}^k d\varepsilon_l \frac{\rho(\varepsilon_l)}{\rho} \right] \left[e^{\beta\varepsilon_1} + 2 \sum_{i=1}^{k-1} e^{\beta(\varepsilon_{i+1} - ieEa)} \right. \\ & \left. + 2e^{-\beta k e E a} \left(1 - e^{-\beta e E a} \right)^{-1} \right]^{-1}. \end{aligned} \quad (4.19)$$

In practice, for not too low E , rather small values of k provide sufficient accuracy. In Fig. 4.3, we have plotted Eq. (4.19) with $k = 8$ for a Gaussian distribution $\rho(\varepsilon)$. For the field range shown in Fig. 4.3, the numerical results have converged well for $k = 8$ (for lower fields, a larger k should be used).

We find that the stretched-exponential law $\mu \propto \exp \sqrt{E}$ is followed over a field range from below 5 MV/m up to 200 MV/m. On the temperature range 200–500 K, which covers the experimentally accessible temperature ranges [4–8], we find good agreement with the empirical law Eq. (4.1). Thus for parameter values $\sigma = 0.1$ eV and $a = 1.0$ nm, which are typical for disordered organic materials [9], our model for the carrier mobility reproduces the experimental results.

In conclusion, we have proposed a model for the field-dependent mobility of charge carriers hopping in a system with energetic disorder and inhomogeneous structural order. The mobility follows the empirical $\mu \propto \exp \sqrt{E}$ law [Eq. (4.1)] over the experimentally observed field and temperature range. The model does not rely on any specific physical or chemical mechanism that is responsible for the disorder, which makes it a good candidate

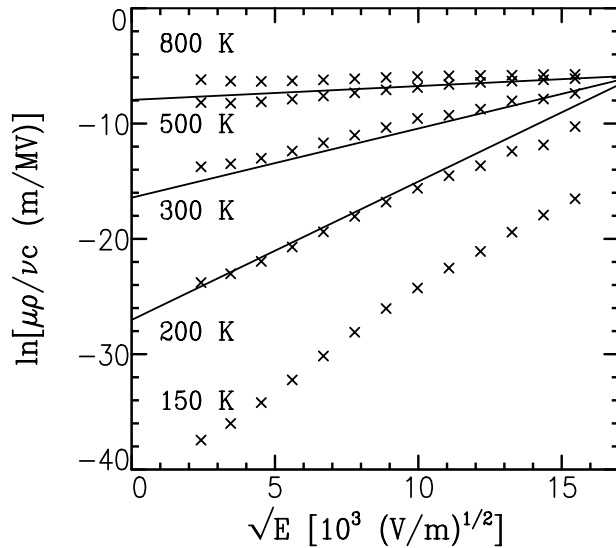


Figure 4.3: *Logarithm of the mobility μ in our model system for a disordered organic semiconductor, as a function of the square root of the electric field E for different temperatures T . Data points are computed by a numerical integration routine, according to Eq. (4.19) with $k = 8$ and a Gaussian distribution of site energies (standard deviation $\sigma = 0.1$ eV, site separation $a = 1.0$ nm). The solid lines follow the empirical law Eq. (4.1) for $T = 200, 300,$ and 500 K, with $\Delta = 0.53$ eV, $B = 3 \times 10^{-5}$ eV(m/V) $^{1/2}$, and $T_0 = 600$ K.*

for explaining the ubiquitously observed behavior. To decide whether a single explanation is in order, or that several mechanisms act in conjunction, a study of systems with inhomogeneous structure as well as strong dipoles might prove worthwhile.

References

- [1] D. M. Pai and B. E. Springett, *Rev. Mod. Phys.* **65**, 163 (1993).
- [2] R. N. Marks, D. D. C. Bradley, R. W. Jackson, P. L. Burn, and A. B. Holmes, *Synth. Met.* **55**, 4128 (1993).
- [3] P. W. M. Blom, M. J. M. de Jong, and J. J. M. Vleggaar, *Appl. Phys. Lett.* **68**, 3308 (1996); P.W.M. Blom and M.C.J.M. Vissenberg, *Phys. Rev. Lett.* **80**, 3819 (1998).
- [4] D. M. Pai, *J. Chem. Phys.* **52**, 2285 (1970).
- [5] W. D. Gill, *J. Appl. Phys.* **43**, 5033 (1972).
- [6] L. B. Schein, A. Peled, and D. Glatz, *J. Appl. Phys.* **66**, 686 (1989); P. M. Borsenberger, *J. Appl. Phys.* **68**, 6263 (1990); M. A. Abkowitz, *Phil. Mag. B* **65**, 817 (1992).
- [7] P. M. Borsenberger, W. T. Gruenbaum, and E. H. Magin, *Physica B* **228**, 226 (1996); J. A. Sinicropi, J. R. Cowdery-Corvan, E. H. Magin, and P. M. Borsenberger, *Chem. Phys.* **218**, 331 (1997).
- [8] P. W. M. Blom, M. J. M. de Jong, and M. G. van Munster, *Phys. Rev. B* **55**, R656 (1997).
- [9] H. Bässler, *Phys. Status Solidi B* **175**, 15 (1993).
- [10] L. Pautmeier, R. Richert, and H. Bässler, *Synth. Met.* **37**, 271 (1990).
- [11] Yu. N. Gartstein and E. M. Conwell, *J. Chem. Phys.* **100**, 9175 (1994); *Phys. Rev. B* **51**, 6947 (1995).
- [12] Yu. N. Gartstein and E. M. Conwell, *Chem. Phys. Lett.* **245**, 351 (1995).

- [13] D. H. Dunlap, P. E. Parris, and V. M. Kenkre, Phys. Rev. Lett. **77**, 542 (1996).
- [14] S. V. Novikov, D. H. Dunlap, V. M. Kenkre, P. E. Parris, and A. V. Vannikov, Phys. Rev. Lett. **81**, 4472 (1998).
- [15] J. Joo, S. M. Long, J. P. Pouget, E. J. Oh, A. G. MacDiarmid, and A. J. Epstein, Phys. Rev. B **57**, 9567 (1998).
- [16] B. Ries and H. Bäessler, Phys. Rev. B **35**, 2295 (1987).
- [17] D. Emin, Phys. Status Solidi B **205**, 69 (1998).
- [18] B. Movaghar, A. Yelon, and M. Meunier, Chem. Phys. **146**, 389 (1990); S. Marianer and B. I. Shklovskii, Phys. Rev. B **46**, 13100 (1992).
- [19] B. Derrida, J. Stat. Phys. **31**, 433 (1983).
- [20] A. Miller and E. Abrahams, Phys. Rev. **120**, 745 (1960).
- [21] R. J. Glauber, J. Math. Phys. **4**, 204 (1963).

Chapter 5

Exciton dynamics in disordered molecular systems

5.1 Introduction

Luminescence, i.e., the de-excitation of excited atoms or molecules by the re-emission of absorbed energy as photons, provides information about the nature and dynamics of excited states of atoms or molecules in a solid. In molecular systems, the covalent binding of atoms within a molecule is much stronger than the van der Waals binding between molecules. For this reason, excitations are usually localized on a molecule. Neutral optical excitations localized on atoms or molecules are generally referred to as Frenkel excitons [1].

An important property of excitons is their ability to transport energy without involving the migration of net electric charge. In general, there are three different basic mechanisms of exciton transport of energy: (i) Radiative transfer, i.e., the emission of a photon by a donor molecule and the subsequent reabsorption of this photon by an acceptor molecule. This process may take place when the emission spectrum of the donor molecule overlaps the absorption spectrum of the acceptor molecule, and when the medium between the two molecules is transparent to the wavelength of the radiation involved. (ii) Resonance transfer, or Förster transfer [2], where the exciton energy is transferred from a donor to an acceptor due to the dipole-dipole coupling between the two molecules. The conditions for resonance transfer are the same as those for radiative transfer, but in

resonance transfer no actual emission and absorption of photons takes place. The dipole-dipole interaction energy is proportional to R^{-3} , where R is the distance between the acceptor and donor molecule. Thus the probability of energy transfer, which is proportional to the square of the interaction energy (Fermi's golden rule), is proportional to R^{-6} . The typical range for resonance transfer is 5-100 Å. (iii) Exciton transfer, when the excited state is not confined to one molecule, but interacts with its surrounding molecules. In case of N coupled molecules, the single excitonic level may split into a band of N levels. This type of splitting is generally referred to as Davydov splitting [3]. Like the hopping transport of charge carriers, this type of exciton transport is very sensitive to disorder in the electronic coupling between adjacent molecules and the transfer steps are restricted to a short range (typically 2-5 Å).

In conjugated polymers, the electronic coupling along the polymer chain is strong, which allows for one-dimensional delocalized bands [4]. Optical excitation of such a one-dimensional semiconductor would give rise to the creation of free electrons and holes (or polarons) instead of strongly bound excitons. To study the nature and dynamics of excited states in conjugated polymers, several spectroscopic techniques have been applied [5], like time and spectrally resolved photoluminescence [6], site-selective fluorescence [7], and energy transfer studies [8]. Although these and related experimental results are still under debate [9], there is a large body of experimental evidence in favor of the notion that photon absorption in PPV-type and other conjugated polymers creates neutral excitons, like in molecular solids. These excitons are localized on segments of the polymer chain that are isolated by structural defects (twists and kinks in the chain) or chemical defects that break the π -conjugation along the chain. The excitons migrate (via energy transfer) to neighboring segments on the same chain or on different chains, decay nonradiatively and emit phonons, or decay radiatively and emit photons. Comparison with experiment [8, 10] has shown that the energy transfer in conjugated polymers is predominantly of the Förster type (resonance transfer).

In energetically disordered systems, the migration of excitons will be accompanied by a relaxation in energy. This leads to a red-shift between the absorption and emission spectrum, often referred to as the Stokes shift. In this Chapter, we describe how this Stokes shift depends on time and on excitation energy. To this end, we will derive an approximate Green function solution for neutral particles hopping in a positionally and energetically disordered system at zero temperature, where we follow the approach by

Movaghar *et al.* [11, 12]. The results of our theory are compared to experimental results on conjugated polymer systems. The Green function solution derived in this Chapter forms the basis of the work presented in the following Chapters 6, 7, and 8.

5.2 Green function formalism

The disordered molecular system is treated as a set of N localized sites i , characterized by random positions \mathbf{R}_i and exciton energies ε_i , distributed according to a density of states $\rho(\varepsilon_i)$. We take the intramolecular vibrational relaxation to this energy ε_i to be much faster than exciton migration or decay, such that higher excited states on the site i need not be taken into account. At low illumination intensities, the probability f_i for an exciton to occupy the site i is small. Hence a linearized master equation may be used to describe the exciton dynamics

$$\frac{\partial}{\partial t} f_i(t) = - \sum_{j \neq i} W_{ji} f_i(t) + \sum_{j \neq i} W_{ij} f_j(t) - \lambda_i f_i(t). \quad (5.1)$$

We take the transition rate W_{ij} from site i to site j to be of the Förster type [2]. At zero temperature, these Förster rates may be written in the form

$$W_{ij} = \begin{cases} \nu_0 \left(\frac{R_0}{R_{ij}} \right)^6, & \varepsilon_j \geq \varepsilon_i, \\ 0, & \varepsilon_j < \varepsilon_i, \end{cases} \quad (5.2)$$

where R_0 is the average nearest neighbour distance, R_{ij} is the distance between the sites i and j and ν_0 is the average nearest neighbour jump frequency. The exciton decay is described by the rate λ_i . In the present Chapter, we take a single rate λ for radiative decay that is the same for all sites. Site-dependent decay rates will be taken into account in the following Chapters.

Formally, the solution of the master equation is given by the Green function $G_{ij}(t)$, which is the probability to find a particle (exciton) on the site i at time t , given that it was at site j at $t = 0$. As described in Sec. 1.4, the luminescence spectrum may be expressed in terms of configurationally averaged Green functions:

$$L(\varepsilon_i, t) = L_1(\varepsilon_i, t) + \int d\varepsilon_j L_2(\varepsilon_i, \varepsilon_j, t), \quad (5.3)$$

$$L_1(\varepsilon_j, t) \equiv \lambda \Omega \rho(\varepsilon_j) f^0(\varepsilon_j) G_1(\varepsilon_j, t), \quad (5.4)$$

$$L_2(\varepsilon_i, \varepsilon_j, t) \equiv \lambda \Omega \rho(\varepsilon_i) \rho(\varepsilon_j) f^0(\varepsilon_j) \int d\mathbf{R}_{ij} G_2(\varepsilon_i, \varepsilon_j, \mathbf{R}_{ij}, t). \quad (5.5)$$

Here, Ω is the volume of the system and $f^0(\varepsilon_j) \equiv f_j(0)$ is the initial condition, which we take independent of site position. The functions $G_1(\varepsilon_j, t)$ and $G_2(\varepsilon_i, \varepsilon_j, \mathbf{R}_{ij}, t)$ denote the configurational average of the local Green function $G_{jj}(t)$ and of the non-local Green function $G_{ij}(t)$ (with $i \neq j$), respectively [see Eqs. (1.42) and (1.43)].

The Laplace transform of the local Green function $G_{jj}(p)$ satisfies the recursion relation (1.36)

$$G_{jj}(p) = \left(1 + \sum_{l \neq j} G_{jl}(p) W_{lj} \right) G_{jj}^0(p). \quad (5.6)$$

Here, $G_{jj}^0(p) = [p + \lambda + \sum_{\mu \neq j} W_{\mu j}]^{-1}$ is the Laplace transform of the probability to remain on the site j [see Eq. (1.37)]. At zero temperature, the probability of ever returning to the initial site vanishes due to the zero probability of jumps to a site with a higher exciton energy. Therefore at $T = 0$ the local Green function is given by $G_{jj}^0(p)$. The configurational average of this function reads

$$\begin{aligned} G_1(\varepsilon_j, t) &= \langle G_{jj}^0(t) \rangle_j = \int \left[\prod_{\nu \neq j} d\mathbf{R}_\nu d\varepsilon_\nu \frac{\rho(\varepsilon_\nu)}{N} \right] e^{-\lambda t - \sum_{\mu \neq j} W_{\mu j} t} \\ &= e^{-\lambda t} \int \left[\prod_{\nu \neq j} d\mathbf{R}_\nu d\varepsilon_\nu \frac{\rho(\varepsilon_\nu)}{N} \right] \prod_{\mu \neq j} e^{-W_{\mu j} t} \\ &= e^{-\lambda t} \left[\int d\mathbf{R}_\mu d\varepsilon_\mu \frac{\rho(\varepsilon_\mu)}{N} e^{-W_{\mu j} t} \right]^{N-1} \\ &= e^{-\lambda t} \left[1 + \frac{n(\varepsilon_j)}{N} 4\pi \int_0^\infty dR R^2 \left(e^{-(R_0/R)^6 \nu_0 t} - 1 \right) \right]^{N-1} \\ &= e^{-\lambda t} \left[1 - \frac{n(\varepsilon_j)}{N} \left(\frac{4}{3} \pi R_0^3 \right) \sqrt{\pi \nu_0 t} \right]^{N-1} \\ &\approx \exp \left(-\lambda t - n(\varepsilon_j) \frac{4}{3} \pi R_0^3 \sqrt{\pi \nu_0 t} \right), \end{aligned} \quad (5.7)$$

where $n(\varepsilon_j)$ denotes the density of sites with energies below ε_j

$$n(\varepsilon_j) = \int_{-\infty}^{\varepsilon_j} d\varepsilon \rho(\varepsilon). \quad (5.8)$$

The stretched exponential time dependence of $G_1(\varepsilon_j, t)$ is characteristic for Förster-type transfer [2]. For the calculation of $G_2(\varepsilon_i, \varepsilon_j, \mathbf{R}_{ij}, t)$, we need

the Laplace transform of Eq. (5.7)

$$\tilde{G}_1(\varepsilon_j, p) = \frac{1}{p + \lambda} \left(1 + \sqrt{\pi} \zeta \exp(\zeta^2) [\operatorname{erf}(\zeta) - 1] \right), \quad (5.9)$$

where we have introduced the dimensionless parameter

$$\zeta = n(\varepsilon_j) \frac{2}{3} \pi R_0^3 \sqrt{\frac{\pi \nu_0}{p + \lambda}} \quad (5.10)$$

and the error function $\operatorname{erf}(x) = \frac{2}{\sqrt{\pi}} \int_0^x dq \exp(-q^2)$.

The Fourier-Laplace transform of the configurationally averaged non-local Green function reads

$$\tilde{G}_2(\varepsilon_i, \varepsilon_j, \mathbf{k}, p) = \int d\mathbf{R}_{ij} e^{-i\mathbf{k} \cdot \mathbf{R}_{ij}} \int_0^\infty dt e^{-pt} G_2(\varepsilon_i, \varepsilon_j, \mathbf{R}_{ij}, t). \quad (5.11)$$

Substituting the recursion relation (1.36) we find

$$\begin{aligned} \tilde{G}_2(\varepsilon_i, \varepsilon_j, \mathbf{k}, p) &= \int d\mathbf{R}_{ij} e^{-i\mathbf{k} \cdot \mathbf{R}_{ij}} \left\langle \sum_{l \neq j} G_{il}(p) W_{lj} G_{jj}^0(p) \right\rangle_{ij} \\ &= \int d\mathbf{R}_{ij} e^{-i\mathbf{k} \cdot \mathbf{R}_{ij}} \left\{ \left\langle G_{ii}(p) W_{ij} G_{jj}^0(p) \right\rangle_{ij} + \right. \\ &\quad \left. \sum_{l \neq i, j} \int d\mathbf{R}_l d\varepsilon_l \frac{\rho(\varepsilon_l)}{N} \left\langle G_{il}(p) W_{lj} G_{jj}^0(p) \right\rangle_{ilj} \right\}. \quad (5.12) \end{aligned}$$

We make the approximation that at zero temperature all hops take place independently. In that case, the average probability of a given series of hops can be written as the product of the average probabilities of each independent hop, e.g.,

$$\left\langle G_{ii}^0(p) W_{il} G_{ll}^0(p) W_{lj} G_{jj}^0(p) \right\rangle_{ilj} \approx \left\langle G_{ii}^0(p) \right\rangle_i \left\langle W_{il} G_{ll}^0(p) \right\rangle_{il} \left\langle W_{lj} G_{jj}^0(p) \right\rangle_{lj}. \quad (5.13)$$

Then the first term on the r.h.s. of Eq. (5.12) becomes

$$\int d\mathbf{R}_{ij} e^{-i\mathbf{k} \cdot \mathbf{R}_{ij}} \tilde{G}_1(\varepsilon_i, p) \left\langle W_{ij} G_{jj}^0(p) \right\rangle_{ij} = \tilde{G}_1(\varepsilon_i, p) \tilde{g}(\varepsilon_j, \mathbf{k}, p) \theta(\varepsilon_j - \varepsilon_i), \quad (5.14)$$

with

$$\tilde{g}(\varepsilon_j, \mathbf{k}, p) \equiv \int d\mathbf{R}_{ij} e^{-i\mathbf{k} \cdot \mathbf{R}_{ij}} \left\langle W_{ij} G_{jj}^0(p) \right\rangle_{ij}. \quad (5.15)$$

Note that $\tilde{g}(\varepsilon_j, \mathbf{k}, p)$ is *not* a function of ε_i due to the zero-temperature ε -dependence of the jump rates (5.2) and the condition $\varepsilon_j > \varepsilon_i$. The same

approximations are used in order to rewrite the second term on the r.h.s. of Eq. (5.12)

$$\begin{aligned}
& \int d\mathbf{R}_{ij} e^{-i\mathbf{k}\cdot\mathbf{R}_{ij}} \sum_{l \neq i,j} \int d\mathbf{R}_l d\varepsilon_l \frac{\rho(\varepsilon_l)}{N} G_2(\varepsilon_i, \varepsilon_l, \mathbf{R}_{il}, p) \langle W_{lj} G_{jj}^0(p) \rangle_{lj} \\
&= \int d\mathbf{R}_{ij} e^{-i\mathbf{k}\cdot\mathbf{R}_{ij}} \int d\mathbf{R}_l d\varepsilon_l \rho(\varepsilon_l) G_2(\varepsilon_i, \varepsilon_l, \mathbf{R}_{il}, p) \langle W_{lj} G_{jj}^0(p) \rangle_{lj} \\
&= \int d\mathbf{R}_{lj} d\mathbf{R}_{il} d\varepsilon_l \rho(\varepsilon_l) e^{-i\mathbf{k}\cdot(\mathbf{R}_{il}+\mathbf{R}_{lj})} G_2(\varepsilon_i, \varepsilon_l, \mathbf{R}_{il}, p) \langle W_{lj} G_{jj}^0(p) \rangle_{lj} \\
&= \int d\varepsilon_l \rho(\varepsilon_l) \tilde{G}_2(\varepsilon_i, \varepsilon_l, \mathbf{k}, p) \int d\mathbf{R}_{lj} e^{-i\mathbf{k}\cdot\mathbf{R}_{lj}} \langle W_{lj} G_{jj}^0(p) \rangle_{lj} \\
&= \int d\varepsilon_l \rho(\varepsilon_l) \tilde{G}_2(\varepsilon_i, \varepsilon_l, \mathbf{k}, p) \tilde{g}(\varepsilon_j, \mathbf{k}, p) \theta(\varepsilon_j - \varepsilon_l) \\
&= \left\{ \int_{-\infty}^{\varepsilon_j} d\varepsilon_l \rho(\varepsilon_l) \tilde{G}_2(\varepsilon_i, \varepsilon_l, \mathbf{k}, p) \right\} \tilde{g}(\varepsilon_j, \mathbf{k}, p). \tag{5.16}
\end{aligned}$$

Thus the following integral equation for $\tilde{G}_2(\varepsilon_i, \varepsilon_j, \mathbf{k}, p)$ is obtained

$$\begin{aligned}
\tilde{G}_2(\varepsilon_i, \varepsilon_j, \mathbf{k}, p) &= \left\{ \tilde{G}_1(\varepsilon_i, p) \theta(\varepsilon_j - \varepsilon_i) + \right. \\
&\quad \left. \int_{-\infty}^{\varepsilon_j} d\varepsilon_l \rho(\varepsilon_l) \tilde{G}_2(\varepsilon_i, \varepsilon_l, \mathbf{k}, p) \right\} \tilde{g}(\varepsilon_j, \mathbf{k}, p). \tag{5.17}
\end{aligned}$$

The corresponding differential equation reads

$$\frac{\partial}{\partial \varepsilon_j} \left[\frac{\tilde{G}_2(\varepsilon_i, \varepsilon_j, \mathbf{k}, p)}{\tilde{g}(\varepsilon_j, \mathbf{k}, p)} \right] = \tilde{G}_1(\varepsilon_i, p) \delta(\varepsilon_j - \varepsilon_i) + \rho(\varepsilon_j) \tilde{G}_2(\varepsilon_i, \varepsilon_j, \mathbf{k}, p). \tag{5.18}$$

The solution reads

$$\tilde{G}_2(\varepsilon_i, \varepsilon_j, \mathbf{k}, p) = \theta(\varepsilon_j - \varepsilon_i) \tilde{G}_1(\varepsilon_i, p) \tilde{g}(\varepsilon_j, \mathbf{k}, p) \exp \left(\int_{\varepsilon_i}^{\varepsilon_j} d\varepsilon_l \rho(\varepsilon_l) \tilde{g}(\varepsilon_l, \mathbf{k}, p) \right). \tag{5.19}$$

We note that an expansion of the exponential function corresponds with the multi-step approach of Movaghar *et al.* [11, 12].

What remains is the calculation of $\tilde{g}(\varepsilon_j, \mathbf{k}, p)$. For the description of luminescence, only $\tilde{g}(\varepsilon_j, \mathbf{k} = 0, p)$ is required

$$\begin{aligned}
\tilde{g}(\varepsilon_j, \mathbf{k} = 0, p) &= \int d\mathbf{R}_{ij} \langle W_{ij} G_{jj}^0(p) \rangle_{ij} \\
&= \left[\int d\mathbf{R}_{ij} \langle W_{ij} G_{jj}^0(p) \rangle_{ij} \right] \frac{1}{n(\varepsilon_j)} \int_{-\infty}^{\varepsilon_j} d\varepsilon_i \rho(\varepsilon_i)
\end{aligned}$$

$$\begin{aligned}
&= \frac{N}{n(\varepsilon_j)} \int d\mathbf{R}_{ij} d\varepsilon_i \frac{\rho(\varepsilon_i)}{N} \langle W_{ij} G_{jj}^0(p) \rangle_{ij} \\
&= \frac{N}{n(\varepsilon_j)} \langle W_{ij} G_{jj}^0(p) \rangle_j \approx \frac{1}{n(\varepsilon_j)} \left\langle \sum_{i \neq j} W_{ij} G_{jj}^0(p) \right\rangle_j \\
&= \frac{1}{n(\varepsilon_j)} \left\langle \frac{\sum_{i \neq j} W_{ij}}{p + \lambda + \sum_{\mu \neq j} W_{\mu j}} \right\rangle_j \\
&= \frac{1 - (p + \lambda) \tilde{G}_1(\varepsilon_j, p)}{n(\varepsilon_j)}. \tag{5.20}
\end{aligned}$$

5.3 Photoluminescence

Having obtained the configurationally averaged Green functions, we can now write down explicit expressions for the luminescence intensity as a function of time, emission energy, and excitation energy. The luminescence intensity $L_1(\varepsilon_j, t)$ of excitons that have not migrated from their initial site follows from substitution of Eq. (5.7) into Eq. (5.4),

$$\begin{aligned}
L_1(\varepsilon_j, t) &= \lambda \Omega \rho(\varepsilon_j) f^0(\varepsilon_j) G_1(\varepsilon_j, t) \\
&= \lambda \Omega \rho(\varepsilon_j) f^0(\varepsilon_j) \exp\left(-\lambda t - n(\varepsilon_j) \frac{4}{3} \pi R_0^3 \sqrt{\pi \nu_0 t}\right). \tag{5.21}
\end{aligned}$$

The luminescence intensity $\tilde{L}_2(\varepsilon_i, \varepsilon_j, p)$ of excitons that have migrated from their initial site is obtained by substitution of Eq. (5.19) into Eq. (5.5),

$$\begin{aligned}
\tilde{L}_2(\varepsilon_i, \varepsilon_j, p) &= \lambda \Omega \rho(\varepsilon_i) \rho(\varepsilon_j) f^0(\varepsilon_j) \tilde{G}_2(\varepsilon_i, \varepsilon_j, \mathbf{k} = 0, p) \\
&= \lambda \Omega \rho(\varepsilon_i) \rho(\varepsilon_j) f^0(\varepsilon_j) \theta(\varepsilon_j - \varepsilon_i) \tilde{G}_1(\varepsilon_i, p) \\
&\times \tilde{g}(\varepsilon_j, \mathbf{k} = 0, p) \exp\left(\int_{\varepsilon_i}^{\varepsilon_j} d\varepsilon_l \rho(\varepsilon_l) \tilde{g}(\varepsilon_l, \mathbf{k} = 0, p)\right). \tag{5.22}
\end{aligned}$$

Here $\tilde{G}_1(\varepsilon_i, p)$ is given by Eq. (5.9) and $\tilde{g}(\varepsilon_j, \mathbf{k}=0, p)$ by Eq. (5.20). The time-dependent luminescence intensity $L_2(\varepsilon_i, \varepsilon_j, t)$ for a given density of states $\rho(\varepsilon)$ and initial condition $f^0(\varepsilon)$ can now be evaluated using a numerical Laplace inversion routine. The time-integrated luminescence intensity is obtained by evaluating Eq. (5.22) at $p = 0$.

When the system is excited at $t = 0$ by a flash of white light [$f^0(\varepsilon) = f^0$], the Laplace transform of the time-dependent PL spectrum is given by

$$\tilde{L}(\varepsilon_i, p) = \lambda \Omega f^0 \rho(\varepsilon_i) \tilde{G}_1(\varepsilon_i, p)$$

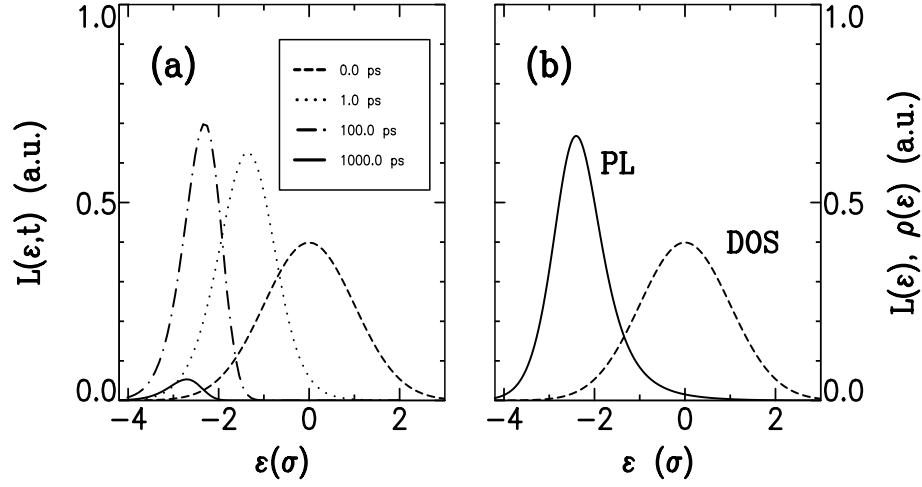


Figure 5.1: a) The transient photoluminescence (PL) spectrum $L(\epsilon, t)$ in a system with a Gaussian density of states as a function of the energy ϵ at various times t after illumination by a short white-light pulse at $t = 0$. The spectrum is being red-shifted in time as the excitons migrate towards sites at lower energy. b) The stationary PL spectrum $L(\epsilon)$ (solid line) as a function of ϵ under constant illumination by a white-light source. The PL spectrum is red-shifted with respect to the Gaussian density of states $\rho(\epsilon)$ (dashed line) due to the exciton migration.

$$\begin{aligned}
& \times \left\{ 1 + \int_{\epsilon_i}^{\infty} d\epsilon_j \rho(\epsilon_j) \tilde{g}(\epsilon_j, 0, p) \exp \left[\int_{\epsilon_i}^{\epsilon_j} d\epsilon_l \rho(\epsilon_l) \tilde{g}(\epsilon_l, 0, p) \right] \right\} \\
& = \lambda \Omega f^0 \rho(\epsilon_i) \tilde{G}_1(\epsilon_i, p) \exp \left[\int_{\epsilon_i}^{\infty} d\epsilon_l \rho(\epsilon_l) \tilde{g}(\epsilon_l, 0, p) \right] \\
& = \lambda N f^0 \rho(\epsilon_i) \frac{\tilde{G}_1(\epsilon_i, p)}{n(\epsilon_i)} \exp \left[-(p + \lambda) \int_{\epsilon_i}^{\infty} d\epsilon_l \rho(\epsilon_l) \frac{\tilde{G}_1(\epsilon_l, p)}{n(\epsilon_l)} \right].
\end{aligned} \tag{5.23}$$

The time-integrated PL spectrum, together with the time dependent PL spectrum is shown in Fig. 5.1 for a system with a Gaussian density of states. Due to the migration of excitons to lower energies, the PL spectrum is red shifted and narrowed with respect to the absorption spectrum. This spectral diffusion and spectral narrowing has been observed experimentally in various disordered organic systems. An example of such an observation

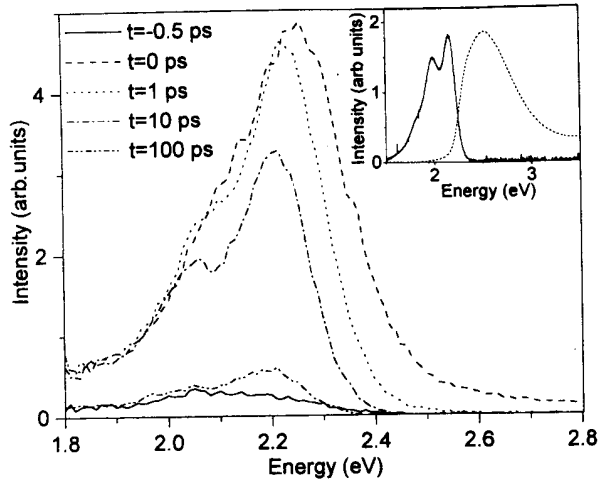


Figure 5.2: Experimentally observed time-resolved PL spectra of poly[2-methoxy,5-(2'-ethyl-hexyloxy)-p-phenylene vinylene] (MEH-PPV) after excitation with 200 fs pulses at 3.06 eV. The inset shows the time-integrated PL spectrum, red shifted with respect to the absorption spectrum. Figure is taken from Ref. [13].

for a conjugated polymer is given in Fig. 5.2.

From Fig. 5.1 we see that the transient PL peak first shifts logarithmically in time to lower energies (as observed experimentally for conjugated polymers, see Fig. 5.2 or Ref. [5]) and then collapses at the so-called localization energy at times of the order λ^{-1} . When the excitons have reached this localization energy, the probability of decay has become greater than the probability to migrate further to lower energies. As a result, the position of the localization energy (marked by the position of the time-integrated PL peak) is a function of intrinsic material properties [$\rho(\varepsilon)$, ν_0 , R_0 , and λ], but *not* of the initial excitation energy [the initial condition $f^0(\varepsilon)$]. When only sites at energies lower than ε_{loc} are selectively excited, the probability of decay on the initial site is larger than the probability to migrate to lower energies. In that case, the Stokes shift between absorption and emission is zero.

This turnover from excitation-independent emission to (quasi) resonant emission—one of the hallmarks of spectral diffusion of excitons—has been observed experimentally in site-selective fluorescence experiments on conjugated polymer systems [7]. A typical example is shown in Fig. 5.3. Let

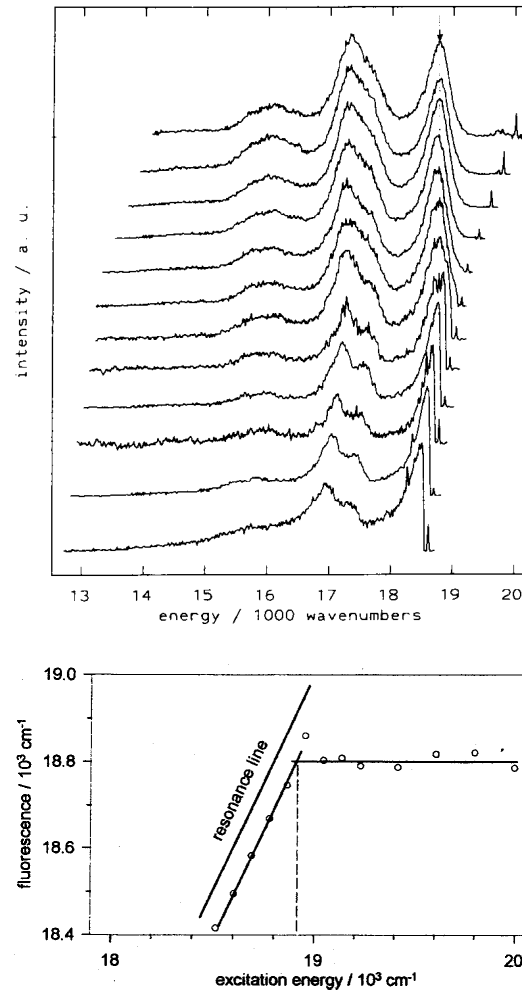


Figure 5.3: *Upper figure: Low temperature (6 K) measured photoluminescence spectra of poly(2-tetrahydrothiophene-p-phenylene vinylene) site-selectively excited at various excitation energies. The high-energy spike marks the laser energy. Lower figure: High energy peak of the photoluminescence spectrum from the upper figure plotted versus excitation energy. For excitation above the localization energy, the position of the PL peak is independent of excitation energy. Below the localization energy, resonant emission is observed, accompanied by a small additional Stokes shift due to vibrational relaxation. Figures taken from the chapter by H. Bässler in Ref. [9].*

us establish the relation between the localization energy and the system parameters describing exciton migration and decay. The value of the localization energy follows directly from the maximum of the time-integrated luminescence intensity. Taking the derivative of $\tilde{L}(\varepsilon_i, p = 0)$ with respect to ε_i , we find

$$\frac{1}{\rho(\varepsilon)} \frac{\partial \rho(\varepsilon)}{\partial \varepsilon} + \frac{n(\varepsilon)}{\lambda \tilde{G}_1(\varepsilon, p = 0)} \frac{\partial}{\partial \varepsilon} \left(\frac{\lambda \tilde{G}_1(\varepsilon, p = 0)}{n(\varepsilon)} \right) + \rho(\varepsilon) \frac{\lambda \tilde{G}_1(\varepsilon, p = 0)}{n(\varepsilon)} = 0. \quad (5.24)$$

We note that this relation is independent of the initial condition. Using Eq. (5.9), we find

$$\lambda^2 \tilde{G}_1^2(\varepsilon, p = 0) + 2b(\varepsilon) \lambda \tilde{G}_1(\varepsilon, p = 0) - 1 = 0, \quad (5.25)$$

with

$$b(\varepsilon) \equiv \zeta^2 + \frac{n(\varepsilon)}{2\rho(\varepsilon)} \frac{d \ln \rho(\varepsilon)}{d\varepsilon}. \quad (5.26)$$

When $\rho(\varepsilon)$ increases with decreasing ε , the maximum intensity will be at the lowest energy possible. For a decreasing $\rho(\varepsilon)$, $b(\varepsilon)$ is positive and the position of the peak is given by:

$$\lambda \tilde{G}_1(\varepsilon, p = 0) = -b(\varepsilon) + \sqrt{b(\varepsilon)^2 + 1}. \quad (5.27)$$

When the density of localized states has an exponential form [$\rho(\varepsilon) = (n/k_B T_0) \exp(\varepsilon/k_B T_0)$ for $-\infty < \varepsilon < 0$], the localization energy can be determined analytically. Substitution of $\rho(\varepsilon)$ into Eq. (5.27) yields

$$1 + \sqrt{\pi} \zeta \exp(\zeta^2) [\operatorname{erf}(\zeta) - 1] = -\zeta^2 - 1/2 + \sqrt{(\zeta^2 + 1/2)^2 + 1}, \quad (5.28)$$

with the solution $\zeta_{loc} = 0.369$. The value for ε_{loc} then follows from definition (5.10) of ζ ,

$$\varepsilon_{loc}/k_B T_0 = \ln(\zeta_{loc}) - \ln \left(n \frac{2}{3} \pi R_0^3 \sqrt{\pi \nu_0 / \lambda} \right). \quad (5.29)$$

For organic systems, the density of localized states is usually modeled by a Gaussian [$\rho(\varepsilon) = n \exp(-\varepsilon^2/2\sigma^2)/\sqrt{2\pi\sigma^2}$]. In that case

$$b(\varepsilon) = \zeta^2 - \frac{\varepsilon n(\varepsilon)}{2\rho(\varepsilon)\sigma^2}. \quad (5.30)$$

Substituting this result into Eq. (5.27), the localization energy as a function of the material parameters can be calculated numerically. The result is shown in Fig. 5.4.

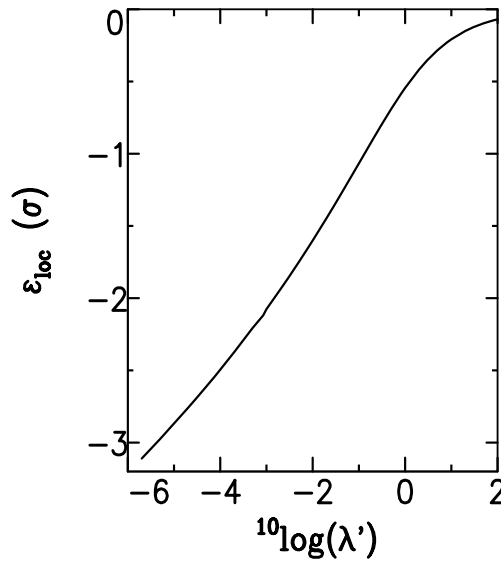


Figure 5.4: Localization energy ε_{loc} as a function of $\lambda' = \lambda[\nu_0\pi(n4\pi R_0^3/3)^2]^{-1}$ in a system with a Gaussian density of states of width σ .

Summarizing, we have described the dynamics of excitons in energetically and spatially disordered molecular systems using a Green function formalism. The configurational average of the Green functions has been calculated explicitly for a system with Förster-type transfer, random site positions, and an arbitrary form of the density of localized states. Two characteristic features of exciton migration in disordered molecular systems, the time evolution of the transient photoluminescence spectrum and the concept of a localization energy, are discussed in detail and compared with experimental results on conjugated polymer systems.

References

- [1] See, e.g., K. C. Kao and W. Hwang, *Electrical Transport in Solids, with Particular Reference to Organic Semiconductors* (Pergamon, Oxford, 1981); M. Pope and C. E. Swenberg, *Electronic Processes in Organic Crystals* (Clarendon, Oxford, 1982).
- [2] Th. Förster, Z. Naturforsch. **4a**, 321 (1949).
- [3] A. S. Davydov and E. F. Sheka, Phys. Status Solidi **11**, 877 (1965).
- [4] A. J. Heeger, S. Kivelson, J. R. Schrieffer, and W. P. Su, Rev. Mod. Phys. **60**, 781 (1988).
- [5] H. Bässler, V. Brandl, M. Deussen, E. O. Göbel, R. Kersting, H. Kurz, U. Lemmer, R. F. Mahrt, and A. Ochse, Pure Appl. Chem. **67**, 377 (1995).
- [6] R. Kersting, U. Lemmer, R. F. Mahrt, K. Leo, H. Kurz, H. Bässler, and E. O. Göbel, Phys. Rev. Lett. **70**, 3820 (1993).
- [7] U. Rauscher, H. Bässler, D. D. C. Bradley, and M. Hennecke, Phys. Rev. B **42**, 9830 (1990).
- [8] U. Lemmer, A. Ochse, M. Deussen, R. F. Mahrt, E. O. Göbel, H. Bässler, P. Haring Bolivar, G. Wegmann, and H. Kurz, Synth. Met. **78**, 289 (1996).
- [9] N. S. Sariciftci (ed.), *Primary Photoexcitations in Conjugated Polymers: Molecular Exciton versus Semiconductor Band Model* (World Scientific, Singapore, 1997).
- [10] B. Mollay, U. Lemmer, R. Kersting, R. F. Mahrt, H. Kurz, H. F. Kauffmann, and H. Bässler, Phys. Rev. B **50**, 10769 (1994).

- [11] B. Movaghar, B. Ries, and M. Grünewald, *Phys. Rev. B* **34**, 5574 (1986).
- [12] M. Grünewald and B. Movaghar, *J. Phys. Condens. Matter* **1**, 2521 (1989).
- [13] G. R. Hayes, I. D. W. Samuel, and R. T. Phillips, *Phys. Rev. B* **52**, R11569 (1995).

Chapter 6

Exciton migration and field-induced dissociation in conjugated polymers

6.1 Introduction

Conjugated polymers (CPs) have been the subject of intensive research during the last decade due to their potential application in opto-electronic devices [1] and the unique properties expected for one-dimensional (1D) systems [2]. Although both electroluminescence (EL) and photoluminescence (PL) are thought to be due to excitonic emission [1], the exact nature and kinetics of excitons in these systems are still under debate. The results of site selective fluorescence (SSF) experiments [3] and of time and spectrally resolved PL spectroscopy [4, 5] have been interpreted by Bässler and co-workers in terms of a molecular model, where the polymer is treated as an array of sites that are subject to both energetic and positional disorder. Photo-absorption creates excitons that are localized on a site. These Frenkel excitons can either migrate towards sites of lower energy, recombine radiatively, or decay non-radiatively. It is believed that the observed red shift between absorption and emission spectra is—at least for a large part—due to the incoherent migration of excitons before recombination. Of specific interest regarding the EL efficiency of polymer light-emitting diodes are the non-radiative decay mechanisms, such as the dissociation of excitons into free charge carriers in the presence of an electric field. The latter process has been studied through field-induced PL-quenching experiments on CP blends by Kersting *et al.* [6] and Deussen *et al.* [7].

Their results have been interpreted in terms of the molecular model, where exciton dissociation requires the intermediate formation of an indirect exciton (charge-transfer state, interchain exciton), i.e., a Coulombically bound electron-hole pair on two neighboring sites. However, there is an ongoing controversy about indirect excitons in CPs, the existence of which seems to depend heavily on the type of material and sample preparation (see, e.g., Refs. [8–10]). Furthermore, the 1D character of the CP chains [2] plays no role within the molecular model. This 1D character can give rise to excitons that are of the Frenkel type perpendicular to the chain direction, but of the Mott-Wannier type along the chain direction [11, 12], thus allowing for a *direct* 1D Onsager-like dissociation process [13] that does not require the formation of an indirect exciton.

In this Chapter, we demonstrate that a *combination* of the molecular migration model and the on-chain dissociation process satisfactorily accounts for the field-induced PL quenching experiments of Kersting *et al.* [6] and Deussen *et al.* [7]. Within our analytic theory, we derive an exact expression for the PL spectrum at zero temperature. Previously, time-dependent PL quenching [6] has been described theoretically by Arkhipov *et al.* [14]. Our theory is different in two respects that are essential for understanding the experimental results [6, 7]: Firstly, unlike in Ref. [14], we take into account recombination of excitons after the first migration step. Secondly and most importantly, Arkhipov *et al.* [14] assume that the formation of an indirect exciton is the primary step of exciton dissociation. Our assumption of on-chain dissociation is supported by the experimental observation that the PL quenching in CP blends is in fact *independent* of the concentration of active material, except for very dilute blends [7]. From comparison with recent PL-quenching experiments on molecularly doped polymer systems [15], which *do* show an increase of quenching efficiency over the whole range of concentrations studied, it was concluded that *intramolecular* dissociation processes indeed play an important role in the CP blends, in contrast with the molecularly doped polymer systems.

6.2 Exciton migration

Let us start with an outline of the theory of exciton migration in disordered media. For more details, the reader is referred to Chapter 5 of this thesis. Consider a system with N localized states i , with position \mathbf{R}_i and exciton energy ε_i . For low excitation densities, the occupational probability $f_i(t)$

of the site i at time t is described by a linearized master equation

$$\frac{\partial}{\partial t} f_i(t) = - \sum_{j \neq i} W_{ji} f_i(t) + \sum_{j \neq i} W_{ij} f_j(t) - \lambda f_i(t), \quad (6.1)$$

where W_{ij} is the transition rate from site j to site i , and λ is the loss rate due to both radiative recombination and non-radiative decay processes, which for the moment is assumed to be constant for all sites. The transitions of neutral optical excitations are described by Förster rates [16], which, at zero temperature, have the form $W_{ij} = w_{ij} \theta(\varepsilon_j - \varepsilon_i)$, with

$$w_{ij} = \nu_0 \left(\frac{R_0}{R_{ij}} \right)^6 \quad (6.2)$$

and $\theta(x) = 1$ if $x > 0$, $\theta(x) = 0$ otherwise. Here, ν_0 is the nearest neighbor jump frequency, R_0 is the nearest neighbor distance, and $R_{ij} \equiv |\mathbf{R}_i - \mathbf{R}_j|$.

Eq. (6.1) can be solved using a Green function formalism [17]. The Green function $G_{ij}(t)$ is the probability to find a particle at site i at a time t , given that it was at site j at $t = 0$, and is a function of all N positions and energies of a given configuration $\{\mathbf{R}_k, \varepsilon_k\}$. Assuming uncorrelated positions and energies, the configurational averages of the local Green function $G_{jj}(t)$ and the non-local Green function $G_{ij}(t)$ (with $i \neq j$) are given by

$$G_1(\varepsilon_j, t) \equiv \int \left[\prod_{k \neq j} d\mathbf{R}_k d\varepsilon_k \frac{\rho(\varepsilon_k)}{N} \right] G_{jj}(t), \quad (6.3)$$

$$G_2(\varepsilon_i, \varepsilon_j, \mathbf{R}_{ij}, t) \equiv \int \left[\prod_{k \neq i, j} d\mathbf{R}_k d\varepsilon_k \frac{\rho(\varepsilon_k)}{N} \right] G_{ij}(t), \quad (6.4)$$

where $\rho(\varepsilon_k)$ denotes the density of localized states at energy ε_k .

The average local Green function has been evaluated exactly for large N by Förster [16],

$$G_1(\varepsilon_j, t) = \exp \left[-\lambda t - n(\varepsilon_j) \frac{4}{3} \pi R_0^3 \sqrt{\pi \nu_0 t} \right], \quad (6.5)$$

with $n(\varepsilon_j) \equiv \int_{-\infty}^{\varepsilon_j} d\varepsilon \rho(\varepsilon)$ the density of sites with energies below ε_j .

Following Movaghar *et al.* [17], we find for the Fourier-Laplace transform of $G_2(\varepsilon_i, \varepsilon_j, \mathbf{R}_{ij}, t)$,

$$\begin{aligned} \tilde{G}_2(\varepsilon_i, \varepsilon_j, \mathbf{k}, p) &= \theta(\varepsilon_j - \varepsilon_i) \tilde{G}_1(\varepsilon_i, p) \tilde{g}(\varepsilon_j, \mathbf{k}, p) \\ &\times \exp \left[\int_{\varepsilon_i}^{\varepsilon_j} d\varepsilon_l \rho(\varepsilon_l) \tilde{g}(\varepsilon_l, \mathbf{k}, p) \right], \end{aligned} \quad (6.6)$$

where $\tilde{G}_1(\varepsilon_i, p)$ is the Laplace transform of $G_1(\varepsilon_i, t)$ and $\tilde{g}(\varepsilon_j, \mathbf{k}, p)$ is the Fourier-Laplace transform of the average probability to jump at time t from site j to site i (given that $\varepsilon_i < \varepsilon_j$). For $\mathbf{k} = \mathbf{0}$, one has [17]

$$\tilde{g}(\varepsilon_j, \mathbf{0}, p) = \frac{1}{n(\varepsilon_j)} \left[1 - (p + \lambda) \tilde{G}_1(\varepsilon_j, p) \right]. \quad (6.7)$$

We note that an expansion of our result (6.6) corresponds to the multi-step approach of Movaghar *et al.* [17].

The PL intensity at time t after photo-absorption can be written as

$$L(t) = \int d\varepsilon_j L_1(\varepsilon_j, t) + \int d\varepsilon_i d\varepsilon_j L_2(\varepsilon_i, \varepsilon_j, t), \quad (6.8)$$

$$L_1(\varepsilon_j, t) \equiv \eta \lambda \Omega \rho(\varepsilon_j) f_j(0) G_1(\varepsilon_j, t), \quad (6.9)$$

$$L_2(\varepsilon_i, \varepsilon_j, t) \equiv \eta \lambda \Omega \rho(\varepsilon_i) \rho(\varepsilon_j) f_j(0) \int d\mathbf{R}_{ij} G_2(\varepsilon_i, \varepsilon_j, \mathbf{R}_{ij}, t), \quad (6.10)$$

with η the efficiency of radiative recombination and Ω the system volume. The PL intensity $L_1(\varepsilon_j, t)$ is due to excitons that recombine at their initial site with energy ε_j and $L_2(\varepsilon_i, \varepsilon_j, t)$ is from excitons that recombine on a site with energy ε_i after migration from the initial site with energy ε_j . Note that the latter contribution has not been taken into account in Ref. [14].

Eqs. (6.5)–(6.2) allow us to study PL spectra for arbitrary initial condition $f_j(0)$ and density of localized states $\rho(\varepsilon)$. In most cases, the system is excited either by a broad-band light source, $f_j(0) = f^0$, or by a narrow-width laser pulse with energy ε_0 , $f_j(0) = f^0 \delta(\varepsilon_j - \varepsilon_0)$. For example, SSF experiments [3] can be described by varying the excitation energy ε_0 . Time-integrated PL spectra can be evaluated directly by substituting $p = 0$ in the Laplace transforms of Eqs. (6.2), whereas time resolution can be obtained using a numerical Laplace inversion routine.

6.3 Field-induced photoluminescence quenching

In the following, our theory of exciton migration is used to interpret field-induced PL-quenching experiments by Deussen *et al.* [7] and Kersting *et al.* [6]. Both study the optical response of thin-film light-emitting diode structures made from blends of poly(phenyl-*p*-phenylene vinylene) (PPPV) and polycarbonate (PC), initially excited by a laser pulse with energy ε_0 . We assume—as they did—that the polymers are perfectly mixed. We further expect the zero-temperature approach to be valid as the experiments are performed at 70–80 K, whereas typical energy differences are of order 0.1 eV.

In the presence of an applied electric field, the PL intensity of these systems, $L^q(t)$, is reduced. In Ref. [7], the relative decrease of the *time-integrated* PL intensity,

$$Q = \frac{\tilde{L}(p=0) - \tilde{L}^q(p=0)}{\tilde{L}(p=0)}, \quad (6.11)$$

is studied as a function of the excitation energy ε_0 , the relative concentration $c \in [0, 1]$ of active material (PPPV), and the strength of the electric field E . In Fig. 6.1, the concentration dependence of Q is given for various field strengths. In Ref. [6], the *transient* PL quenching,

$$Q(t) = \frac{L(t) - L^q(t)}{L(t)}, \quad (6.12)$$

is studied for a system with fixed ε_0 , c , and E . Their results are given in Fig. 6.2.

In the absence of an electric field, the PL intensity is described by

$$\begin{aligned} \tilde{L}(p) = & \eta\lambda\Omega f^0 \rho(\varepsilon_0) \left\{ \tilde{G}_1(\varepsilon_0, p) + \tilde{g}(\varepsilon_0, \mathbf{0}, p) \int_{-\infty}^{\varepsilon_0} d\varepsilon_i \rho(\varepsilon_i) \right. \\ & \left. \times \tilde{G}_1(\varepsilon_i, p) \exp \left[\int_{\varepsilon_i}^{\varepsilon_0} d\varepsilon_l \rho(\varepsilon_l) \tilde{g}(\varepsilon_l, \mathbf{0}, p) \right] \right\}. \end{aligned} \quad (6.13)$$

The energy integration can be evaluated exactly for arbitrary $\rho(\varepsilon)$, resulting in an exponential time decay as found in PL experiments on CP blends and solutions (see, e.g., Refs. [8, 10]). From time-resolved PL experiments [4, 8–10], we estimate $\lambda \approx (300 \text{ ps})^{-1}$ and $\nu_0 \approx 10^{13} \text{ Hz}$. We take $n \frac{4}{3} \pi R_0^3 = c$, with $n \equiv n(\varepsilon \rightarrow \infty) = N/\Omega$.

To describe the quenched PL intensity in the presence of an electric field, our key assumption is an on-chain dissociation of excitons. One may expect that the dissociation of an exciton on a given site depends on the strength of the electric field, the orientation of the CP chain segment with respect to the electric field, and the exciton binding energy. We model this as follows: dissociation can only occur on a fraction α of the sites with a loss rate λ_d , so that the total loss rate is $\lambda + \lambda_d$; on the other sites the total loss rate is just λ . The specific on-chain character of the dissociation process is reflected in the concentration independence of the parameters λ_d and α . In the following, we will just fit these parameters to the experiments, leaving a detailed physical interpretation to future work. We do not take into account the second-order Stark effect, which leads to an additional red shift in the PL spectrum and a reduction of η .

When dissociation sites are present, the average local Green function reads

$$\tilde{G}_1^q(\varepsilon_j, p) = (1 - \alpha)\tilde{G}_1(\varepsilon_j, p) + \alpha\tilde{G}_1^d(\varepsilon_j, p), \quad (6.14)$$

where $\tilde{G}_1^d(\varepsilon_j, p)$ is the Laplace transform of Eq. (6.5) with λ replaced by $\lambda + \lambda_d$. For the average probability to jump from site j one has

$$\begin{aligned} \tilde{g}^q(\varepsilon_j, \mathbf{0}, p) &= \frac{1}{n(\varepsilon_j)} \left[1 - (1 - \alpha)(p + \lambda)\tilde{G}_1(\varepsilon_j, p) \right. \\ &\quad \left. - \alpha(p + \lambda + \lambda_d)\tilde{G}_1^d(\varepsilon_j, p) \right]. \end{aligned} \quad (6.15)$$

The quenched PL intensity, $\tilde{L}^q(p)$, follows from substitution of Eqs. (6.14) and (6.15) into Eq. (6.13).

Although many microscopic parameters have been introduced, we find from Eq. (6.11) that Q is a function of only four independent parameters: the fraction of sites with energies below the excitation energy $n(\varepsilon_0)/n$; the fraction of dissociation sites α ; the relative recombination and dissociation rates λ' and λ'_d , given by

$$\frac{\lambda}{\lambda'} = \frac{\lambda_d}{\lambda'_d} = \pi\nu_0 \left(n \frac{4}{3} \pi R_0^3 \right)^2. \quad (6.16)$$

As an important consequence, our expression for the PL quenching is *independent* of the form of the density of states $\rho(\varepsilon)$. Taking experimental parameters, we estimate $\lambda' = 10^{-4}/c^2$.

Conforming to the results of Ref. [7], we find that Q is approximately constant as a function of excitation energy [or $n(\varepsilon_0)/n$] except for very low energies. Consequently, the PL quenching is only weakly dependent on the initial condition $f_j(0)$.

The concentration dependence of Q , as given in Fig. 6.1, can be understood as follows: At very low c , the excitons are immobile ($\lambda' \rightarrow \infty$) and Q is given by the quenching efficiency of an isolated site,

$$\lim_{c \rightarrow 0} Q = \alpha \frac{\lambda_d}{\lambda + \lambda_d}. \quad (6.17)$$

With increasing c , the excitons visit more sites during their lifetime yielding a higher probability of an encounter with a dissociation site, so that Q increases. As c further increases, migration from dissociation sites before dissociation takes place results in a saturation of Q . This competition between dissociation and migration depends on λ'_d .

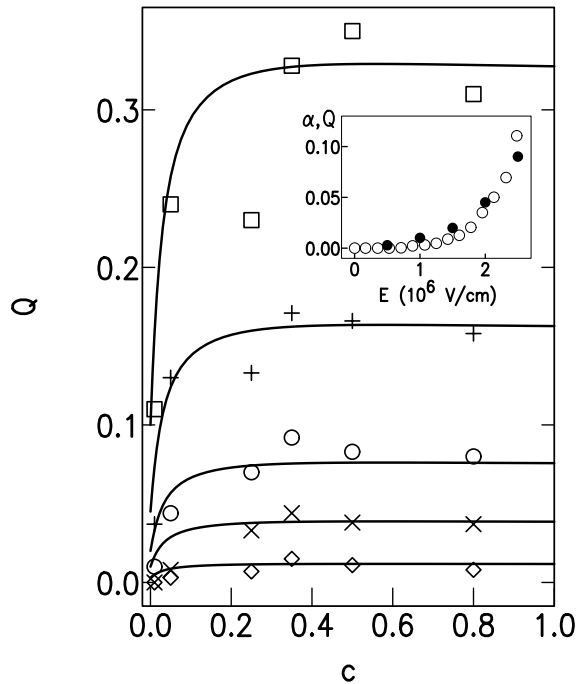


Figure 6.1: Photoluminescence quenching Q as a function of concentration c for an electric field $E = 0.5, 1.0, 1.5, 2.0$, and 2.5 MV/cm (bottom to top). The parameters used are $n(\varepsilon_0)/n = 0.9$, $\lambda' = 10^{-4}/c^2$, and $\lambda'_d = 0.1/c^2$. The values of α are given in the inset (dots), together with Q for $c = 0.01$ (circles). Experimental data are taken from Ref. [7].

In Fig. 6.1, the experimental values of Q as a function of c for various E are compared with our theory. Given the minimal assumptions put in our model, the agreement is quite good. The values of λ'_d and α are determined from the onset of saturation at $c \approx 0.3$ and the saturation values of Q for different E . We find good agreement using $\lambda'_d = 0.1/c^2$ for all values of E , which corresponds to $\lambda_d \approx (300 \text{ fs})^{-1}$. The values of α for each E are depicted in the inset of Fig. 6.1. According to Eq. (6.17), these values should match the experimental values of Q at $c = 0.01$ (see the inset of Fig. 6.1). We note that further improvement may be achieved taking into account, e.g., an E -dependence of η or a sample-dependent trap density.

We stress that recombination of migrating excitons, i.e. $L_2(\varepsilon_i, \varepsilon_0, t)$, is required to describe the increase of Q at low c and that the concentration-independence of the dissociation process is essential to obtain the saturation of Q at high c .

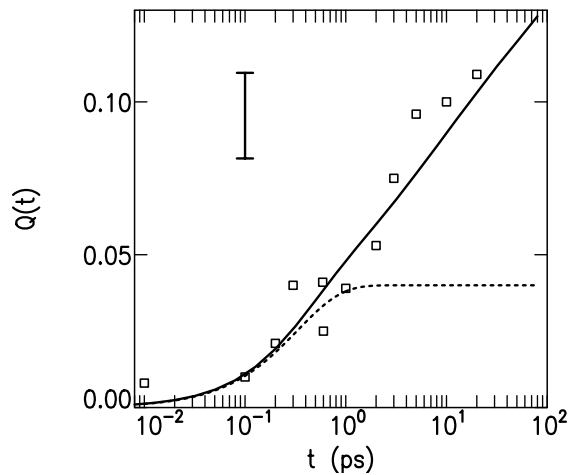


Figure 6.2: *Transient photoluminescence quenching $Q(t)$ as a function of time t (solid line). The same parameters are used as in Fig. 1, with $c = 0.2$ and $\alpha = 0.04$. The dashed line denotes the quenching when the luminescence of migrated excitons, $L_2(\varepsilon_i, \varepsilon_0, t)$, is neglected. Experimental data are taken from Ref. [6]. An indication of the experimental error is given in the upper left corner.*

Let us make the comparison with the experimental results of Kersting *et al.* [6] on a PPPV/PC sample with $c = 0.2$. We simply use the same set of parameters as above. The time-integrated PL quenching $Q = 0.135$ yields $\alpha = 0.04$. The transient PL quenching $Q(t)$ [Eq. (6.12)] is compared with experiment in Fig. 6.2. Given the fact that we have not used any fitting parameters, the agreement is remarkable. For comparison, we have also plotted the quenching when recombination *after* migration, i.e. $L_2(\varepsilon_i, \varepsilon_0, t)$, is not taken into account. We see that, after the first picosecond, the increase of $Q(t)$ is entirely due to the migration of excitons, which, for long times, leads to $Q(t \rightarrow \infty) = 1$.¹ This is in stark contrast with the

¹For the intermediate time regime, Fig. 2 suggests that $Q(t) \propto \ln(t)$. Indeed, one can

model proposed in Ref. [14], where $Q(t)$ saturates towards the value of Q , but it is in agreement with the experimental findings of Kersting *et al.* [6], who report a further PL quenching on a time scale of several hundred picoseconds.

6.4 Conclusion

We have presented an analytic zero-temperature theory of exciton migration and PL in a disordered medium which can be used to interpret a variety of spectroscopic experiments. The theory has been applied to describe field-induced PL-quenching experiments in PPPV blends. We find that the effect is governed by a subtle balance of recombination, migration, and *on-chain* dissociation and that close agreement with experiment is obtained for realistic values of the parameters involved. It would be interesting to ascertain to which extent the on-chain dissociation occurs in other CPs.²

6.5 Appendix

The results presented in this Chapter have led to the following discussion with dr. E.M. Conwell from Xerox Wilson Center for Research and Technology/University of Rochester, New York.

Comment by E.M. Conwell

Exciton dissociation by high electric field in conducting polymers such as poly(phenylene vinylene) (PPV) and poly(phenyl-*p*-phenylene vinylene) (PPPV) has been demonstrated experimentally [6, 7] and attributed to the electron and hole separating onto different chains or different conjugation segments [6, 7, 14]. In a recent Letter Vissenberg and de Jong [20] challenged the view that dissociation may involve separation onto two chains. They showed that good agreement with experiment can be obtained with a theory in which the dissociation takes place on chain, suggesting that it is due to a one-dimensional (1D) Onsager-like process. Unfortunately their

derive that, up to linear order in α , $Q(t) = \alpha [1 + 1/2 \ln(1 + \pi\nu_0[cn(\varepsilon_0)/n]^2 t)]$.

²Recent photoconductivity studies [18] and time-resolved pump-probe experiments [19] on a ladder-type poly(*p*-phenylene) show indications of a direct on-chain dissociation mechanism.

theory ignores some facts about these polymers that make their suggested process quite improbable.

The experiments on electric-field-induced quenching of photoluminescence (PL) for PPPV dispersed in an inert polymer [polycarbonate (PC)] matrix show that quenching (1) becomes quite small at low PPPV concentrations and (2) saturates at higher concentrations [7]. The observation (1) is clearly evidence against exciton dissociation on chain. Vissenberg and de Jong state that the observation (2) supports their assumption of on-chain dissociation [20]. They take it to be evidence that the PPPV is distributed uniformly in the PC matrix. That is most unlikely. It is well known that polymers are in general immiscible. Mixtures of polymers tend to phase segregate so that there are likely to be other chains of the same polymer near by except for extreme dilution. Such segregation has been found in many recent investigations of conducting polymers, particularly polyaniline [21] and polypyrrole [22], in inert polymer matrices. The evidence comes from transmission electron microscopy and scanning electron microscopy images and from the fact that percolation thresholds are much lower than expected for uniform dispersion of the conducting polymers. Thus the observation of concentration independence except for very low concentrations of the luminescent polymer in all likelihood results from phase segregation and cannot be taken as evidence for the existence of well separated chains. It is quite consistent with this explanation that PL quenching experiments on molecularly doped polymers [15] do not show saturation but rather an increase of quenching efficiency over the entire concentration range studied. Entropy considerations dictate that on insertion into an inert polymer molecules are much less likely to phase separate than a second polymer.

It is well known that, although these polymers may have very long chains, the average conjugation length, which determines the delocalization of the π wave functions, is quite short. For PPPV, to which they have applied their theory, the average conjugation length is ~ 6 monomers [23]. For standard PPV estimates on the basis of many different properties give the average conjugation length as 7 to 8 monomers. This is not much greater than the length of an on-chain exciton in this type of polymer, ~ 6 monomers in PPV [24]. It is clearly not possible for the exciton to dissociate by an Onsager-type process on the average length segment. Of course it is still possible that dissociation occurs by the electron or hole jumping to another conjugation segment on the same chain.

The authors' statement that there is an ongoing controversy about the existence of indirect excitons, i.e., electron and hole on separate chains,

deserves comment. Although exciton dissociation to form such a pair is admittedly sample dependent [25], their formation is well established for cyano-PPV, as evidenced by the excimer emission seen in that case [26]. Evidence that such pairs exist in MEH-PPV (poly[2-methoxy,5-(2-ethylhexyloxy) phenylene vinylene]) and PPV, although they do not show excimer emission because the electron-hole distance is too large, has also been presented [27]. In light of these facts it is difficult to believe that field-induced exciton dissociation proceeds exclusively through formation of electron-hole pairs on different conjugation segments of the same chain when there are other chains near by.

Reply

In Ref. [7], the electric-field induced quenching of photoluminescence (PL) in blends of poly(phenyl-*p*-phenylene vinylene) (PPPV) and polycarbonate (PC) as a function of the applied electric field and of the PPPV concentration has been reported. It was found that the quenching is small but finite at low concentrations and that it saturates at concentrations above 30 %. We have shown that this concentration dependence can be well understood using a theory that combines the migration of excitons between different PPPV chain segments with a field-induced dissociation of excitons that takes place on chain [20]. Conwell [28] opposes to the on-chain dissociation process in favor of an interchain dissociation process that involves the formation of an indirect exciton, *i.e.*, a bound electron-hole pair on separate chains.

This type of (intermolecular) dissociation can account for field-induced PL quenching in molecularly doped polymers [15]. Unlike in the PPPV/PC blends, the quenching is zero at low concentrations and increases over the entire concentration range studied. In agreement with our interpretation, Deussen *et al.* ascribe these differences to the occurrence of on-chain dissociation in the polymer PPPV [15]. Conwell argues that the saturation of quenching may be due to a phase segregation in the polymer blend [28]. Although we can not exclude the possibility of phase segregation, there are several reasons to expect on-chain dissociation to play an important role.

According to Conwell, the small quenching at low concentrations of PPPV is “clearly evidence against exciton dissociation on chain” [28]. However, our theory applies to the *whole* range of concentrations and gives good agreement with experiment. In particular, we have found that the quenching at low concentrations corresponds with the probability of dissociation on an isolated chain (see Fig. 1, Ref. [20]).

Furthermore, Conwell claims that the average conjugation length in PPPV is too short for on-chain dissociation to take place. We note that, although the exciton is *delocalized* along ~ 6 monomers, its *size*, *i.e.* the distance between the electron and hole, may be as small as 2 monomers [12]. Most importantly, however, an on-chain dissociation mechanism does not necessarily imply that the dissociation takes place within one conjugated segment of the polymer chain. After an initial charge separation within the chain segment, the on-chain dissociation mechanism may be completed by a subsequent jump of a charge carrier towards the next segment on the same chain. Note that this process does not depend on the nearest neighbor distance, in contrast with indirect exciton formation.

Regarding the existence of indirect excitons, Conwell points out that various indications of this species have been found in derivatives of poly(*p*-phenylene vinylene) [28]. If such indications, like excimer emission, were to be found in PPPV/PC blends, one would indeed expect an additional contribution of interchain dissociation to the field-induced PL quenching. The real question is, however, which is the dominant mechanism for the dissociation of excitons in the presence of a strong electric field.

The model presented in Ref. [20] is not specific for the details of the dissociation mechanism. Consequently, it can be applied to describe on-chain as well as interchain dissociation. We have found that agreement with experiment can only be reached with dissociation parameters that are strictly concentration independent. This has led us to the conclusion that on-chain dissociation is the dominant process in PPPV blends. Conwell's interpretation in terms of interchain dissociation would imply that the formation of indirect excitons is independent of the concentration of PPPV. However, even in the presence of phase segregation, complete independence over the full range of concentrations seems very unlikely.

Finally, we would like to stress that our model of on-chain dissociation can not only quantitatively describe the concentration dependence of field-induced PL quenching in PPPV blends, but the time dependence of the quenching as well. Although alternative explanations, like phase segregation, can not be excluded, this remains a strong indication for the validity of our model.

References

- [1] J. H. Burroughes, D. D. C. Bradley, A. R. Brown, R. N. Marks, K. MacKay, R. H. Friend, P. L. Burn, and A. B. Holmes, *Nature (London)* **347**, 539 (1990).
- [2] A. J. Heeger, S. Kivelson, J. R. Schrieffer, and W. P. Su, *Rev. Mod. Phys.* **60**, 781 (1988).
- [3] U. Rauscher, H. Bässler, D. D. C. Bradley, and M. Hennecke, *Phys. Rev. B* **42**, 9830 (1990).
- [4] R. Kersting, U. Lemmer, R. F. Mahrt, K. Leo, H. Kurz, H. Bässler, and E. O. Göbel, *Phys. Rev. Lett.* **70**, 3820 (1993).
- [5] H. Bässler, V. Brandl, M. Deussen, E. O. Göbel, R. Kersting, H. Kurz, U. Lemmer, R. F. Mahrt, and A. Ochse, *Pure & Appl. Chem.* **67**, 377 (1995).
- [6] R. Kersting, U. Lemmer, M. Deussen, H. J. Bakker, R. F. Mahrt, H. Kurz, V. I. Arkhipov, H. Bässler, and E. O. Göbel, *Phys. Rev. Lett.* **73**, 1440 (1994).
- [7] M. Deussen, M. Scheidler, and H. Bässler, *Synth. Met.* **73**, 123 (1995).
- [8] M. Yan, L. J. Rothberg, E. W. Kwock, and T. M. Miller, *Phys. Rev. Lett.* **75**, 1992 (1995).
- [9] G. R. Hayes, I. D. W. Samuel, and R. T. Philips, *Phys. Rev. B* **52**, R11569 (1995).
- [10] J. W. Blatchford, S. W. Jessen, L. B. Lin, J. J. Lih, T. L. Gustafson, A. J. Epstein, D. K. Fu, M. J. Marsella, T. M. Swager, A. G. MacDiarmid, S. Yamaguchi, and H. Hamaguchi, *Phys. Rev. Lett.* **76**, 1513 (1996).

- [11] H. X. Wang and S. Mukamel, *Chem. Phys. Lett.* **192**, 417 (1992); D. Beljonne, Z. Shuai, R. H. Friend, and J. L. Brédas, *J. Chem. Phys.* **102**, 2042 (1995).
- [12] Á. Horváth, H. Bässler, and G. Weiser, *Phys. Status Solidi B* **173**, 755 (1992).
- [13] M. Gailberger and H. Bässler, *Phys. Rev. B* **44**, 8643 (1991).
- [14] V. I. Arkhipov, H. Bässler, M. Deussen, E. O. Göbel, R. Kersting, H. Kurz, U. Lemmer, and R. F. Mahrt, *Phys. Rev. B* **52**, 4932 (1995).
- [15] M. Deussen, P. Haring Bolivar, G. Wegmann, H. Kurz, and H. Bässler, *Chem. Phys.* **207**, 147 (1996).
- [16] Th. Förster, *Z. Naturforsch.* **4a**, 321 (1949).
- [17] B. Movaghar, B. Ries, and M. Grünewald, *Phys. Rev. B* **34**, 5574 (1986); M. Grünewald and B. Movaghar, *J. Phys. Condens. Matter* **1**, 2521 (1989).
- [18] S. Barth, H. Bässler, U. Scherf, and K. Müllen, *Chem. Phys. Lett.* **288**, 147 (1998).
- [19] W. Graupner, G. Cerullo, G. Lanzani, M. Nisoli, E. J. W. List, G. Leising, and S. De Silvestri, to be published in *Phys. Rev. Lett.*
- [20] M. C. J. M. Vissenberg and M. J. M. de Jong, *Phys. Rev. Lett.* **77**, 4820 (1996) [this Chapter].
- [21] For a summary of a number of studies, see A. B. Kaiser, C. K. Subramaniam, P. W. Gilberd, and B. Wessling, *Synth. Met.* **69**, 197 (1995).
- [22] M. Omastova, S. Kösina, J. Pointeck, A. Janke, and J. Pavlinec, *Synth. Met.* **81**, 49 (1996).
- [23] S. Heun, R. F. Mahrt, A. Greiner, U. Lemmer, H. Bässler, D. A. Halliday, D. D. C. Bradley, P. L. Burn, and A. B. Holmes, *J. Phys. Condens. Matter* **5**, 247 (1993).
- [24] S. C. Graham, D. D. C. Bradley, and R. H. Friend, *Synth. Met.* **41–43**, 1277 (1991).
- [25] E. M. Conwell, *Synth. Met.* **53**, 101 (1996).

-
- [26] I. D. W. Samuel, G. Rumbles, and C. J. Collison, Phys. Rev. B **52**, R11573 (1995).
- [27] E. M. Conwell, J. Perlstein, and S. Shaik, Phys. Rev. B **54**, R2308 (1996).
- [28] E. M. Conwell, preceding Comment, Phys. Rev. Lett. **78**, 4301 (1997).

Chapter 7

Electric field-induced photoluminescence quenching in disordered molecular solids

7.1 Introduction

The interest in the photophysics of organic molecular solids is related to their broad range of applications and to the theoretical challenge of understanding the excited-state dynamics and transport properties of these disordered materials. The electrical and optical properties of organic dyes are determined by π -electrons, which have a relatively small energy gap between the highest occupied molecular orbital (HOMO) and the lowest unoccupied molecular orbital (LUMO). The mechanical properties in the solid state can be improved by dispersing the molecular dye in a polymer matrix. These molecularly doped polymers (MDPs) are broadly utilized in laser printers and photocopiers [1]. Polymers with chromophores built into the backbone or into side chains, and fully π -conjugated polymers (CPs) show promising potential for applications in thin-film devices such as light-emitting diodes [2].

In molecular solids, the excited states are strongly bound electron-hole pairs, localized on a molecular site. In case of energetic disorder, these excitons relax in the course of a random walk to sites with lower energies. This results in a Stokes shift between the absorption and the emission spectrum. In CPs, the π -electrons are not confined to a small molecule, but are delo-

calized over part of the polymer chain. Nevertheless, several spectroscopic studies support a similar molecular exciton picture for CPs [3]. Among these experiments are two complementary studies of electric-field induced photoluminescence (PL) quenching, which provide a direct comparison between a CP [4, 5] and a MDP [6]. The system consists of a polycarbonate matrix, blended with poly(phenyl-*p*-phenylene vinylene) (PPPV) or with tris(stilbene)amine (TSA), which has a chemical structure related to that of PPPV (see inset to Fig. 7.3). In both systems, the dynamics of the PL quenching indicates that the effect is due to the field-induced dissociation of a molecular exciton into separate charge carriers [4, 6]. However, clear differences have been observed in the concentration dependence as well as the ultrafast transient behavior of the electric field-induced PL quenching.

In the CP blends [4, 5], (a) the PL quenching at very low PPPV concentrations is small, but finite, as becomes evident at high fields; (b) the PL quenching first increases and then saturates with increasing concentration; (c) the transient PL quenching keeps increasing at longer times. Recently, we have demonstrated that all these observations can be accounted for using a model that combines the migration of a molecular exciton with an *intramolecular* dissociation mechanism, in which the electron and the hole are separated along the polymer chain [7]. For instance, the finite quenching at low concentrations is a direct reflection of this intramolecular dissociation mechanism. It is also observed in transient photoconductivity studies on CP solutions [8]. However, our conclusion of *intramolecular* dissociation has been opposed by Conwell [9], who suggests an *intermolecular* dissociation process, which involves a jump of one of the charge carriers to a neighboring site. The saturation at higher concentrations was ascribed to phase segregation in the polymer blend. We have replied [10] that phase segregation can not be excluded *a priori*, but that the good agreement with experiments remains a strong indication of the validity of our model.

In MDPs, where exciton dissociation must be of intermolecular nature, it has been observed [6] that (a) the PL quenching at very low TSA concentrations goes to zero, *i.e.* the probability of dissociation on an isolated site is zero; (b) the PL quenching increases with concentration over the whole range of concentrations; (c) after an initial increase, the transient PL quenching saturates at longer times (see Figs. 7.2 and 7.3). In this chapter, we demonstrate that exciton migration, combined with *intermolecular* dissociation of excitons, can account for these observations. This work, combined with our previous work [7], provides a consistent picture of electric field-induced PL quenching in CP and MDP systems, where both the

similarities and the differences can be explained.

7.2 Exciton migration

Let us first recapitulate the general theory, presented in Refs. [7, 11, 12] and in Chapter 5 of this thesis. We consider a system consisting of localized states i , with random positions \mathbf{R}_i and exciton energies ε_i , distributed according to the density of states $\rho(\varepsilon)$. The transition rate from site j to i is of the Förster [13] type, i.e. $W_{ij} = \nu_0 (R_0/R_{ij})^6 \theta(\varepsilon_j - \varepsilon_i)$. Here, the constant R_0 is the average nearest neighbor distance in an undiluted molecular film, ν_0 is the corresponding nearest neighbor jump frequency, $R_{ij} \equiv |\mathbf{R}_i - \mathbf{R}_j|$, and $\theta(x) = 1$ if $x > 0$, $\theta(x) = 0$ otherwise. Only jumps that are downward in energy are considered, as the thermal energy $k_B T$ is usually much smaller than the energy differences between the sites. The exciton decay is described by a site-independent rate λ .

Let the system be excited at $t = 0$ by an incident light pulse, such that all sites have an initial occupational probability f_0 . (Both theory [7, 12] and experiment [5, 6] indicate that the final result is insensitive to the precise initial condition.) Then the PL intensity at time t is given by

$$L(t) = \lambda f_0 \int d\varepsilon \rho(\varepsilon) G_1(\varepsilon, t) + \lambda f_0 \int d\mathbf{R} d\varepsilon d\varepsilon' \rho(\varepsilon) \rho(\varepsilon') G_2(\varepsilon, \varepsilon', \mathbf{R}, t). \quad (7.1)$$

The local Green function $G_1(\varepsilon, t)$ is the average probability that an exciton remains at its initial site,

$$G_1(\varepsilon, t) = \exp \left[-\lambda t - n(\varepsilon) \frac{4}{3} \pi R_0^3 \sqrt{\pi \nu_0 t} \right], \quad (7.2)$$

with $n(\varepsilon) = \int_{-\infty}^{\varepsilon} d\varepsilon' \rho(\varepsilon')$ the density of sites with energies below ε . We note that this probability decays exponentially due to exciton decay, but non-exponentially due to the migration of excitons to different sites. In Eq. (7.1), the non-local Green function $G_2(\varepsilon, \varepsilon', \mathbf{R}, t)$ is the average probability that an exciton has migrated at time t to a site with energy ε at a relative position \mathbf{R} from the initial site with energy ε' . This non-local Green function can be decomposed into local Green functions, describing the different paths an exciton may take to end up at the final site. The expression for the non-local Green function is given in Refs. [7, 12].

7.3 Exciton dissociation

In the presence of an electric field \mathbf{F} , excitons may dissociate into separate charge carriers. The dissociation of excitons is taken into account through an additional decay rate λ_d : on a fraction α of the sites, dissociation can take place and the excitons decay at a total rate $\lambda + \lambda_d$; on the remaining fraction $1 - \alpha$ of the sites, the decay rate is just λ . The *quenched* local Green function is then given by

$$G_1^q(\varepsilon, t) = (1 - \alpha)G_1(\varepsilon, t) + \alpha G_1^d(\varepsilon, t), \quad (7.3)$$

where $G_1^d(\varepsilon, t)$, *i.e.* the local Green function on a site where dissociation can take place, is given by Eq. (7.2) with λ replaced by $\lambda + \lambda_d$. Substitution into Eq. (7.1) yields the time-integrated PL quenching,

$$Q = \frac{\int_0^\infty dt [L(t) - L^q(t)]}{\int_0^\infty dt L(t)}, \quad (7.4)$$

as well as the transient PL quenching

$$Q(t) = \frac{L(t) - L^q(t)}{L(t)}, \quad (7.5)$$

where $L^q(t)$ denotes the quenched PL intensity in the presence of an electric field.

In the following, we will assume that the process of exciton migration is the same in both the CP blend and the MDP. Hence we use the same parameters as in Ref. [7]: $\nu_0 = 10^{13}$ Hz, $\lambda = (300 \text{ ps})^{-1}$. The relative concentration $c = n \frac{4}{3} \pi R_0^3 \in [0, 1]$ is proportional to the density of sites $n = n(\infty)$. The density of states $\rho(\varepsilon)$ is a Gaussian with standard deviation $\sigma = 0.1$ eV. The results are not heavily dependent on the precise values of the parameters.

Regarding the dissociation of excitons, a microscopic model of intermolecular dissociation is used in order to determine the dependence of the dissociation parameters λ_d and α on the electric field strength F , the TSA concentration c , and the exciton energy ε . The dissociation rate for an exciton located on site i with a neighbor j is given by

$$\lambda_d = \nu_0 \exp(-2\gamma R_{ij}) \theta(E_{ij}), \quad (7.6)$$

where we follow Scheidler *et al.* [14] in taking the attempt frequency $\nu_0 = 10^{13}$ Hz identical to the nearest-neighbor exciton transition rate. The localization length is of order $\gamma^{-1} = 1.5 \text{ \AA}$, as obtained from carrier transport

measurements in MDPs [15]. The energy difference E_{ij} between an electron and a hole on separate sites and an exciton on the site with lowest energy is given by (see Fig. 7.1)

$$E_{ij} = E_C - E_b - \frac{1}{2} |\varepsilon_i - \varepsilon_j| + eFR_{ij} |\cos \chi|, \quad (7.7)$$

where E_C is the Coulomb energy of the dissociated electron-hole pair and χ is the angle between the electric field \mathbf{F} and the vector $\mathbf{R}_j - \mathbf{R}_i$. Here, we have assumed that the exciton binding energy E_b is the same on all sites, *i.e.* the disorder in exciton energies is solely due to the inhomogeneous broadening of the HOMO and LUMO levels. We have further assumed a symmetric distribution of HOMO and LUMO levels. Then a hole tunneling to a site j in the field direction gives the same result as an electron tunneling to the same site j in the opposite direction.

In contrast with exciton migration, the dissociation of excitons is a short-range process. We can therefore neglect the dissociation between sites at a distance $> R_0$, as these dissociation rates are exponentially smaller than the rates between nearest neighbors. The probability of finding k sites within the “nearest neighbor volume” $\frac{4}{3}\pi R_0^3$ around the initial site is given by a Poisson distribution. Hence the probability of having at least one neighbor at a distance shorter than R_0 is $1 - \exp\left(-n\frac{4}{3}\pi R_0^3\right) = 1 - e^{-c}$. As the TSA molecule is anisotropic, the dissociation rate is not determined by the average center-to-center distance R_0 , but by the minimum tunneling distance R , which may be much smaller. Therefore, we replace the distribution of rates $\lambda_d(R_{ij})$ by the dominant rate $\lambda_d(R)$.

Let us now calculate the probability that $E_{ij} > 0$, given that the site i has a nearest neighbor j . This probability, which is a function of the site energy ε , is found by integrating over all energies ε' and orientations χ of the nearest neighbor,

$$\begin{aligned} p(\varepsilon) &= \frac{1}{n} \int d\varepsilon' \rho(\varepsilon') \int_0^1 d\cos \chi \\ &\quad \times \theta\left(\Delta E - \frac{1}{2} |\varepsilon - \varepsilon'| + eFR \cos \chi\right) \\ &= \int_{\max(0, 2\Delta E)}^{\max(0, 2\Delta E + 2eFR)} d\varepsilon' \frac{n(\varepsilon + \varepsilon') - n(\varepsilon - \varepsilon')}{2neFR}, \end{aligned} \quad (7.8)$$

where $\Delta E = E_C - E_b$. If $\Delta E < 0$, all excitons are stable in the absence of an electric field. The stability of excitons is *enhanced* by the disorder in the system, as the excitons migrate to sites with lower energies, from which

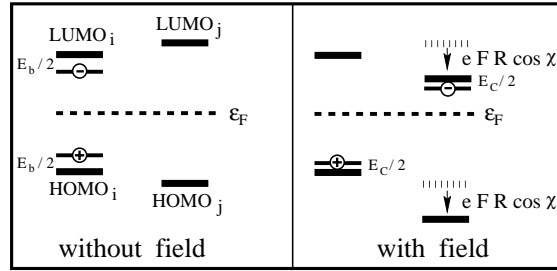


Figure 7.1: Energy level diagram describing field-induced exciton dissociation between two molecules i and j . Left figure: energy levels of molecules i and j without applied electric field. An exciton, located on molecule i , has an energy $\varepsilon_i = \text{HOMO}_i + \text{LUMO}_i - E_b$. Right figure: energy levels of molecules i and j are shifted by $eFR \cos \chi$ in the presence of an applied electric field \mathbf{F} . The energy of the electron-hole pair is given by $\text{HOMO}_i + \text{LUMO}_j - E_C - eFR \cos \chi$. (For $\cos \chi < 0$, the hole jumps to j .) When the distribution of HOMO and LUMO levels is symmetric with respect to the Fermi energy ε_F , the energy condition (7.7) is obtained.

a dissociating jump is difficult. When $\Delta E + eFR < 0$, the electric field can never overcome the exciton binding and $p(\varepsilon) = 0$. Combining Eq. (7.8) with the probability to find a nearest neighbor, we find for the dissociation parameters

$$\alpha(\varepsilon) = 1 - e^{-cp(\varepsilon)}, \quad (7.9)$$

$$\lambda_d = \nu_0 e^{-2\gamma R}. \quad (7.10)$$

The time-integrated PL quenching Q and the transient PL quenching $Q(t)$ can now be calculated as a function of the concentration c and the electric field strength F , where the tunneling distance R and the energy difference ΔE are the only free parameters.

In Fig. 7.2, the time-integrated PL quenching Q is shown as a function of the TSA concentration c for different field strengths F . We find that the complete set of experiments is well described using $R = 2.0 \text{ \AA}$ and $\Delta E = -7.5 \times 10^{-3} \text{ eV}$. Our theory reproduces both the zero quenching at low c and the increasing Q over the whole range of c . Deussen *et al.* [6] have interpreted their results in terms of a localization length $\gamma^{-1} \simeq 15 - 20 \text{ \AA}$.

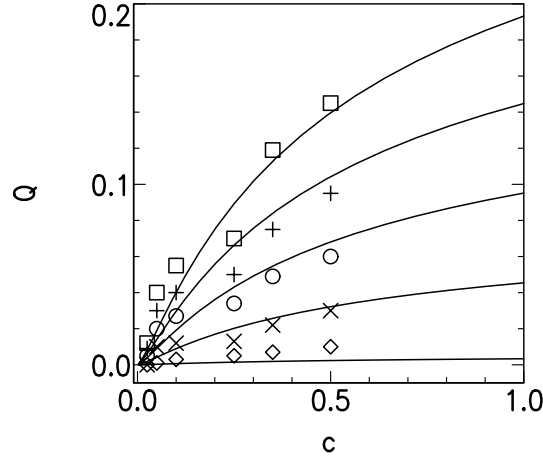


Figure 7.2: Photoluminescence quenching Q as a function of concentration c for an electric field $F = 0.5, 1.0, 1.5, 2.0,$ and 2.5 MV/cm (bottom to top). The parameters used are $R = 2.0$ Å and $\delta = -7.5 \times 10^{-3}$ eV. Experimental data (at a temperature $T = 77$ K) are taken from Ref. [6].

This value is an order of magnitude too large because exciton migration is not taken into account.

The obtained values for R and ΔE allow us to make a rough estimate of the exciton binding energy E_b . We use the approach by Scheidler *et al.* [14]

$$\Delta E = E_C - E_b = \frac{e^2}{4\pi\epsilon_r\epsilon_0} \left(\frac{1}{R_{\text{eh}}} - \frac{1}{R_{\text{exc}}} \right), \quad (7.11)$$

with R_{eh} the electron-hole distance and R_{exc} the distance between the electron and the hole in the excitonic state. Due to the anisotropic shape of the TSA molecules, the shortest dissociating jump is perpendicular to the molecule, $R_{\text{eh}} = \sqrt{R_{\text{exc}}^2 + R^2}$. Substituting $\epsilon_r = 3$, $R = 2.0$ Å and $\delta = -7.5 \times 10^{-3}$ eV, we find that the exciton size R_{exc} is about 11 Å, which corresponds with the size of one of the three “legs” of the TSA molecule (see inset to Fig 7.3). Furthermore, we find $E_b = 0.45$ eV, which agrees well with the value of 0.4 eV estimated in Refs. [5, 6].

Equation (7.11) can also be used to explain the experimentally observed increase in Q with increasing polarity of the polymer matrix [6]. An increase in polarity enhances the relative dielectric constant ϵ_r . Consequently, $|\Delta E|$ decreases and the exciton becomes more liable to dissociation.

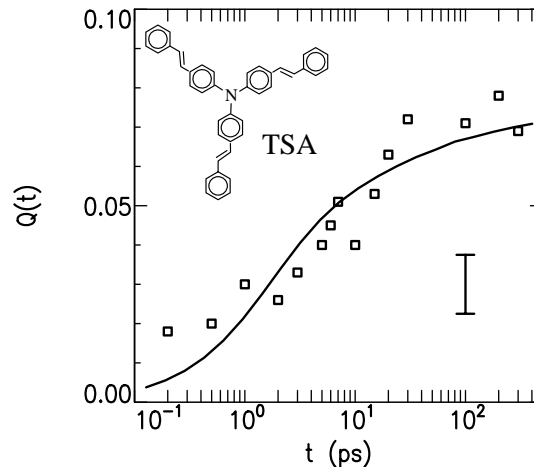


Figure 7.3: *Transient photoluminescence quenching $Q(t)$ as a function of time t (solid line). The same parameters are used as in Fig. 7.2, with $c = 0.5$ and $F = 1.5$ MV/cm. Experimental data are taken from Ref. [6] ($T = 15$ K). An indication of the experimental error is given in the lower right corner. The chemical structure of tris(stilbene)amine (TSA) is given in the upper left corner.*

Let us now compare our theory with the experimental results on *transient* electric field-induced PL quenching $Q(t)$ [6], using the same parameters as above. In Fig. 7.3, the time evolution of transient electric field-induced PL quenching $Q(t)$ is shown for a 50% TSA blend with an applied electric field $F = 1.5$ MV/cm. Given the fact that we have not used any fitting parameters, the agreement is quite good. We see that, after the onset of PL quenching in the first few picoseconds, $Q(t)$ first increases and then saturates at longer time scales. The saturation of $Q(t)$ is due to the migration of excitons to sites with a low energy ε , which have a very low dissociation probability $\alpha(\varepsilon)$. This saturation effect may be part of the answer to the question why on-chain dissociation is dominant in CPs [9]. At low concentrations, interchain dissociation is suppressed simply due to the large distances between the chains. At higher concentrations the chains are closer together, but then the excitons migrate rapidly to the sites with the lowest energies, where they are stable against intermolecular dissociation.

7.4 Conclusion

We have combined our analytic theory of exciton migration with a microscopic model of intermolecular exciton dissociation, in order to describe electric field-induced PL quenching experiments on MDPs. The theory accounts well for the dependence of PL quenching on the electric field strength and on the dopant concentration. We estimate an exciton binding energy $E_b = 0.45$ eV and an exciton size $R_{\text{exc}} = 11$ Å. Using the same set of parameters, good agreement is obtained with the observed time evolution of transient PL quenching. This work, together with our previous work [7], provides a consistent picture of electric field-induced PL quenching in MDPs as well as CP blends, underlining their distinct dissociation mechanisms, *i.e.* intermolecular dissociation in MDPs and intramolecular dissociation in CP blends.

References

- [1] P. M. Borsenberger and D. S. Weiss, in *Organic Photoreceptors for Imaging Systems* (Marcel Dekker, New York, 1993).
- [2] J. H. Burroughes, D. D. C. Bradley, A. R. Brown, R. N. Marks, K. MacKay, R. H. Friend, P. L. Burn, and A. B. Holmes, *Nature (London)* **347**, 539 (1990); For recent reviews, see A. J. Epstein and Y. Yang (eds.), *MRS Bull.* **22**, 6 (1997).
- [3] See, *e.g.*, H. Bässler, V. Brandl, M. Deussen, E. O. Göbel, R. Kersting, H. Kurz, U. Lemmer, R. F. Mahrt, and A. Ochse, *Pure & Appl. Chem.* **67**, 377 (1995); J. J. M. Halls, K. Pichler, R. H. Friend, S. C. Moratti, and A. B. Holmes, *Appl. Phys. Lett.* **68**, 3120 (1996); S. V. Frolov, M. Liess, P. A. Lane, W. Gellermann, Z. V. Vardeny, M. Ozaki, and K. Yoshino, *Phys. Rev. Lett.* **78**, 4285 (1997).
- [4] R. Kersting, U. Lemmer, M. Deussen, H. J. Bakker, R. F. Mahrt, H. Kurz, V. I. Arkhipov, H. Bässler, and E. O. Göbel, *Phys. Rev. Lett.* **73**, 1440 (1994).
- [5] M. Deussen, M. Scheidler, and H. Bässler, *Synth. Met.* **73**, 123 (1995).
- [6] M. Deussen, P. Haring Bolivar, G. Wegmann, H. Kurz, and H. Bässler, *Chem. Phys.* **207**, 147 (1996).
- [7] M. C. J. M. Vissenberg and M. J. M. de Jong, *Phys. Rev. Lett.* **77**, 4820 (1996) [Chapter 6].
- [8] G. H. Gelinck, J. M. Warman, and E. G. J. Staring, *J. Phys. Chem.* **100**, 5485 (1996).
- [9] E. M. Conwell, *Phys. Rev. Lett.* **78**, 4301 (1997) [Section 6.5].
- [10] M. C. J. M. Vissenberg and M. J. M. de Jong, *Phys. Rev. Lett.* **78**, 4302 (1997) [Section 6.5].

- [11] B. Movaghar, B. Ries, and M. Grünewald, *Phys. Rev. B* **34**, 5574 (1986); M. Grünewald and B. Movaghar, *J. Phys. Condens. Matter* **1**, 2521 (1989).
- [12] M. C. J. M. Vissenberg and M. J. M. de Jong, in *Excitonic Processes in Condensed Matter*, edited by M. Schreiber (Dresden University Press, Dresden, 1996); *Phys. Rev. B* **56**, 6681 (1997).
- [13] Th. Förster, *Z. Naturforsch.* **4a**, 321 (1949).
- [14] M. Scheidler, U. Lemmer, R. Kersting, S. Karg, W. Riess, B. Cleve, R. F. Mahrt, H. Kurz, H. Bässler, E. O. Göbel, and P. Thomas, *Phys. Rev. B* **54**, 5536 (1996).
- [15] P. M. Borsenberger, *J. Appl. Phys.* **68**, 6263 (1990).

Chapter 8

Photobleaching and spectral diffusion in disordered media

8.1 Introduction

The photochemical bleaching of organic dyes, resulting in the fading of colors, is a well-known problem for the textile and graphics industries [1]. The same process poses a fundamental limit to the lifetime of optical devices based on organic materials, such as organic dye lasers [2–4] and polymer light-emitting diodes [5–8]. The photochemical stability of these materials is described by the quantum yield for bleaching γ , which is the probability that a chromophore (optical absorber) is destroyed after a photon is absorbed. In this description, it is implicitly assumed that the destroyed chromophore is identical to the chromophore which absorbed the photon. However, in an energetically disordered system, an excitation may relax in the course of a random walk towards sites of lower energy, a process known as spectral diffusion [9]. This effect causes a relatively stronger bleaching of chromophores with a low excitation energy, as observed in organic dye aggregates [10]. The bleaching of dye aggregates has recently been described by Tomioka and Miyano [11] using a numerical simulation of coherent exciton transport on a two-dimensional lattice with on-site energy disorder.

The present work has been instigated by the observation that photobleaching of poly(*p*-phenylene-vinylene) (PPV) films causes a blue shift of the absorption spectrum [7, 12, 13]. Experiments suggest that the optical properties of conjugated polymers are well modeled by replacing the polymer chains by a set of chain segments with a distribution of effective conjugation lengths [14]. Upon illumination, on-chain singlet excitons [12, 15] are

formed that relax in the course of an incoherent random walk between different polymer chain segments [14]. The bleaching of the polymer appears to be due to a photo-oxidation [5] reaction, resulting in a chain scission of the macromolecule [6, 8]. The simulation of Ref. [11] is not applicable here, because the system is three-dimensional, the lattice structure is absent, and the exciton transport is incoherent.

In this Chapter, the incoherent migration of excitons in a system with positional and energetic disorder is described analytically using an effective medium approximation (EMA). This transport formalism is used to calculate the excited-state occupational probability of a given site, which determines its bleaching rate. When the system is then excited by a broadband light source, spectral diffusion leads to a red shift of the excited-state occupational probability and hence to a relatively stronger bleaching of the lower-lying states. In some systems, specifically in PPV [5], photobleaching not only reduces the absorption of the material, but the photoluminescence (PL) efficiency as well. Apparently, the excitons in these systems are quenched in the presence of a bleached chromophore. In our model, this is accounted for by attributing an additional non-radiative decay channel to excitons on sites that are next to bleached sites. These sites are referred to as ‘quenching sites’.

This Chapter is organized as follows. The incoherent migration of excitons is described in Sec. 8.2. This formalism is used in Sec. 8.3 to model the photochemical bleaching. The influence of quenching sites is described in Sec. 8.4. In Sec. 8.5, the applicability of the model to photobleaching of PPV is discussed. A short summary of the main results is given in Sec. 8.6.

8.2 Spectral diffusion

Consider a system with N localized states, with position \mathbf{R}_i and excited state energy ε_i , for $i = 1 \dots N$. For low excitation densities, the occupational probability $f_i(t)$ of the site i at time t is described by a linearized master equation

$$\frac{\partial}{\partial t} f_i(t) = - \sum_{j \neq i} W_{ji} f_i(t) + \sum_{j \neq i} W_{ij} f_j(t) - \lambda f_i(t), \quad (8.1)$$

where W_{ij} is the transition rate from site j to site i , and λ is the decay rate due to both radiative recombination and non-radiative decay processes, which is assumed to be constant for all sites. For the moment, the effect of photobleaching is not taken into account. At zero temperature, only

transitions to sites with lower energy are possible, implying

$$W_{ij} = w(\mathbf{R}_{ij})\theta(\varepsilon_j - \varepsilon_i), \quad (8.2)$$

with $\mathbf{R}_{ij} \equiv \mathbf{R}_i - \mathbf{R}_j$ and $\theta(x) = 1$ if $x > 0$, $\theta(x) = 0$ otherwise. The function $w(\mathbf{R}_{ij})$ depends on the exciton transfer mechanism.

Equation (8.1) can be solved using a Green function formalism [16–18]. The Green function $G_{ij}(t)$ is the probability to find a particle at site i at a time t , given that it was at site j at $t = 0$, and is a function of all N positions and energies of a given configuration $\{\mathbf{R}_k, \varepsilon_k\}$. To determine the configurational averages of the Green function, we assume that the positions and energies are uncorrelated and denote the density of states (DOS) at energy ε as $\rho(\varepsilon)$. The local Green function, *i.e.* the average of $G_{jj}(t)$, and the non-local Green function, *i.e.* the average of $G_{ij}(t)$ with $i \neq j$, are given by

$$G_1(\varepsilon_j, t) \equiv \int \left[\prod_{k \neq j} d\mathbf{R}_k d\varepsilon_k \frac{\rho(\varepsilon_k)}{N} \right] G_{jj}(t), \quad (8.3)$$

$$G_2(\varepsilon_i, \varepsilon_j, \mathbf{R}_{ij}, t) \equiv \int \left[\prod_{k \neq i, j} d\mathbf{R}_k d\varepsilon_k \frac{\rho(\varepsilon_k)}{N} \right] G_{ij}(t). \quad (8.4)$$

We calculate the Green functions (8.3) and (8.4) in the EMA [16], which allows us to proceed with analytical expressions. Here, the migration from a site is described by a single effective rate, rather than by the sum of all distinct transition rates. This approximation tends to be inaccurate for long times [16], which is not of importance for this work in view of the finite exciton life time. The local Green function is given by

$$G_1(\varepsilon, t) \simeq e^{-\lambda[1+Kn(\varepsilon)]t}, \quad (8.5)$$

where

$$K = \frac{1}{\lambda} \int d\mathbf{R} w(\mathbf{R}), \quad (8.6)$$

$$n(\varepsilon) = \int_{-\infty}^{\varepsilon} d\varepsilon' \rho(\varepsilon'). \quad (8.7)$$

The first term in the exponent of Eq. (8.5) describes the exciton decay, the second the exciton migration. The exact value of K depends on $w(\mathbf{R})$ and thus on the exciton transfer mechanism. For example, when using rates

of the Förster type [16–19], $K = \frac{4}{3}\pi R_0^3 \nu_0 / \lambda$, with R_0 the nearest neighbor distance and ν_0 the nearest neighbor transition rate.

Following Movaghar *et al.* [16], we found for the Fourier-Laplace transform of the non-local Green function (8.4) [17, 18]

$$\begin{aligned} \tilde{G}_2(\varepsilon, \varepsilon', \mathbf{k}, p) &= \theta(\varepsilon' - \varepsilon) \tilde{G}_1(\varepsilon, p) \tilde{g}(\varepsilon', \mathbf{k}, p) \\ &\times \exp \left[\int_{\varepsilon}^{\varepsilon'} d\varepsilon'' \rho(\varepsilon'') \tilde{g}(\varepsilon'', \mathbf{k}, p) \right], \end{aligned} \quad (8.8)$$

where $\tilde{g}(\varepsilon', \mathbf{k}, p)$ is the Fourier-Laplace transform of $g(\varepsilon', \mathbf{R}, t)$, which is the average probability to jump at time t from the initial site with energy ε' to a site at a distance \mathbf{R} with lower energy. The exponential function results from the summation over all different paths to go from the initial site to the final site and $\tilde{G}_1(\varepsilon, p)$ denotes the probability to remain on the final site. It follows from Eq. (8.5) that

$$\tilde{G}_1(\varepsilon, p) = \frac{1}{p + \lambda + \lambda K n(\varepsilon)}. \quad (8.9)$$

For $\mathbf{k} = \mathbf{0}$, the jump probability reads [16]

$$\tilde{g}(\varepsilon, \mathbf{0}, p) = \frac{\lambda K}{p + \lambda + \lambda K n(\varepsilon)}, \quad (8.10)$$

which is the product of the local Green function and the transition rate for a jump to a site with lower energy, integrated over all space. Substitution into Eq. (8.8) yields

$$\tilde{G}_2(\varepsilon, \varepsilon', \mathbf{k} = \mathbf{0}, p) = \frac{\theta(\varepsilon' - \varepsilon) \lambda K}{[p + \lambda + \lambda K n(\varepsilon)]^2}. \quad (8.11)$$

Equations (8.9) and (8.11) constitute the effective medium description of spectral diffusion in an energetically disordered system.

Under constant illumination, sites with energy ε absorb photons at a rate $\alpha(\varepsilon)$. The total absorption rate per unit volume is given by

$$\alpha_{tot} = \int d\varepsilon \rho(\varepsilon) \alpha(\varepsilon). \quad (8.12)$$

Using Eqs. (8.9) and (8.11), we find for the steady-state occupational probability $f(\varepsilon)$

$$f(\varepsilon) = \alpha(\varepsilon) \tilde{G}_1(\varepsilon, 0) + \int d\varepsilon' \rho(\varepsilon') \alpha(\varepsilon') \tilde{G}_2(\varepsilon, \varepsilon', \mathbf{0}, 0)$$

$$\begin{aligned}
&= \frac{\alpha(\varepsilon)}{\lambda + \lambda K n(\varepsilon)} \\
&+ \frac{K \lambda}{[\lambda + \lambda K n(\varepsilon)]^2} \int_{\varepsilon}^{\infty} d\varepsilon' \rho(\varepsilon') \alpha(\varepsilon').
\end{aligned} \tag{8.13}$$

We note that in the absence of spectral diffusion ($K = 0$) the occupational probability is just $\alpha(\varepsilon)/\lambda$. The photoluminescence (PL) spectrum follows from the occupational probability,

$$L(\varepsilon) = \eta \lambda \rho(\varepsilon) f(\varepsilon), \tag{8.14}$$

where η is the PL efficiency, *i.e.*, the fraction of excitons that recombine radiatively.

We will consider excitation by a broad-band light source, described by

$$\alpha(\varepsilon) = \alpha_0, \tag{8.15}$$

so that all chromophores have the same excitation rate. Now Eqs. (8.12) and (8.13) imply

$$\alpha_{tot} = \alpha_0 n(\infty), \tag{8.16}$$

$$f(\varepsilon) = \frac{\alpha_0 [1 + K n(\infty)]}{\lambda [1 + K n(\varepsilon)]^2}. \tag{8.17}$$

The occupation, and hence the PL spectrum, is clearly red shifted with respect to the situation in the absence of spectral diffusion, as $n(\varepsilon)$ increases with increasing energy.

8.3 Photobleaching

Under illumination, photochemical reactions may modify the optical properties of chromophores. In the present work, we will follow Tomioka and Miyano [11] in assuming that the chromophore has negligible absorption after photobleaching. Below, we will describe photochemical bleaching using the results of the previous Section in combination with a decreasing DOS.

The bleaching of a site is described by a bleaching rate $\beta(\varepsilon, t)$. This rate is proportional to the occupational probability,

$$\beta(\varepsilon, t) = \lambda_b f(\varepsilon, t), \tag{8.18}$$

where λ_b is the bleaching rate for an excited state. The occupational probability $f(\varepsilon, t)$ is now a function of time, as—due to the continuous bleaching

of sites—a steady state can not be reached. The effect of the bleaching process is modeled by removing the bleached site from the system,

$$\frac{\partial \rho(\varepsilon, t)}{\partial t} = -\beta(\varepsilon, t)\rho(\varepsilon, t). \quad (8.19)$$

Of experimental interest is the case where bleaching is much slower than exciton decay ($\lambda_b \ll \lambda$). Then the average occupational probability of excited states at a given time t can be obtained using a quasi-stationary approach,

$$f(\varepsilon, t) = f[\varepsilon, \rho(\varepsilon, t)]. \quad (8.20)$$

The functional on the right-hand side is given by substituting a time-dependent DOS $\rho(\varepsilon, t)$ for $\rho(\varepsilon)$ in Eq. (8.13).

The speed at which the system evolves depends on the intensity of the incident light. Hence the total number of absorbed photons per unit volume,

$$A(t) \equiv \int_0^t dt' \alpha_{tot}[\rho(\varepsilon, t')], \quad (8.21)$$

is a convenient measure of time. (The total absorption rate α_{tot} , cf. Eq. (8.12), has become a functional of the time-dependent DOS.)

Combining Eqs. (8.18)–(8.21) and using A instead of t to measure time, we find that the evolution of the DOS $\rho(\varepsilon, A)$ is described by

$$\frac{\partial \rho(\varepsilon, A)}{\partial A} = -\rho(\varepsilon, A) \frac{\lambda_b f[\varepsilon, \rho(\varepsilon, A)]}{\alpha_{tot}[\rho(\varepsilon, A)]}. \quad (8.22)$$

A check on the formalism is performed by substituting the total absorption rate (8.12) and the occupational probability (8.13) into Eq. (8.22) and integrating both sides of this equation over all energies. We then find that the total density of sites $n(A) \equiv n(\infty, A)$ decreases according to

$$\frac{\partial n(A)}{\partial A} = -\frac{\lambda_b}{\lambda} \equiv -\gamma. \quad (8.23)$$

Here γ is the quantum yield for bleaching, which is constant in time and independent of spectral diffusion. This must hold for any model in which the exciton decay rate is independent of the site energy. The total density of sites decreases linearly with the number of absorbed photons,

$$n(A) = n(0) - \gamma A. \quad (8.24)$$

Let us now consider the evolution of the DOS, focussing on the energy dependence of the bleaching process. Substituting Eqs. (8.16) and (8.17)

into Eq. (8.22) and integrating both sides of this equation up to the energy ε , we find that the evolution of $n(\varepsilon, A)$ is described by

$$\frac{\partial n(\varepsilon, A)}{\partial A} = -\gamma \frac{n(\varepsilon, A)[1 + Kn(A)]}{n(A)[1 + Kn(\varepsilon, A)]}. \quad (8.25)$$

Using Eq. (8.24), we find

$$n(\varepsilon, A) = \mathcal{W}[h(\varepsilon, A)] / K, \quad (8.26)$$

with Lambert's \mathcal{W} function, which is defined by [20]

$$\mathcal{W}(x) \exp[\mathcal{W}(x)] = x, \quad (8.27)$$

and

$$h(\varepsilon, A) \equiv Kn(\varepsilon, 0) \left[1 - \frac{\gamma A}{n(0)} \right] e^{K[n(\varepsilon, 0) - \gamma A]}. \quad (8.28)$$

The density of states $\rho(\varepsilon, A)$ is obtained by taking the derivative of Eq. (8.26) with respect to ε ,

$$\rho(\varepsilon, A) = \rho(\varepsilon, 0) \frac{1 + 1/[Kn(\varepsilon, 0)]}{1 + 1/[Kn(\varepsilon, A)]}. \quad (8.29)$$

The quasi-stationary PL spectrum of the system follows from Eq. (8.14),

$$L(\varepsilon, A) = \eta \lambda \rho(\varepsilon, A) f[\varepsilon, \rho(\varepsilon, A)]. \quad (8.30)$$

Without spectral diffusion ($K = 0$), the DOS and the PL spectrum decrease uniformly

$$\rho(\varepsilon, A) = \rho(\varepsilon, 0) \left[1 - \frac{\gamma A}{n(0)} \right], \quad (8.31)$$

$$L(\varepsilon, A) = \eta \alpha_0 \rho(\varepsilon, A). \quad (8.32)$$

In Figs. 8.1(a) and 8.1(b), it is shown that, when the spectral diffusion is weak, the DOS decreases almost uniformly and that the PL spectrum is only slightly red shifted with respect to the DOS.

When the spectral diffusion is strong, the DOS decreases at the low energy side [Fig. 8.1(c)]. The PL spectrum is narrower than the DOS and red shifted. Upon bleaching, the blue shift of the PL spectrum follows the blue shift of the low-energy flank of the DOS [Fig. 8.1(d)]. In the limit $K \rightarrow \infty$, all excitons are immediately transferred towards the sites with

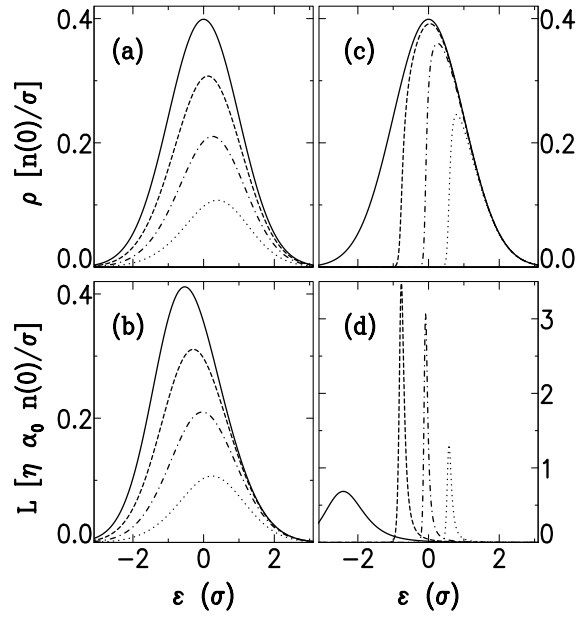


Figure 8.1: Evolution of the DOS $\rho(\varepsilon, A)$ (a,c) and the PL spectrum $L(\varepsilon, A)$ (b,d) for a medium that is bleached by a broadband light source, as given by Eqs. (8.29) and (8.30), respectively. The initial DOS is a Gaussian with standard deviation σ . The plots show $\rho(\varepsilon, A)$ and $L(\varepsilon, A)$ after $A = 0.00, 0.25, 0.50$, and $0.75 n(0)/\gamma$ photons per unit volume have been absorbed. Plots (a,b) show the case of weak spectral diffusion ($Kn(0) = 1.0$), whereas the spectral diffusion is strong ($Kn(0) = 100.0$) in (c,d).

the lowest energy. Hence, there is only emission by and bleaching of these lowest-energy sites. The DOS and the PL spectrum are then given by

$$\rho(\varepsilon, A) = \rho(\varepsilon, 0) \theta [n(\varepsilon, 0) - \gamma A], \quad (8.33)$$

$$L(\varepsilon, A) = \eta \alpha_0 \rho(\varepsilon, 0) n(A) \delta [n(\varepsilon, 0) - \gamma A], \quad (8.34)$$

where $\delta(x)$ is the Dirac delta function.

With or without spectral diffusion, the decrease of the PL intensity upon bleaching is proportional to the decrease in absorption. This is due to the constant PL efficiency η .

The effect of spectral diffusion on photobleaching can be demonstrated

experimentally by monitoring the density of sites in a given energy interval $[\varepsilon_0, \varepsilon_1]$ as a function of time, while the system is bleached by white light. The time evolution of this site density $\Delta n(A) = n(\varepsilon_1, A) - n(\varepsilon_0, A)$ is qualitatively different for weak and for strong spectral diffusion, as shown in Fig. 8.2. Without spectral diffusion ($K = 0$), the sites in the interval are bleached with an efficiency that is time independent [$\partial\Delta n(A)/\partial A = -\gamma\Delta n(0)/n(0)$]. When spectral diffusion is strong, sites are bleached from the low-energy side. Initially, the bleaching efficiency of sites in the interval is zero, as only lower-energetic sites are bleached. After all sites with energy $\varepsilon < \varepsilon_0$ have been bleached, we have $\partial\Delta n(A)/\partial A = -\gamma$ until all sites in the interval have been bleached.

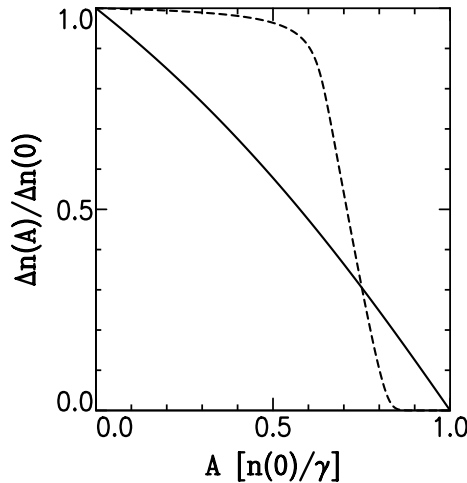


Figure 8.2: Evolution of the total density of sites $\Delta n(A) = n(\varepsilon_1, A) - n(\varepsilon_0, A)$ in an energy interval $[\varepsilon_0, \varepsilon_1]$, as given by Eq. (8.26). The system is bleached by a broad-band light source. The initial densities are $n(\varepsilon_0, 0) = 0.6n(0)$ and $n(\varepsilon_1, 0) = 0.8n(0)$. The full line shows the case of weak spectral diffusion [$Kn(0) = 1.0$], whereas the case of strong spectral diffusion [$Kn(0) = 100.0$] is given by the dashed line. The results are independent of the form of the DOS.

8.4 Influence of quenching sites

In the preceding discussion, it is assumed that the bleached chromophores do not interact with the excited states in the system. However, as shown by, e.g., Yan *et al.* [5], the PL efficiency in conjugated polymer films decreases drastically upon bleaching. Apparently, the excited states are quenched by the bleached chromophores.

In this Section, we study the case where bleached sites induce an additional non-radiative decay channel for excitons on sites within a certain range of the bleached site. We assume a short-range interaction, i.e., only the Z nearest neighbors of the bleached site are affected. The intact (unbleached) sites can now be subdivided into normal sites and quenching sites. A quenching site is a site next to a bleached site, so that an exciton decays at a rate $\lambda + \lambda_q$, where λ_q is the additional quenching rate induced by the bleached site. The density of quenching sites is given by $n^q(A)$, and the DOS by $\rho^q(\varepsilon, A)$. On the normal sites, the exciton decays at a lower rate λ . The density and the DOS of these (non-quenching) sites are denoted as $n^{nq}(A)$ and $\rho^{nq}(\varepsilon, A)$, respectively. The density and DOS of intact sites are given by $n(A) = n^q(A) + n^{nq}(A)$ and $\rho(\varepsilon, A) = \rho^q(\varepsilon, A) + \rho^{nq}(\varepsilon, A)$.

Let us first consider the exciton dynamics *without photobleaching* in a system that contains both normal sites and quenching sites, analogous to Sec. 8.2. We can use the model we have developed in Ref. [17] for field-induced PL quenching in conjugated polymers. There are two distinct local Green functions, depending on which kind of site the exciton is located,

$$\tilde{G}_1^q(\varepsilon, p) = \frac{1}{p + \lambda + \lambda_q + \lambda K n(\varepsilon)}, \quad (8.35)$$

$$\tilde{G}_1^{nq}(\varepsilon, p) = \frac{1}{p + \lambda + \lambda K n(\varepsilon)}. \quad (8.36)$$

The same holds for the jump probabilities [cf. Eq. (8.10)] from either a quenching site or a normal site,

$$\tilde{g}^q(\varepsilon, \mathbf{0}, p) = \frac{\lambda K}{p + \lambda + \lambda_q + \lambda K n(\varepsilon)}, \quad (8.37)$$

$$\tilde{g}^{nq}(\varepsilon, \mathbf{0}, p) = \frac{\lambda K}{p + \lambda + \lambda K n(\varepsilon)}. \quad (8.38)$$

There are four distinct non-local Green functions, as both the initial site and the final site may be a quenching site or not,

$$\tilde{G}_2^{a,b}(\varepsilon, \varepsilon', \mathbf{k}, p) = \theta(\varepsilon' - \varepsilon) \tilde{G}_1^a(\varepsilon, p) \tilde{g}^b(\varepsilon', \mathbf{k}, p)$$

$$\times \exp \left[\int_{\varepsilon}^{\varepsilon'} d\varepsilon'' \rho(\varepsilon'') \tilde{g}(\varepsilon'', \mathbf{k}, p) \right]. \quad (8.39)$$

Here, $a = q, nq$ indicates the type of the final site and $b = q, nq$ that of the initial site. The function $\tilde{g}(\varepsilon, \mathbf{k}, p)$ is the average probability to jump away from any site

$$\tilde{g}(\varepsilon, \mathbf{k}, p) = \frac{\rho^q(\varepsilon)}{\rho(\varepsilon)} \tilde{g}^q(\varepsilon, \mathbf{k}, p) + \frac{\rho^{nq}(\varepsilon)}{\rho(\varepsilon)} \tilde{g}^{nq}(\varepsilon, \mathbf{k}, p). \quad (8.40)$$

Unlike in Sec. 8.2, there is no simple $\mathbf{k} = \mathbf{0}$ expression for the non-local Green function. The integral in the exponent of Eq. (8.39) can only be evaluated numerically, due to the fact that $\tilde{g}(\varepsilon, \mathbf{0}, p)$ is explicitly energy dependent according to Eq. (8.40).

Let us again study the situation of constant illumination. We assume an equal absorption rate $\alpha(\varepsilon)$ for normal sites as well as quenching sites. The steady-state occupational probabilities $f^{nq}(\varepsilon)$ for normal sites and $f^q(\varepsilon)$ for quenching sites are given by

$$\begin{aligned} f^a(\varepsilon) &= \alpha(\varepsilon) \tilde{G}_1^a(\varepsilon, 0) \\ &\quad + \int d\varepsilon' \alpha(\varepsilon') \sum_{b=q, nq} \rho^b(\varepsilon') \tilde{G}_2^{a,b}(\varepsilon, \varepsilon', \mathbf{0}, 0) \\ &= \tilde{G}_1^a(\varepsilon, 0) \left\{ \alpha(\varepsilon) + \int_{\varepsilon}^{\infty} d\varepsilon' \rho(\varepsilon') \alpha(\varepsilon') \tilde{g}(\varepsilon', \mathbf{0}, 0) \right. \\ &\quad \left. \times \exp \left[\int_{\varepsilon}^{\varepsilon'} d\varepsilon'' \rho(\varepsilon'') \tilde{g}(\varepsilon'', \mathbf{0}, 0) \right] \right\}. \end{aligned} \quad (8.41)$$

The average occupational probability reads

$$f(\varepsilon) = \frac{\rho^q(\varepsilon)}{\rho(\varepsilon)} f^q(\varepsilon) + \frac{\rho^{nq}(\varepsilon)}{\rho(\varepsilon)} f^{nq}(\varepsilon). \quad (8.42)$$

We can now take into account the influence of quenching sites on the bleaching process. Two processes take place simultaneously: normal and quenching sites are destroyed (albeit with different bleaching efficiencies) and normal sites are transformed into quenching sites when a neighboring site is bleached. Equation (8.22), which describes the time evolution of the DOS, is now replaced by two coupled equations,

$$\frac{\partial \rho^q(\varepsilon, A)}{\partial A} = -\frac{\lambda_b f^q}{\alpha_{tot}} \rho^q(\varepsilon, A) + \frac{Z\gamma(A)}{n(0)} \rho^{nq}(\varepsilon, A), \quad (8.43)$$

$$\frac{\partial \rho^{nq}(\varepsilon, A)}{\partial A} = -\frac{\lambda_b f^{nq}}{\alpha_{tot}} \rho^{nq}(\varepsilon, A) - \frac{Z\gamma(A)}{n(0)} \rho^{nq}(\varepsilon, A), \quad (8.44)$$

where the first term on the right hand side describes the bleaching process and the second term describes the transformation of normal sites into quenching sites. We have again used the quasi-stationary approach, i.e., the occupational probabilities and the total absorption rate are functionals $f^q[\varepsilon, \rho^q(\varepsilon, A), \rho^{nq}(\varepsilon, A)]$, $f^{nq}[\varepsilon, \rho^q(\varepsilon, A), \rho^{nq}(\varepsilon, A)]$ and $\alpha_{tot}[\rho(\varepsilon, A)]$. (The absorption rate $\alpha_{tot}[\rho(\varepsilon, A)]$ is only a functional of the total DOS, as we have taken identical absorption rates for both types of intact sites.) For brevity, we have omitted these functional dependencies in the notation of Eqs. (8.43) and (8.44). The quantum yield for bleaching $\gamma(A)$, which is no longer constant in time, is given by

$$\begin{aligned} \gamma(A) &\equiv -\frac{\partial n(A)}{\partial A} \\ &= \frac{\lambda_b \int d\varepsilon' \rho(\varepsilon', A) f[\varepsilon', \rho^q(\varepsilon, A), \rho^{nq}(\varepsilon, A)]}{\alpha_{tot}[\rho(\varepsilon, A)]}. \end{aligned} \quad (8.45)$$

The transformation of normal sites into quenching sites has been modeled as follows. When a photon is absorbed, it has a probability $\gamma(A)$ of bleaching a site. For a further unbleached system, such a bleached site has Z nearest neighbors on which the excited states can be quenched. This implies that, for a partially bleached system, a fraction $n^{nq}(A)/n(0)$ of these Z nearest neighbors will be transformed from normal sites into quenching sites. There is no effect on bleached sites or on sites that already are quenching sites, which form the remaining fraction of the Z nearest neighbors. As the site energies are uncorrelated, there are $Z\rho^{nq}(\varepsilon, A)/n(0)$ nearest neighbors with energy ε that are transformed into quenching sites. Thus, per photon that is absorbed, $Z\gamma(A)\rho^{nq}(\varepsilon, A)/n(0)$ non-quenching sites with energy ε are transformed into quenching sites [see Eqs. (8.43) and (8.44)].

The evolution of the system is completely defined by Eqs. (8.35)–(8.45) for given initial conditions $\rho^q(\varepsilon, 0)$ and $\rho^{nq}(\varepsilon, 0)$. In the following, the properties of this system are discussed according to a typical example. We take a Gaussian DOS with initially no quenching sites. The system is bleached by a broad-band light source [$\alpha(\varepsilon) = \alpha_0$]. The spectral diffusion is strong [$Kn(0) = 100.0$] and exciton quenching takes place at a high rate, comparable to the fastest transition rates [$\lambda_q = \lambda Kn(0)$], such that an escape from a quenching site is unlikely. A bleached site can induce exciton quenching on one neighboring site ($Z = 1.0$).

Figure 8.3 shows the evolution of the total density of sites $n(A)$, the density of quenching sites $n^q(A)$, and the bleaching efficiency $\gamma(A)$ as a function of the number of absorbed photons A . Initially, $n(A)$ decreases

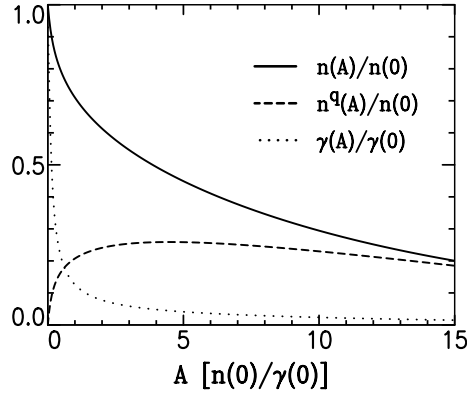


Figure 8.3: *Evolution of the total density of sites $n(A)$, the density of quenching sites $n^q(A)$, and the quantum yield for bleaching $\gamma(A)$ with the number of absorbed photons per unit volume A . The system is bleached by a broad-band light source. The bleached sites induce exciton quenching on neighboring sites. Parameters are given in the text.*

with a quantum yield for bleaching $\gamma(0) = \lambda_b/\lambda$. Without quenching, the system would then be fully bleached at $A = n(0)/\gamma(0)$. When quenching sites are formed, the quantum yield for bleaching rapidly decreases. In the long-time limit, the value $\gamma(\infty) = \lambda_b/(\lambda + \lambda_q)$ is reached, which is the quantum yield for bleaching on a quenching site.

The evolution of the DOS of the system is shown in Fig. 8.4. Indeed, we observe that the DOS of the normal sites decreases faster than that of all the sites. The difference is of course due to the formation of quenching sites. As the number of quenching sites increases, the migration of excitons gets suppressed. As a result, the evolution of $\rho(\varepsilon, A)$ resembles that of Fig. 8.1 (c) in the beginning, where spectral diffusion is strong, and that of Fig. 8.1 (a) later on, where spectral diffusion is weak.

The evolution of the PL spectrum $L(\varepsilon, A)$ can be calculated according to Eqs. (8.30) and (8.42), and is depicted in Fig. 8.5. Unlike in Fig. 8.1, the PL intensity decreases faster than the total absorption. This reduction of the PL *efficiency* is due to the formation of quenching sites. The PL efficiency can be calculated using Eqs. (8.30) and (8.45),

$$\eta [\rho^q(\varepsilon, A), \rho^{nq}(\varepsilon, A)] \equiv \frac{\int d\varepsilon L(\varepsilon, A)}{\alpha_{tot}[\rho(\varepsilon, A)]} = \frac{\eta\lambda}{\lambda_b}\gamma(A), \quad (8.46)$$

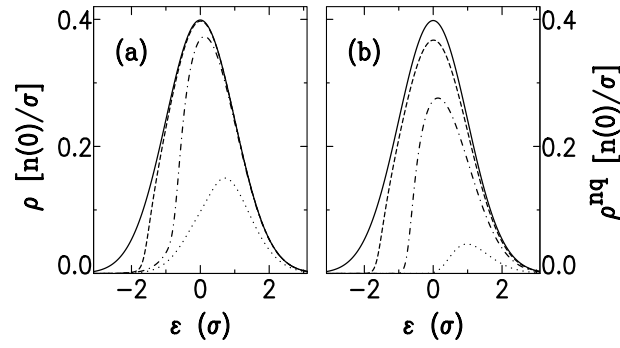


Figure 8.4: Evolution of the total DOS $\rho(\varepsilon, A)$ (a) and the DOS $\rho^{nq}(\varepsilon, A)$ for the normal sites (b) with the number of absorbed photons per unit volume A . Initially, the DOS is a Gaussian (with standard deviation σ) without quenching sites. The system is bleached by a broad-band light source. The bleached sites induce exciton quenching on neighboring sites. Both $\rho(\varepsilon, A)$ and $\rho^{nq}(\varepsilon, A)$ are shown after $A = 0.00, 0.10, 1.00,$ and 10.0 $n(0)/\gamma(0)$ photons per unit volume have been absorbed. Parameters are given in the text.

and appears to be proportional to the quantum yield for bleaching, shown in Fig. 8.3. Furthermore, one can observe in Fig. 8.5 that the PL peak is broadened after long bleaching times. This is due to the transition from strong towards weak spectral diffusion.

Due to the energy distribution of quenching sites, the PL efficiency of excitons is strongly dependent on their initial energy. This energy dependence can be probed in a photoluminescence excitation (PLE) experiment. In such an experiment the system is excited site-selectively, *i.e.*, at a specific energy. This can be modeled by an excitation rate of the form

$$\alpha(\varepsilon) = \alpha_0 \delta(\varepsilon - \varepsilon_0). \quad (8.47)$$

Substituting this excitation rate in Eq. (8.42), we find the PLE efficiency $\eta_{\text{PLE}}[\varepsilon_0, \rho^q(\varepsilon, A), \rho^{nq}(\varepsilon, A)]$, analogous to Eq. (8.46). This PLE efficiency is plotted in Fig 8.6 for the same system as in Figs. 8.3–8.5. We stress that the site-selective excitation is only used to measure the PLE spectrum of the system; the bleaching of the system is still performed through the broad-band light source [Eq. (8.15)].

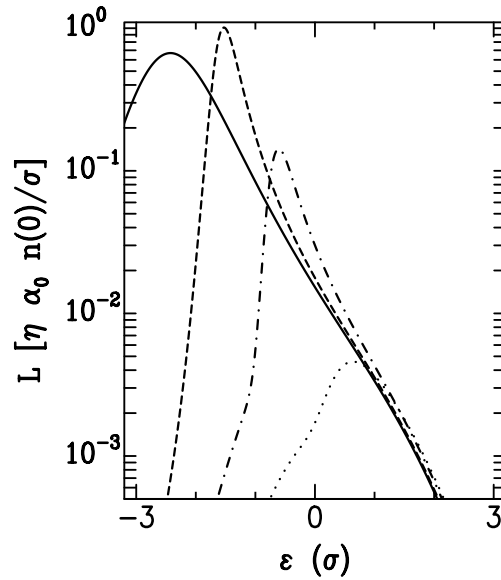


Figure 8.5: *Evolution of the PL spectrum $L(\varepsilon, A)$ with the number of absorbed photons per unit volume A . The system is bleached by a broad-band light source. The bleached sites induce quenching of excitons on the intact sites. The PL spectrum is shown after $A = 0.00, 0.10, 1.00$, and 10.0 $n(0)/\gamma(0)$ photons per unit volume have been absorbed. Parameters are given in the text.*

In Fig. 8.6, it is shown that, without quenching sites, the PLE efficiency is η , independent of energy. When quenching sites are formed, the PLE efficiency is lowered and has a pronounced energy dependence. Starting at high energies, the PLE efficiency increases when the excitation energy is lowered. This is due to the lower mobility of lower-energetic excitons, which gives rise to a decreased probability to encounter a quenching site. In the low-energy tail of the spectrum, all sites are quenching sites, as follows from Fig. 8.4. Thus the PLE efficiency of excitons created at these energies is low, $\eta_{\text{PLE}} = \eta\lambda/(\lambda + \lambda_q)$.

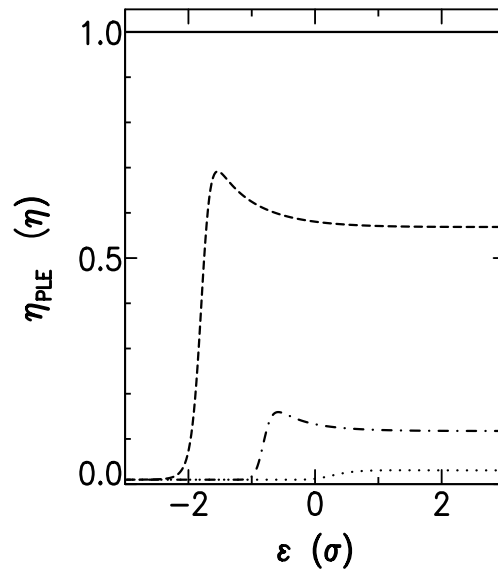


Figure 8.6: *The photoluminescence excitation efficiency η_{PLE} as a function of the excitation energy ε . The system is bleached by a broad-band light source. The bleached sites induce quenching of excitons on the intact sites. The PLE efficiency is shown after $A = 0.00, 0.10, 1.00,$ and 10.0 $n(0)/\gamma(0)$ photons per unit volume have been absorbed. Parameters are given in the text.*

8.5 Photobleaching of PPV

In Sec. 8.3, it is described how spectral diffusion in a system with energetic disorder gives rise to a stronger bleaching at lower energies. In Sec. 8.4, it is shown that bleaching in combination with exciton quenching, besides the obvious drop in the PL efficiency, leads to a crossover from strong to weak spectral diffusion and a non-trivial energy dependence of the PLE efficiency. These effects have been observed in bleaching experiments on PPV and its derivatives [5, 7, 12, 13].

The following reaction mechanism for the photobleaching of PPV and its derivatives has been suggested [6, 8]. Upon illumination, singlet excited states are formed in PPV that relax energetically through spectral diffusion. These singlet excited states can form triplet excited states through an intersystem crossing. Then the energy of the PPV triplet state can be used

to excite molecular oxygen from its triplet ground state to its singlet excited state. The excited oxygen reacts with the vinyl double bond in the PPV backbone, which results in a scission of the polymer chain and the creation of two carbonyl groups (C=O bonds). Experiments on solutions of a PPV derivative show that part of the reaction is self-sensitized, i.e., the oxidation occurs at the initially excited PPV chain segment, and that the remainder is diffusion-controlled, i.e., the reaction occurs at a random (ground state) PPV chain segment to which the singlet oxygen has diffused [8]. The branching ratio of these two reaction paths varies for different solvents; it is unknown for solid PPV films. The diffusion-controlled reaction can be suppressed by adding a singlet oxygen quencher to the system [8].

In our model, we have combined the singlet excited-state dynamics with a self-sensitized bleaching reaction of the molecular sites. Bleaching through the oxygen diffusion-controlled reaction may be taken into account by adding [in Eq. (8.18)] a bleaching rate that is independent of the site occupation. However, we do not expect the diffusion-controlled reaction to be the dominant mechanism, as it would lead to a uniform decrease of the DOS instead of the experimentally observed blue shift. The dynamics of triplet excitons in PPV may be included as well. Although this would make the description of the excited-state dynamics more complex, we do not expect that this would lead to qualitative changes in our results.

The quenching of the PL efficiency in bleached PPV has been ascribed to the creation of carbonyl groups [5]. It is believed that, due to the high electron affinity of the carbonyls, immediate (≤ 200 fs) charge transfer takes place between an intact segment of the polymer and an oxidated segment, thereby dissociating the exciton and quenching the PL [5, 7, 12, 21]. This reaction is well described by the fast, short-range quenching mechanism used in our model.

The recent experiments of Harrison *et al.* [12] show an energy independent PLE efficiency in unbleached PPV, which indicates the absence of quenching sites in the initial material. In photo-oxidized PPV, the PLE efficiency is lower and has a pronounced energy-dependence: starting at the low-energy flank of the absorption spectrum, the PLE efficiency decreases until a saturation value is reached at high energies. This behavior is reminiscent of our results shown in Fig. 8.6. Harrison *et al.* [12] ascribe this effect to the fact that the measurements have been performed on a thick layer that was not uniformly oxidized. Due to the blue shift of the bleached absorption spectrum, the response of the PLE measurement at low energies is mainly from deeper, less oxidized parts of the sample, which have

a higher PL efficiency [12]. Our calculations show that this energy dependence of the PLE efficiency is inherent to oxidized PPV and that it should be present in uniformly oxidized layers as well. To describe the experiments on thicker layers, our theory should be combined with the approach of Kaminow *et al.* [2] or more recent extensions of this approach [3, 4, 22].

8.6 Conclusion

The influence of spectral diffusion on the photobleaching of an energetically disordered system in the low temperature regime has been described using an analytical effective medium theory. Due to spectral diffusion, the excited states are transferred towards chromophores with lower excitation energies, which results in a relatively stronger bleaching of these chromophores. As a consequence, both the absorption spectrum and the PL spectrum are blue shifted in the course of the bleaching process.

When the excited states are quenched on sites that are next to a bleached site, the reduced lifetime of the excitons gives rise to a decrease of the PL efficiency. Furthermore, the reduction of the exciton lifetime results in increasingly less spectral diffusion, which is reflected in the bleaching behavior and the broadening of the PL spectrum. Finally, excitons that are created on the sites with higher excitation energies have a lower PL efficiency, as these excitons are more mobile and have a higher probability to encounter a quenching site. This, in combination with the time dependent DOS of the quenching sites, gives rise to a pronounced energy dependence of the photoluminescence excitation efficiency.

The effects described above have all been observed in photobleaching experiments on PPV and its derivatives. At present, however, the exact nature of both the excited-state dynamics and the photochemical bleaching reaction in PPV is still under debate. Consequently, as experimental information on many system parameters is lacking, a quantitative microscopic modelling of these photobleaching experiments would be unrealistic. However, we believe that our model contains the essential physics. More experiments are clearly needed. An ideal experiment would be on a thin layer of PPV that is uniformly bleached at low temperatures. After different bleaching times, all relevant spectra, such as the absorption spectrum, the PL spectrum, and the PLE spectrum, should be measured for the same sample.

References

- [1] J. Kosar, *Light-Sensitive Systems* (Wiley, New York, 1965).
- [2] I. P. Kaminow, L. W. Stulz, E. A. Chandross, and C. A. Pryde, *Appl. Opt.* **11**, 1563 (1972).
- [3] K. K. Boyarskii, A. Yu. Vorobev, V. I. Zenskii, Yu. L. Kolesnikov, and I. K. Meshovskii, *Opt. Spectrosk.* **65**, 909 (1988) [*Opt. Spectrosc. (USSR)* **65**, 536 (1988)].
- [4] A. Dubois, M. Canva, A. Brun, F. Chaput, and J.-P. Boilot, *Appl. Opt.* **35**, 3193 (1996); *Synth. Met.* **81**, 305 (1996).
- [5] M. Yan, L. J. Rothberg, F. Papadimitrakopoulos, M. E. Galvin, and T. M. Miller, *Phys. Rev. Lett.* **73**, 744 (1994); L. J. Rothberg, M. Yan, S. Son, M. E. Galvin, E. W. Kwock, T. M. Miller, H. E. Katz, R. C. Haddon, and F. Papadimitrakopoulos, *Synth. Met.* **78**, 231 (1996).
- [6] B. H. Cumpston and K. F. Jensen, *Synth. Met.* **73**, 195 (1995).
- [7] T. Zyung and J.-J. Kim, *Appl. Phys. Lett.* **67**, 3420 (1995).
- [8] R. D. Scurlock, B. Wang, P. R. Ogilby, J. R. Sheats, and R. L. Clough, *J. Am. Chem. Soc.* **117**, 10194 (1995).
- [9] See, e.g., R. Richert and H. Bässler, *Chem. Phys. Lett.* **118**, 235 (1985).
- [10] A. Nabetani, A. Tomioka, H. Tamaru, and K. Miyano, *J. Chem. Phys.* **102**, 5109 (1995).
- [11] A. Tomioka and K. Miyano, *Phys. Rev. B* **54**, 2963 (1996).
- [12] N. T. Harrison, G. R. Hayes, R. T. Phillips, and R. H. Friend, *Phys. Rev. Lett.* **77**, 1881 (1996).

- [13] A. J. M. Berntsen and R. H. Cuijpers (private communication) [see Section 1.5].
- [14] For a recent review, see H. Bässler, V. Brandl, M. Deussen, E. O. Göbel, R. Kersting, H. Kurz, U. Lemmer, R. F. Mahrt, and A. Ochse, *Pure & Appl. Chem.* **67**, 377 (1995).
- [15] N. C. Greenham, I. D. W. Samuel, G. R. Hayes, R. T. Phillips, Y. A. R. R. Kessener, S. C. Moratti, A. B. Holmes, and R. H. Friend, *Chem. Phys. Lett.* **241**, 89 (1995); J. J. M. Halls, K. Pichler, R. H. Friend, S. C. Moratti, and A. B. Holmes, *Appl. Phys. Lett.* **68**, 3120 (1996).
- [16] B. Movaghar, B. Ries, and M. Grünewald, *Phys. Rev. B* **34**, 5574 (1986).
- [17] M. C. J. M. Vissenberg and M. J. M. de Jong, *Phys. Rev. Lett.* **77**, 4820 (1996) [Chapter 6].
- [18] M. C. J. M. Vissenberg and M. J. M. de Jong, in *Excitonic Processes in Condensed Matter*, edited by M. Schreiber (Dresden University Press, Dresden, 1996) [see also Chapter 5].
- [19] Th. Förster, *Z. Naturforsch.* **4a**, 321 (1949).
- [20] R. M. Corless, G. H. Gonnet, D. E. G. Hare, D. Jeffrey, and D. E. Knuth, *Adv. Comput. Maths.* **5**, 329 (1996).
- [21] H. Antoniadis, L. J. Rothberg, F. Papadimitrakopoulos, M. Yan, M. E. Galvin, and M. A. Abkowitz, *Phys. Rev. B* **50**, 14911 (1994).
- [22] J.-J. Kim, T. Zyung, and W. Y. Hwang, *Appl. Phys. Lett.* **64**, 3488 (1994).

Samenvatting

Opto-elektronische eigenschappen van wanordelijke organische halfgeleiders

Dit proefschrift beschrijft de resultaten van een theoretische studie naar de optische respons en de elektrische transporteigenschappen van wanordelijke organische halfgeleiders. Organische materialen, met name plastics, worden veelal toegepast vanwege hun mechanische of hun isolerende eigenschappen. Sinds het begin van de jaren zestig is echter bekend dat kristallen bestaande uit organische pigmenten halfgeleidende eigenschappen vertonen, zoals een sterke toename van de elektrische geleidbaarheid met de temperatuur of met de intensiteit van opvallend licht (fotogeleiding). De interesse in organische halfgeleiders nam tegen het einde van de jaren tachtig een grote vlucht toen aangetoond werd dat met wanordelijke lagen van deze materialen werkende transistoren en efficiënte licht-emitterende diodes (LEDs) gemaakt kunnen worden. Geconjugeerde polymeren combineren de halfgeleidende eigenschappen van organische pigmenten met de mechanische eigenschappen van plastics. De mogelijkheid om met deze materialen goedkope en flexibele transistoren en LEDs te maken wordt momenteel door een aantal bedrijven onderzocht, waaronder Philips.

In essentie bestaat een organische LED uit een organische halfgeleidende laag tussen twee elektroden. Wanneer een spanning wordt aangelegd, komen vanuit de ene elektrode elektronen de organische laag in. Bij de tegenoverliggende elektrode verlaten elektronen de laag. De achterblijvende positieve ladingen worden volgens de halfgeleiderterminologie aangeduid als 'gaten' (chemici zouden eerder spreken van kationen). De elektronen en gaten bewegen in tegengestelde richting door de organische laag tot ze elkaar tegenkomen en recombineren tot een neutrale aangeslagen toestand: een *exciton*. Dit exciton verdwijnt tenslotte via een energieomzetting naar warmte of licht. De werking van een organische LED berust dus zowel op de injectie en het transport van ladingsdragers, als op de vorming en het

verval van excitonen.

Het doel van deze studie is het leggen van verbanden tussen enerzijds materiaalparameters en anderzijds fenomenologische parameters uit halfgeleidermodellen, die gebruikt worden voor de karakteristatie van organische transistoren en LEDs. Het transport van lading door een organische halfgeleider vindt plaats via sprongen van molecuul tot molecuul. Deze sprongen zijn sterk afhankelijk van zowel de *energetische* als de *structurele* wanorde in de organische laag. De invloed van beide vormen van wanorde op de transporteigenschappen van organische transistoren en LEDs wordt bestudeerd in hoofdstuk 2, 3 en 4 van dit proefschrift. De dynamica van excitonen wordt gewoonlijk bestudeerd door excitonen met licht aan te maken, en vervolgens het uitgezonden licht te detecteren (fotoluminescentie). Een probleem bij de interpretatie van fotoluminescentie-experimenten aan deze materialen is het complexe samenspel van processen: het exciton stralend of niet-stralend vervallen, maar het kan ook zijn energie overdragen aan naburige moleculen alvorens te vervallen. Dit laatste proces bepaalt voor een groot deel de uiteindelijke kleur van de emissie, als ook de efficiëntie van stralend verval. In hoofdstuk 5 wordt een theorie gepresenteerd voor de excitodynamica in wanordelijke moleculaire materialen. Hiermee is het mogelijk om het samenspel van processen te relateren aan de experimenteel waargenomen verschijnselen. In hoofdstuk 6, 7 en 8 passen we deze theorie toe in studies naar de invloed van sterke elektrische velden en van de degradatie van de organische halfgeleider op de efficiëntie van stralend verval. In het volgende worden de verschillende onderwerpen wat verder uitgediept.

In hoofdstuk 2 wordt een model gepresenteerd voor de mobiliteit (beveeglijkheid) van ladingsdragers in organische transistoren. In analogie met de LEDs loopt de stroom hierin van de ene elektrode naar de andere via een halfgeleidende organische laag. Echter de hoeveelheid lading in het halfgeleidende kanaal, en daardoor de stroomsterkte, is regelbaar met behulp van een derde elektrode. Het blijkt dat de spanning op deze elektrode niet alleen de ladingsdichtheid, maar ook de mobiliteit van de ladingsdragers beïnvloedt: met toenemende spanning neemt de gemiddelde energie per ladingsdrager toe, zodat energiever schillen tussen moleculen gemakkelijker overbrugd kunnen worden. Onderzoek aan verschillende materialen laat zien dat verschillen in de mobiliteit voornamelijk veroorzaakt worden door de structurele wanorde.

In hoofdstuk 3 worden experimenten aan de schakeltijd, d.w.z. de vertraging tussen het aanleggen van de spanning en de emissie van licht, van

polymeren LEDs beschreven. Deze schakeltijd is het directe gevolg van het feit dat de ladingsdragers eerst de polymeerlaag over moeten steken, voordat recombinatie plaats kan vinden. Uit de experimenten blijkt dat de gemeten schakeltijd voornamelijk wordt bepaald door de spreiding in mobiliteit (d.w.z. door de snelste ladingsdragers) en niet door de gemiddelde mobiliteit. Zowel energetische als structurele wanorde kunnen bijdragen tot deze spreiding. Experimenteel blijkt de spreiding onafhankelijk van de temperatuur, hetgeen duidt op een dominante rol van structurele wanorde.

In hoofdstuk 4 wordt een theoretisch model voorgesteld voor de gemiddelde ladingsdragersmobiliteit in wanordelijke organische halfgeleiders. In vrijwel alle soorten organische halfgeleiders blijkt deze mobiliteit op ongeveer dezelfde wijze toe te nemen met de temperatuur en met het aangelegde elektrische veld. Modellen, waarin de energetische en structurele wanorde homogeen verdeeld zijn, geven alleen kwalitatieve overeenstemming met het waargenomen gedrag. Recent onderzoek heeft aangetoond dat de overeenstemming verbetert wanneer correlaties tussen de energieën van naburige moleculen meegenomen worden. We laten zien dat kwantitatieve overeenstemming ook bereikt wordt met een model waarin de *structuur* sterk inhomogeen is.

In de hoofdstukken 6 en 7 gebruiken we de theorie voor excitodynamica (hoofdstuk 5) om de experimenteel waargenomen afname in fotoluminescentie in een aangelegd elektrisch veld te beschrijven. Hierbij behandelt hoofdstuk 6 in het bijzonder geconjugeerde polymeren en hoofdstuk 7 organische pigmenten. De afname in fotoluminescentie wordt veroorzaakt door de dissociatie van excitonen. (Dit dissociatieproces is juist tegenovergesteld aan het recombinatieproces in een LED.) Uit de analyse van de experimenten volgt dat het dissociatieproces voor beide klassen van materialen verschillend is: bij organische pigmenten vereist dissociatie de overdracht van een ladingsdrager naar een naburig molecuul, terwijl in een geconjugeerd polymeer het exciton langs de polymeerketen, dus intra-moleculair, uit elkaar getrokken wordt.

Tot slot behandelt hoofdstuk 8 het verbleken van kleurstoffen onder intense of langdurige belichting. Bij het bleken van geconjugeerde polymeren is experimenteel waargenomen dat de absorptie en emissie van licht niet alleen afnemen door dit blekingsproces, maar ook verschuiven naar een meer blauwe kleur. Dit gedrag is te begrijpen vanuit de invloed van de excitodynamica op de degradatie van het polymeer en vice versa.

List of Publications

1. “Theory of exciton migration in conjugated polymers”,
M.C.J.M. Vissenberg and M.J.M. de Jong,
in *Excitonic Processes in Condensed Matter*, proceedings of the International Conference, edited by M. Schreiber (Dresden University Press, Dresden, 1996), p. 263.
2. “Theory of exciton migration and field-induced dissociation in conjugated polymers”,
M.C.J.M. Vissenberg and M.J.M. de Jong,
Physical Review Letters **77**, 4820-4823 (1996) [Chapter 6].
3. “Generalized Landau–de Gennes theory of uniaxial and biaxial nematic liquid crystals”,
M.C.J.M. Vissenberg, S. Stallinga, and G. Vertogen,
Physical Review E **55**, 4367-4377 (1997).
4. Reply to Comment on “Theory of exciton migration and field-induced dissociation in conjugated polymers”,
M.C.J.M. Vissenberg and M.J.M. de Jong,
Physical Review Letters **78**, 4302 (1997) [Section 6.5].
5. “Photobleaching and spectral diffusion in disordered media”,
M.C.J.M. Vissenberg and M.J.M. de Jong,
Physical Review B **56**, 6681-6688 (1997) [Chapter 8].
6. “Electric field-induced luminescence quenching in conjugated polymers and in molecularly doped polymers”,
M.C.J.M. Vissenberg and M.J.M. de Jong,
Physica Status Solidi B **205**, 347-350 (1998)
(*Proceedings of the International Conference on Hopping and Related Phenomena, Ráckeve, 1997*).

7. “Theory of electric field-induced photoluminescence quenching in disordered molecular solids”,
M.C.J.M. Vissenberg and M.J.M. de Jong,
Physical Review B **57**, 2667-2670 (1998) [Chapter 7].
8. “Dispersive hole transport in poly(p-phenylene vinylene)”,
P.W.M. Blom and M.C.J.M. Vissenberg,
Physical Review Letters **80**, 3819-3822 (1998) [Chapter 3].
9. “Theory of the field-effect mobility in amorphous organic transistors”,
M.C.J.M. Vissenberg and M. Matters,
Physical Review B **57**, 12964-12967 (1998) [Chapter 2].
10. “Theory of luminescence quenching and photobleaching in conjugated polymers”,
M.J.M. de Jong and M.C.J.M. Vissenberg,
Philips Journal of Research **51**, 495-510 (1998)
(*Special Issue on Polymer Light-Emitting Diodes*).
11. “Organic field-effect transistors and all-polymer integrated circuits”,
M. Matters, D.M. de Leeuw, M.C.J.M. Vissenberg, C.M. Hart, P.T. Herwig, T. Geuns, C.M.J. Mutsaers, and C.J. Drury,
to appear in Optical Materials
(*Proceedings of the E-MRS Spring Meeting, Strasbourg, 1998*).
12. “Transient hole transport in poly(*p*-phenylene vinylene) LEDs”
M.C.J.M. Vissenberg and P.W.M. Blom,
to appear in Synthetic Metals
(*Proceedings of the International Conference on the Science and Technology of Synthetic Metals, Montpellier, 1998*) [Section 3.4].
13. “Theory of the field-dependent mobility in disordered organic semiconductors”,
M.C.J.M. Vissenberg,
submitted [Chapter 4].
14. Reply to Comment on “Dispersive hole transport in poly(*p*-phenylene vinylene)”,
P.W.M. Blom and M.C.J.M. Vissenberg,
submitted.

Curriculum Vitæ

Op 22 januari 1972 ben ik geboren te Philipsburg, Sint Maarten. Middellaar onderwijs volgde ik vanaf 1984 aan het Moller Lyceum te Bergen op Zoom. Daar deed ik in 1990 eindexamen Gymnasium- β in 9 vakken. In hetzelfde jaar behaalde ik de tweede plaats op de Nederlandse Natuurkunde Olympiade en een eervolle vermelding op de Internationale Natuurkunde Olympiade.

Vervolgens begon ik de studie Natuurkunde aan de Katholieke Universiteit Nijmegen. In september 1991 slaagde ik voor het propædeutisch examen, met lof. Tijdens mijn studie heb ik werkcolleges gegeven in wis- en natuurkunde vakken. Mijn afstudeeronderzoek verrichtte ik in de vakgroep Theoretische Fysica I. Onder begeleiding van prof. dr. G. Vertogen en dr. S. Stallinga onderzocht ik de oriëntationele elasticiteitstheorie van nematische vloeibare kristallen. In augustus 1995 slaagde ik voor het doctoraal examen, met lof.

In september 1995 ben ik met financiële steun van Philips in dienst getreden van de Stichting voor Fundamenteel Onderzoek der Materie, om als Onderzoeker In Opleiding promotieonderzoek te verrichten bij prof. dr. C.W.J. Beenakker. Dit onderzoek is in zijn geheel verricht op het Philips Natuurkundig Laboratorium, eerst in de groep “Exploratory Physics” van dr. H. van Houten, later in de groep “Microsystems Technology” van dr. G.F.A. van de Walle, onder begeleiding van dr. ir. M.J.M. de Jong en dr. ir. P.W.M. Blom. De belangrijkste resultaten van dit onderzoek zijn beschreven in dit proefschrift. Ik heb deze resultaten kunnen presenteren bij verscheidene nationale symposia en op internationale conferenties in Bad Schandau, Ráckeve, Cambridge, Trieste en Montpellier.

Met ingang van 1 februari 1999 ben ik als Wetenschappelijk Medewerker in dienst van Philips Research te Eindhoven.

STELLINGEN

behorende bij het proefschrift

Opto-Electronic Properties of Disordered Organic Semiconductors

van M.C.J.M. Vissenberg

1. Transport van lading door een wanordelijk organisch materiaal verloopt via het huppelmechanisme en niet via het valstrikmechanisme.

Hoofdstuk 2 van dit proefschrift

2. De karakteristieke veldafhankelijkheid van de ladingsdragersmobiliteit in een wanordelijke laag poly(-*p*-phenyleen vinyleen) wordt grotendeels bepaald door inhomogeniteiten in de structurele ordening.

Hoofdstuk 4 van dit proefschrift

3. De afname van de fotoluminescentie van geconjugeerde polymeren in sterke elektrische velden wordt veroorzaakt door de intramoleculaire dissociatie van excitonen.

Hoofdstuk 6 en 7 van dit proefschrift

4. Door uit dezelfde fotogeleidingsmeting zowel de ladingsdragersmobiliteit als de dispersieparameters te bepalen, maken Lebedev *et al.** beide resultaten ongeloofwaardig.

**E. Lebedev, Th. Dittrich, V. Petrova-Koch, S. Karg en W. Brütting, Appl. Phys. Lett. 71, 2686 (1997).*

Paragraaf 3.4 van dit proefschrift

5. Het feit dat in chemisch gedoteerde geconjugeerde polymeren met een metallische geleiding de statische diëlektrische constante positief is, geeft aan dat slechts een fractie van de ladingsdragers participeert in het metallisch transport.

6. Sommige suggesties ter verbetering van polymeren lichtgevende diodes kan men maar beter met een korreltje zand¹, zeep² of zout³ nemen.
¹*S.A. Carter, J.C. Scott en P.J. Brock, Appl. Phys. Lett.* **71**, 1145 (1997).
²*Y. Cao, G. Yu en A.J. Heeger, Adv. Mater.* **10**, 917 (1998).
³*Q. Pei, G. Yu, C. Zhang, Y. Yang en A.J. Heeger, Science* **269**, 1086 (1995).
7. Voor de beschrijving van alle elastische oriëntationele vervormingen in een chiraal biaxiaal nematisch medium met inhomogene ordening zijn 48 onafhankelijke elasticiteitsconstanten nodig.
M.C.J.M. Vissenberg, S. Stallinga en G. Vertogen, Phys. Rev. E **55**, 4367 (1997).
8. De verzadiging van de effectieve voortplantingssnelheid van een aardshok met toenemende meetafstand duidt op een percolatieovergang.
M. Roth, G. Müller en R. Snieder, Geophys. J. Int. **115**, 552 (1993).
9. In een niet-ontaard elektronengas met korte-dracht elastische strooicentra neemt de stroom toe met de drie-tweede macht van de spanning.
10. De benaming “gestrekte exponent” voor de functie e^{-x^α} slaat op de rekbaarheid van deze functie bij het passen aan meetpunten.
11. Het voor de Openbaar-Vervoer-Reisinformatie ontwikkelen van een spraakherkenningssysteem dat uitgaat van een open dialoog in plaats van een menu-gestuurde dialoog heeft alleen zin wanneer ook de OVR-telefonistes volgens open dialogen gaan communiceren.
12. Van antiflogistische additieven in tandpasta—met uitzondering van de stof triclosan—is het gingivitisverlagend effect minder significant dan het prijsverhogend effect.